DESIGN AND FABRICATION OF TRAVELLING-WIRE ELECTRO-CHEMICAL SPARK

MACHINE AND MACHINING OF PIEZOELECTRIC CERAMIC (PZT)

A Thesis Submitted
in Partial Fulfilment of the Requirements
for the Degree of
MASTER OF TECHNOLOGY

BY
YATINDER PRATAP SINGH

to the
DEPARTMENT OF MECHANICAL ENGINEERING
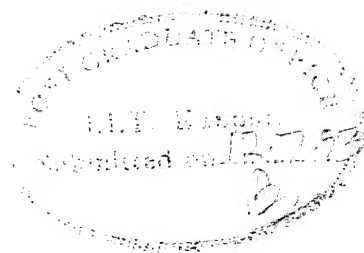INDIAN INSTITUTE OF TECHNOLOGY KANPUR
JULY 1993

DEDICATED TO
MY PARENTS,
WIFE KAMNA
AND
BELOVED SISTER
ANU

CERTIFICATE

This is to certify that the present work entitled "DESIGN AND FABRICATION OF TRAVELLING WIRE ELECTRO-CHEMICAL SPARK MACHINE (TW-ECSM) AND MACHINING OF PIEZOELECTRIC CERAMICS (PZT)" has been carried out by Yatinder Pratap Singh under our supervision and has not been submitted elsewhere for a degree.

D.C.Agrawal
Professor
Material Science Programme
Indian Institute of Technology
Kanpur - 208016

Vijay.K.Jain
Professor
Dept. of Mechanical Engineering
Indian Institute of Technology
Kanpur - 208016

ABSTRACT

Machining of advanced engineering materials such as ceramics and composites is gaining tremendous potential primarily because of its vast applications in various field. As a result newer techniques are being discovered for the machining of these materials. The conventional machining techniques have proved to be incompetent as compared to the non-conventional techniques.

In ceramics, the piezoelectric ceramics are gaining importance for the reason of their application as transducer in the fields of engineering and sciences. Recently the main emphasis of some of the researchers has been in the machining of non-conducting materials (ceramics and composites) using non-conventional methods in general and *Electro-Chemical Spark Machining (ECSM)* in particular.

Here, the author has attempted to explore the feasibility of using ECSM for the machining of electrically partially conducting materials like piezoelectric ceramics. Experiments are conducted on Lead Zirconate Titanate (PZT) which dominates in the field of piezoelectric ceramics.

A *Travelling Wire Electro-Chemical Spark Machining (TW-ECSM)* set up is fabricated. Various experiments are conducted to investigate into the effects of supply voltage and concentration of electrolyte on average diametral overcut and material removal rate (MRR). The surface texture is also analyzed using Scanning Electron Microscope (SEM). With the help of an oscilloscope, the minimum voltage at which the sparking occurs is also recorded. It

has been observed that the machining of partially electrically conductive materials using ECSM process is comparatively more difficult than non-conducting materials for the simple reason that physical contact between the cathode and the workpiece (partially conductive) or the wire and the debris in the cut slot results in arcing which deteriorates the machined surface characteristics. Repeated arcing finally results in wire breakage. Overcut is found to be a function of applied voltage and concentration.

In the end some means are suggested for minimization of the arcing and attaining better surface characteristics.

ACKNOWLEDGEMENT

CONTENTS

LIST OF FIGURES

LIST OF PHOTOGRAPHS

LIST OF TABLES

INTRODUCTION

1.1 Electrically assisted non-conventional machining

With the development of new alloys with high strength, high temperature resistant (HSTR); more and more challenging problems are faced by the scientists and the technologists in the field of manufacturing. The major difficulties in adopting the traditional manufacturing processes were identified as,

1) new materials with a low machinability,

2) dimensional and geometrical accuracy requirements,

3) a higher production rate and economy.

This gave development of non-conventional machining techniques in the early 1930s.

The non-conventional processes vary widely in their basic features, mechanics of the process and the type of energy used in the material removal, but are dependent on the electrical energy. Thus they can be grouped under a common heading of 'electrically assisted non-conventional machining processes'. The more common processes under this heading are

(i) Electro Chemical Machining (ECM),

(ii) Electric Discharge Machining (EDM),

(iii) Electron Beam Machining (EBM) and

(iv) Plasma Arc Machining (PAM).

From the point of view of material removal, accuracy and shape capabilities, ECM and EDM processes have the maximum potential.

Unfortunately, these processes have a major limitation in the fact that only electrically conducting work materials can be machined. To overcome this, a hybrid of ECM and EDM has been conceived in the early '70s in which the phenomenon of electro-chemical discharge (ECD) is employed for the material removal. Use of ECD for conducting material were also attempted and was termed as "Electro Chemical Arc Machining (ECAM)". For the non-conducting material it was termed as "Electro Chemical Discharge Machining (ECDM)".

1.2 Comparative study of various processes

It will be convenient to understand the process of ECDM using a comparative illustration of ECM, EDM, ECAM and ECDM. Fig.1.1 illustrates the voltage and current density ranges that are used in various electrolyte system of machining [1]. Usual voltage ranges of ECM is 8 to 20 volts, for ECAM it is 20 to 40 volts and that of ECDM is in the range of 20 to 100 volts depending upon the type of workpeice, tool size, electrolyte etc. Typical ranges of the tool size and the work-tool gap for these processes are presented in Fig.1.2 [1].

Very high current density is attained by ECAM process upto a value of 800 A/cm^2 and MRR obtained is as high as five times compared to ECM and about forty times compared to EDM [1].

The mechanism of material removal in ECM, EDM and ECAM have been investigated thoroughly and understood reasonably well. In ECM, electrochemical anodic dissolution causes material removal and in EDM melting, vaporization and mechanical shock are
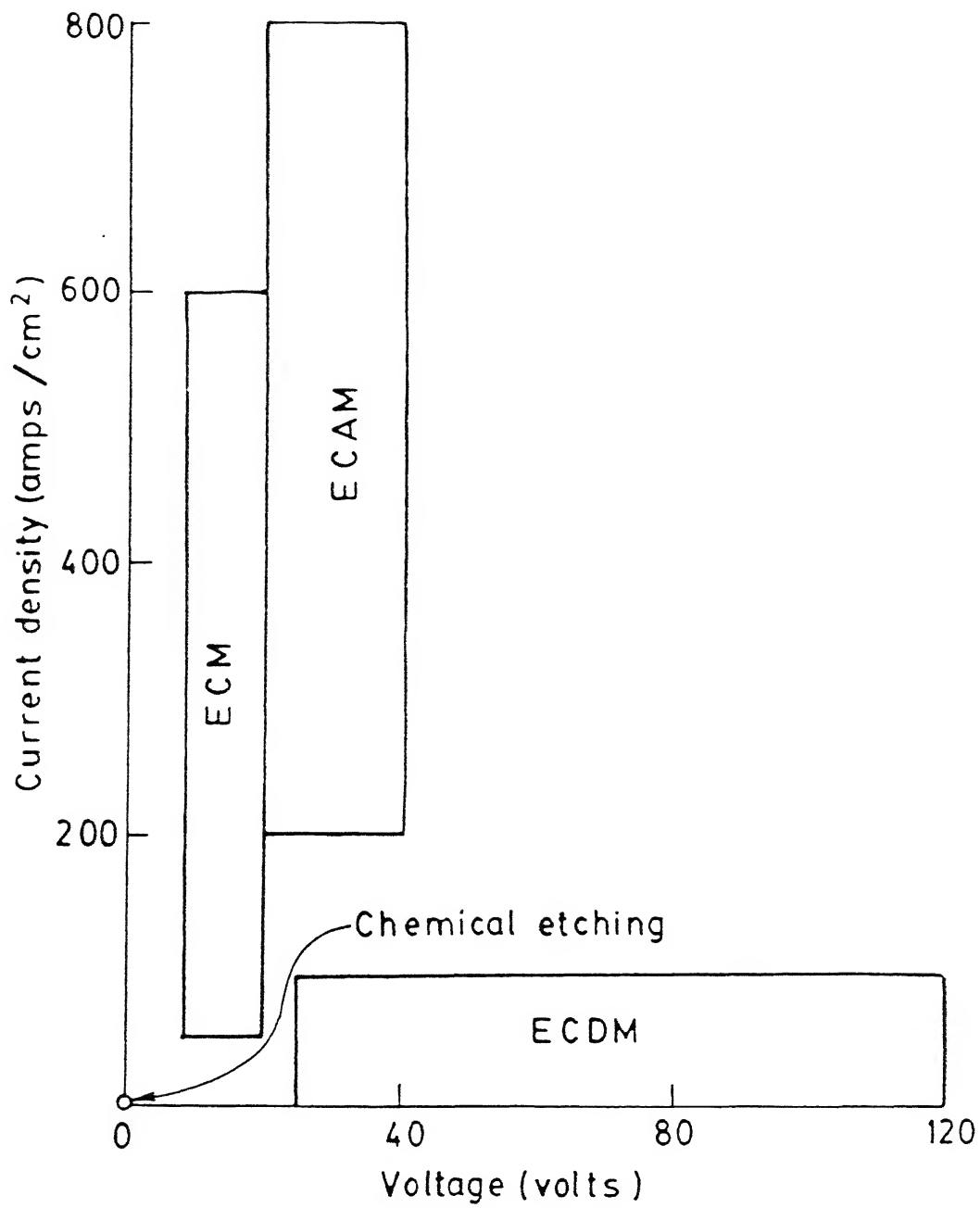
FIG 1.1   VOLTAGE AND CURRENT DENSITY   RANGES   OF   THE   MACHINING
                 SYSTEMS USING ELECTROLYTE SOLUTIONS [1]
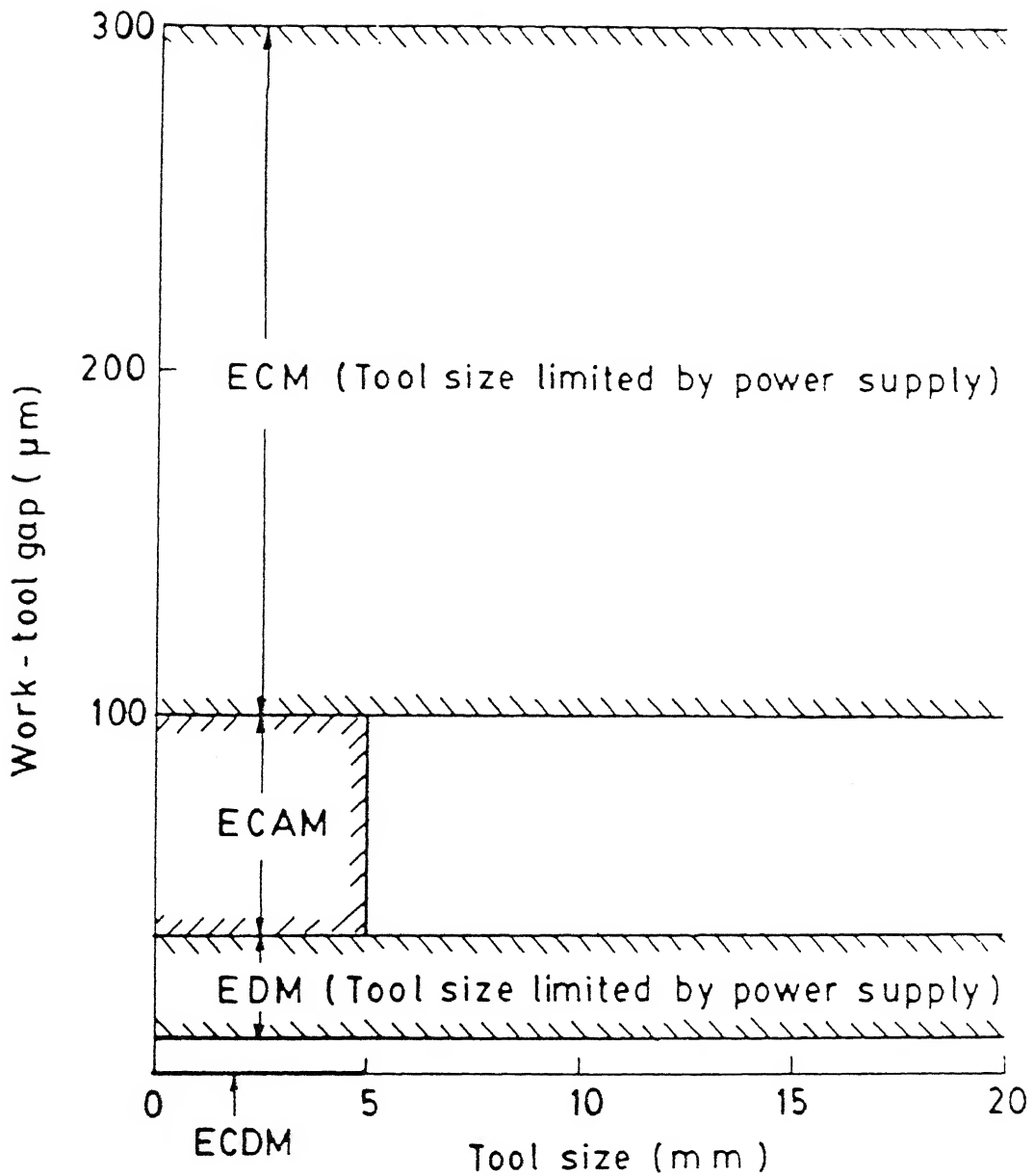
FIG 1.2   TOOL SIZE AND WORK-TOOL GAP IN ELECTRICALLY ASSISTED
           MACHINING PROCESSES [1]

responsible for material removal producing a crater. In ECAM both the mechanisms described above are acting simultaneously. However, in ECAM it is the arc instead of the sparks which produce the thermal effects. The mechanism of material removal in ECDM is not yet very clear and is supposed to be melting, vaporization and mechanical shock responsible for the material removal [1,3,19].

A major difference between ECAM and ECDM is that, in ECAM discharge takes place between the electrodes, but in ECDM it is between one electrode and the electrolyte across the hydrogen gas bubble.

1.3 Electro Chemical Discharge (ECD) phenomena

Electrochemical discharge cell primarily consists of two electrodes dipped in an electrolyte as shown in Fig.1.3. Application of external potential between the electrodes causes an electric current to flow in the cell resulting in electrochemical reactions, such as anodic dissolution, cathodic deposition, electrolysis of the electrolyte etc., depending on the electrode-electrolyte combination. If a suitable electrolyte is chosen and the electrodes are of grossly different sizes, then, beyond a certain value of the applied potential electric sparks appear at the smaller electrode and the cell current drops. This phenomenon is known as Electro-chemical discharge phenomenon. The mechanism of ECD, by and large, is not clear, though the observations of this process have established the fact that the discharge takes place due to bubble generation resulting from electro-chemical reaction and thermal processes.

Power supply

Large electrode

Tool electrode
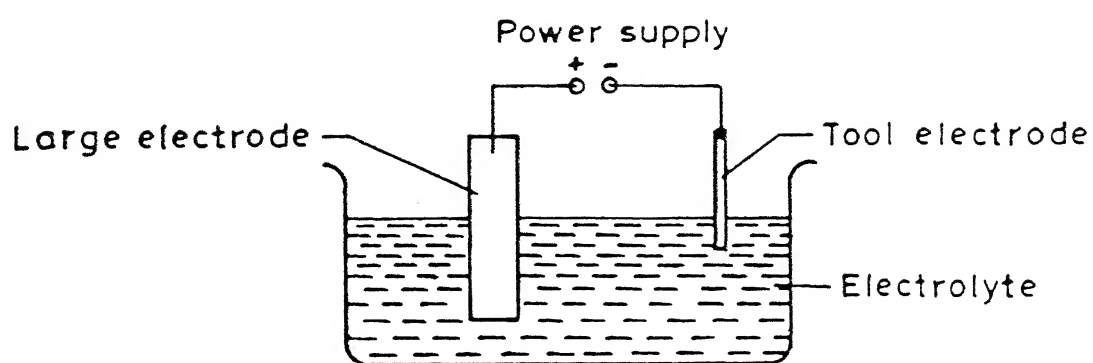
Electrolyte

FIG 1.3   SCHEMATIC DIAGRAM OF ECD SET-UP

1.4 Discharge phenomena in electrolytes

Electrical discharge can take place either due to the dielectric breakdown of the medium or due to the switching action. When the applied potential between two electrodes separated by a dielectric medium is high enough, the breakdown of the medium takes place. Sparks appear between the electrodes through the highly ionized channel developed due to dielectric breakdown [1,3] shown in Fig.1.4. In a similar manner discharges between electrodes can take place when the medium is gaseous one. The required potential difference between the electrodes to cause such discharge through the air is given by Paschen's Curve [16] Fig.1.5. The X-axis represents the product of the pressure of the gas and the distance between the electrodes. The Y-axis represents the required potential difference. For other gases the value of the potential required is of the same order. From Paschen's Curve it can be observed that the minimum required potential difference to initiate a discharge through an air gap is in the order of 280 volts. Whereas,in the ECD cell it has been observed that discharge occurs at an applied voltage in the range of 15V to 50V. Hence, it is logical to conclude that the discharge in the electrochemical cell is not due to the electrical breakdown of the gas bubble [3].

The other type of the discharge takes place at the interrupter switches of electrical circuit. If the inductance of the circuit is L, then at instant of opening the circuit the induced e.m.f. V_s, is given by $V_s = - L (dI/dt)$ where, "I" is the current at any instant of the circuit opening and "t" is the time to break the circuit. This e.m.f. is termed as back or switching

ionised column

Dielectric fluid

- • Electron
- ⊕ +ve ion
- ○ Dielectric molecule
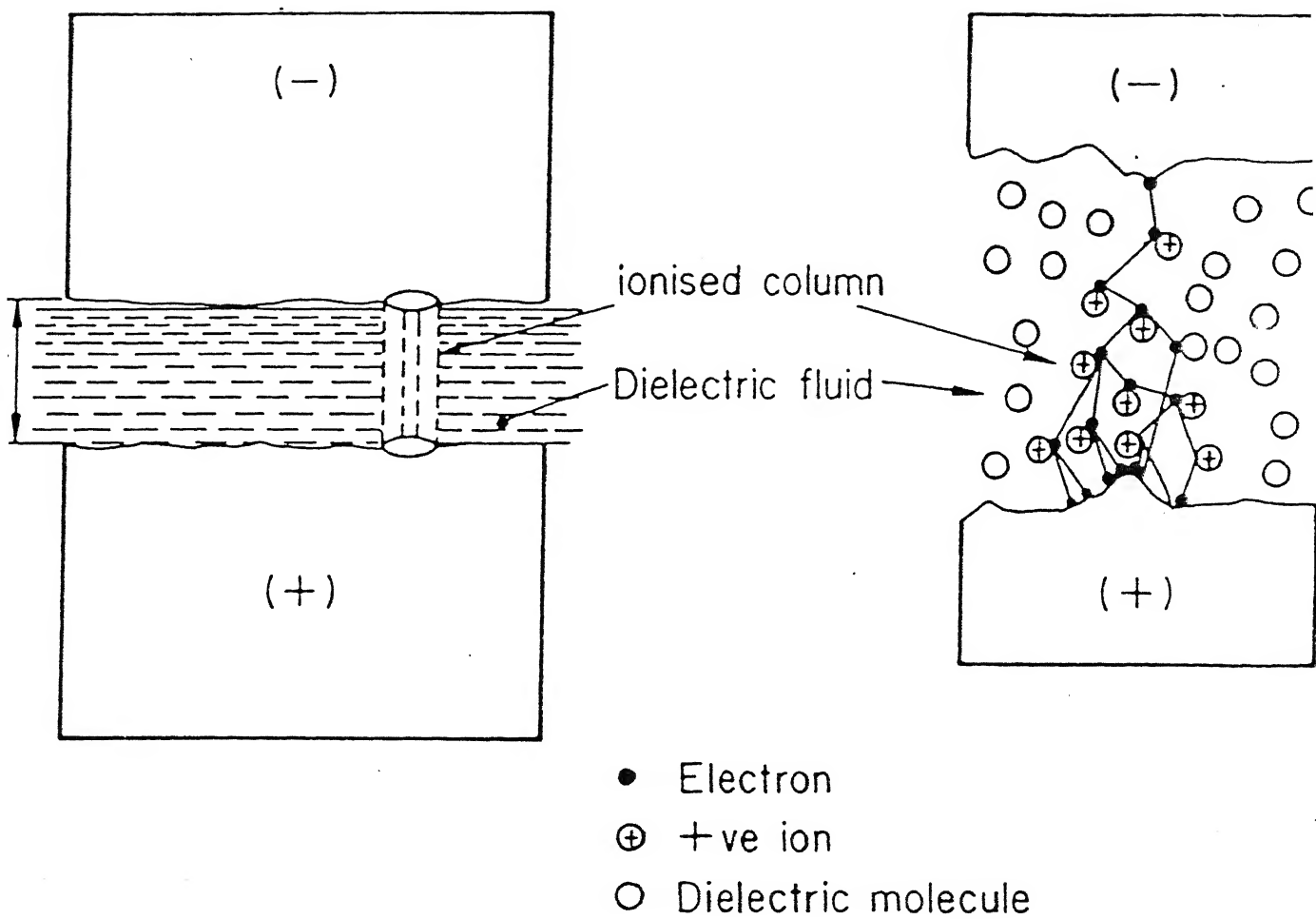
FIG 1.4   DISCHARGE IN LIQUID DIELECTRICS [1]
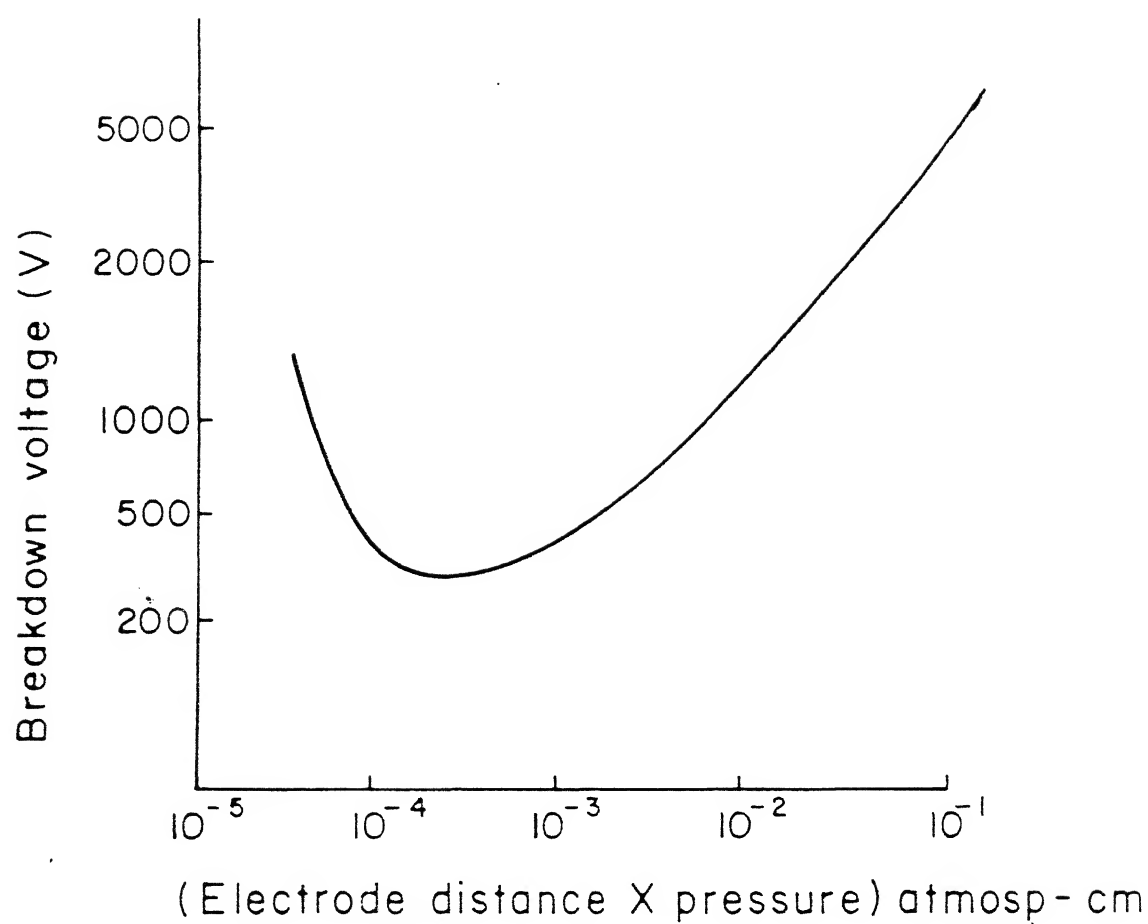
FIG 1.5   PASCHEN'S CURVE FOR BREAKDOWN VOLTAGE (FOR AIR FILLED GAP AT 20°C FOR PLANE PARALLEL ELECTRODE) [16]

e.m.f. The energy stored in the inductance is released through this spark [3].

In an ECD cell, hydrogen gas is liberated in the form of bubbles at the cathode, due to electrochemical reaction. The contact area between the electrode and the electrolyte constricts due to the bubble nucleation on the electrode surface. Constriction of the current due to the bubble formation causes non-uniformity in the current path. The bubble generally grow in size and after attaining a critical size, they detach from the electrode surface. Nucleation site density of H_2 bubble increases with the applied voltage (i.e.with the current density) to the cell. When the nucleation site density of H_2 becomes sufficiently high, substantial constriction of the current path takes place at the interface resulting in increased resistance. The ohmic heating of the electrolyte also becomes significant. This causes the onset of vapour bubble nucleation on the electrode surface in addition to the hydrogen bubbles. Beyond this stage the number of combined nucleation sites increases very rapidly with the voltage. As the nucleation site density reaches a critical value, vapour blanketing of the electrode occurs. At this stage the points of contact between the electrolyte and the tool electrode, known as bubble bridge, blows of instantly due to intense heating. Consequently, the current through the circuit drops in a very short time span, which is analogous to the switching off in an electrical circuit. Discharge takes place along the location of the bubble bridge. The bubble dislodge from the electrode surface due to bridge blowing off and the contact between the electrode and the electrolyte is re-established. This cycle repeats continuously [3].

1.5 Ceramic Material

Ceramic materials are assuming increasing industrial importance in the machine building and apparatus engineering fields, mainly owing to the way in which technological limitations can be overcome by the use of these non-metallic materials.

The name ceramic applies to a wide variety of materials including glasses, single crystals and polycrystalline ceramics.

We are more concerned of the engineering ceramics, also referred to as high performance ceramics, belong to the group of oxide and non-oxide ceramics.

Important representatives of the oxide ceramic group are aluminum oxide (Al_2O_3) also known as corundum, followed by zirconium oxide (ZrO_2) and titanium oxide (TiO_2).

Silicon nitride and silicon carbide are the most important members of the group of non-oxide ceramics.

Ceramics, compared with metals, have peculiar characteristics—excellent high temperature resistance but excessive brittleness too. It should be emphasized that virtually no metals can be used at temperature over $1100^\circ C$ without cooling. The ceramics are the sole practical materials to be used as structural components. The other largest advantage of adopting ceramics as structural components is their resistance to fatigue at high temperature and highly corrosion resistance at high temperature.

Ceramic materials are employed on account of their special thermodynamic and mechanical properties, and their light weight characteristics. High flexural strength in conjunction with low density, extreme hardness and hence great brittleness, accompanied

11

by a certain degree of chemical resistance and great mechanical strength even at high temperature, are the predominant features of ceramics[10].

1.5.1 Piezoelectric ceramics

The Lead Zirconate Titanate ceramic, $Pb(ZrTi)O_3$, commonly known as PZT, has vast application primarily because of its piezoelectric property.

Piezoelectric ceramics can serve as transducers between electrical and mechanical energy. They can compete with all other electromechanical transducers. To be transduced, piezoelectric energy must be applied as elastic energy. Elastic energy storage may involve high stresses, limited only by mechanical strength, but invariably the relative deformations are small, rarely exceeding one part in 1000 [7].

The piezoelectric ceramics has wide applications in different fields such as, phonograph pickups, air transducers eg. hearing aid, tuned ultrasonic microphones in remote control of television sets, under water sound detection and many more. PZT ceramics have become the dominant material for piezoelectric accelerometers.

1.6 Machining of ceramics

The investigation about high performance ceramics has advanced mainly in the process of fabricating higher strength, highly corrosion resistance and temperature resistance materials.

However, at the present time, in the steps of practical application of these materials for structural parts, the development

of utilization technology becomes more essential. Especially, the machining technology of the ceramics will be very important among them.

The problems in machining technology for high performance ceramics are to realize lower cost, higher accuracy and higher efficiency at the same time. These problems are really common to all usual materials. But ceramics are typically brittle materials and the strength is decided by the existence of defects. The surface flaw formed during machining, influence the strength of a machined part. Thus, the reliability of the machined part depends on the machining process, considerably. This point is the most important one particularly in ceramic machining. But the requirement of high efficiency and reliability are contrary to each other. Therefore, at first, most suitable machining conditions for the individual requirements must be searched experimentally, and then optimum conditions for both requirement should be evolved and employed.

1.7 Literature survey

The grinding process by a diamond wheel is the most widely used machining method for high performance ceramics. However the low accuracy and efficiency and large wheel wear are its major drawbacks. During grinding of ceramics the normal forces are unusually high, compared with the tangential ones. This ratio may be as high as ten to twenty for silicon nitride. This high normal force gives rise to elastic deformation of the structural parts of the grinding machine, leading to inefficient cut of the specimen. This results in low machining efficiency and also low finishing accuracy

[6,9].

Some newly developed ceramics, such as ZrB_2, reaction bonded silicon carbide (RB-SiC) and SiC fiber reinforced Si_3N_4 are electro-conductive which can be machined using EDM regardless of their hardness, strength and brittleness. But the non-conducting ceramics still remainsunmachined because of the limitation of this process [6,10,15 & 17]. Comparing with grinding, it is easier to make a complex shaped member with an EDM process.

The typical relationship between the machining conditions, pulse current and pulse duration vs removal rate is shown in Fig.1.6. MRR increases with the increase in pulse current and pulse duration. The surface roughness was increased with increase in pulse current and pulse duration. pulse current had more influence on the surface roughness and pulse duration had more effect in degrading the strength of the material [6,10,15,17].

As laser machining doesn't need mechanical force, it has the advantage of flexibility for the work shape, easy setting up and high machining rate. With an increase in the power of the laser, cutting rate becomes several times more but the machined surface finish becomes poorer. Even at at low cutting rate which gives good surface finish, there is always a possibility of inducing thermal cracks. Thickness of heat affected layer which deteriorates the strength of the machined component was found to be around $70 \mu m$ [6,20].

A comparison of ECDM with USM (ultrasonic machining) has been made by Kumar [21]. ECDM is reported to be having some distinct advantages over USM. The initial investment required for USM would
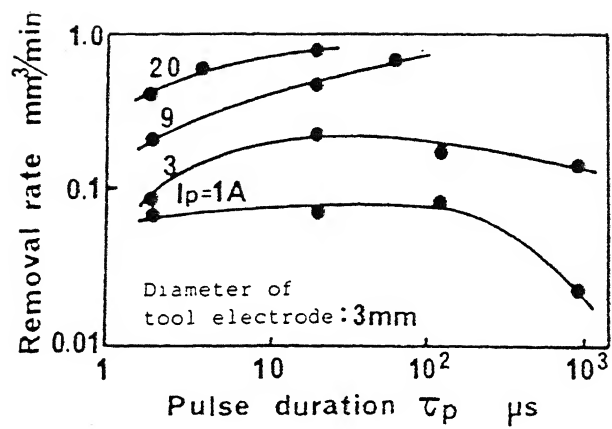
FIG 1.6   EFFECT OF MACHINING CONDITIONS ON MATERIAL REMOVAL
           RATE [6]

be larger than that required for ECDM. The penetration rate of 2mm/min obtained in ECDM is 1.5mm/min faster than obtained in USM (using stainless steel circular tool of 1.6mm diameter). Moreover, the surface roughness of about 0.3 microns obtained with ECDM is also smaller by 0.5 microns obtained with USM (for a glass workpeice).

ECDM has been successfully applied by Tandon [18] and Sreenivasa [19]. Effect of voltage, electrolyte conductivity, fiber volume fraction and tool diameter on MRR (material removal rate), tool wear rate (TWR), relative tool wear and overcut were studied by them.

Tandon [18] reported increase in MRR, TWR and overcut with increase in voltage and electrolyte conductivity, and with decrease in tool diameter. Fiber volume fraction was reported to have no effect on TWR and overcut and slight decrease in MRR with increase in fiber volume fraction.

Sreenivasa [19] reported, increase in MRR, TWR and overcut with increase in voltage, NaOH electrolyte concentration upto 20% beyond which it decreased, primarily because the specific conductance decreases beyond 20% concentration.

Cook, Foot, Jordan and Kalyani [4] have studied the discharge machining of glass. The process is shown to be electrolyte sensitive, and also varies somewhat with polarity. Further, for a given voltage, the rate of machining decreases with time. Machining rate increases both with concentration and temperature of the electrolyte. A pulsed d-c supply was also used to test the effect of high frequency pulse current. It is found that for pulsed power

supply, with pulses in micro-sec range, MRR increases by a factor of two. More striking is the effect of pulsed power (ms or μs) on the surface finish. The surface produced by pulsed power is found to be much smoother than that from a d-c power supply.

A special mention needs to be made about the sparking in ECM. Larsson and Bauxter [11] discussed about the reasons for sparking in ECM. For sparking to occur, metal-to-metal contact does not seem to be necessary. The onset of sparking coincides with the formation of large bubbles. Such bubbles blanket a much larger area of the electrode than the more spherical bubbles. The sparking between the electrode and the electrolyte was seen when two wire electrode were held just touching onto the surface of static electrolyte with a voltage of 100 volts. Potential gradient is probably more important than the potential difference. In an ECM cell, if the cathode becomes covered with a layer of thin, large area bubbles, the current will be conducted by the streamers of the electrolyte between the bubbles thus causing a high potential gradient.

According to Loutrel and Cook [12], fields in the order of 10^6V/cm are generally required to produce field emission arcs in the dielectrics. For the case of the electrolyte found in ECM, they theorize that arcs always form across voids. If the voltage gradient across the voids exceeds the dielectric strength or breakdown voltage, an arc will occur. Once an arc has initiated, it may either die or grow larger. After an arc has initiated, the heat produced will begin to vaporize the surrounding electrolyte. In extreme machining conditions, the arc will continue to grow, bridging the gap and causing melting of the electrode surface. This is a typical

failure point in ECM.

Loutrel [12] has suggested the following seven mechanisms leading to high voltage gradients in the presence of voids :

(1) electrolytic gas evolution at the electrode surfaces,

(2) depletion layer,

(3) electrode passivation and activation over voltage,

(4) local stagnation of flow,

(5) steam generation and cavitation,

(6) vapour blanketing of the electrode surfaces, and

(7) particles in electrolyte flow.

McGeough and Crichton [13] have reported, from the observation made using high speed photography that both spark and arc discharges are possible in an electrolyte. According to them, on application of a voltage pulse between two electrodes immersed in an electrolyte, three phenomena may occur :

(a) electro-chemical action only (as in normal ECM),

(b) electro-chemical action followed by discharge between one electrode and the electrolyte, and

(c) electro-chemical action followed by discharge between the electrodes.

Cook et.al [4] conducted experiments with ECD for machining glass and other electrically non-conducting materials and identified the applied voltage, tool polarity, electrolyte temperature and concentration as input parameter for determining the MRR. They suggested that the possible mechanism of material removal in ECDM could be due to the thermo-mechanical, chemical, field effect or due to some other unknown effects. Cook et.al did the experiments with

positive tools but Umesh Kumar [2] had concentrated on negative tool. He noticed that the discharge vanished with the flowing electrolyte. The mechanism of material removal suggested by him were thermo-mechanical and electrochemical action.

Allesu [1] conducted experiments of ECDM. Glass wafer of 0.2 mm thickness was cut along the length using razor blade. He suggested , mechanism of material removal depends on thermal heating, cavitation and electrochemical action. He also examined the effect of the electrolyte flow on the discharge voltage and found that the discharge voltage increases with the electrolyte flow velocity. The most useful observation made by him is the distribution of voltage drop in an ECDM (Fig.1.7) and the sources of the resistance (Fig.1.8).

Recently, Indrajit Basak [3] conducted experiments on ECD and ECDM. He laid major stress in determining the critical voltage and critical current to onset a discharge for different given condition and to explore the possibility of enhancing the MRR characteristics of ECDM. The electrolyte and its concentration are the leading factors to determine the critical voltage for discharge initiation. Along with, these two factors the equivalent surface area of the tool electrode determines the critical current. The electrode material has no significant effect on critical voltage or critical current. He suggested that by introducing inductance in the ECD circuit, more than 200% increase in MRR can be achieved. He also suspects that this enhancement of the MRR is achieved at the cost of the surface quality. Therefore, such extra inductance can be employed only for rough machining operations.
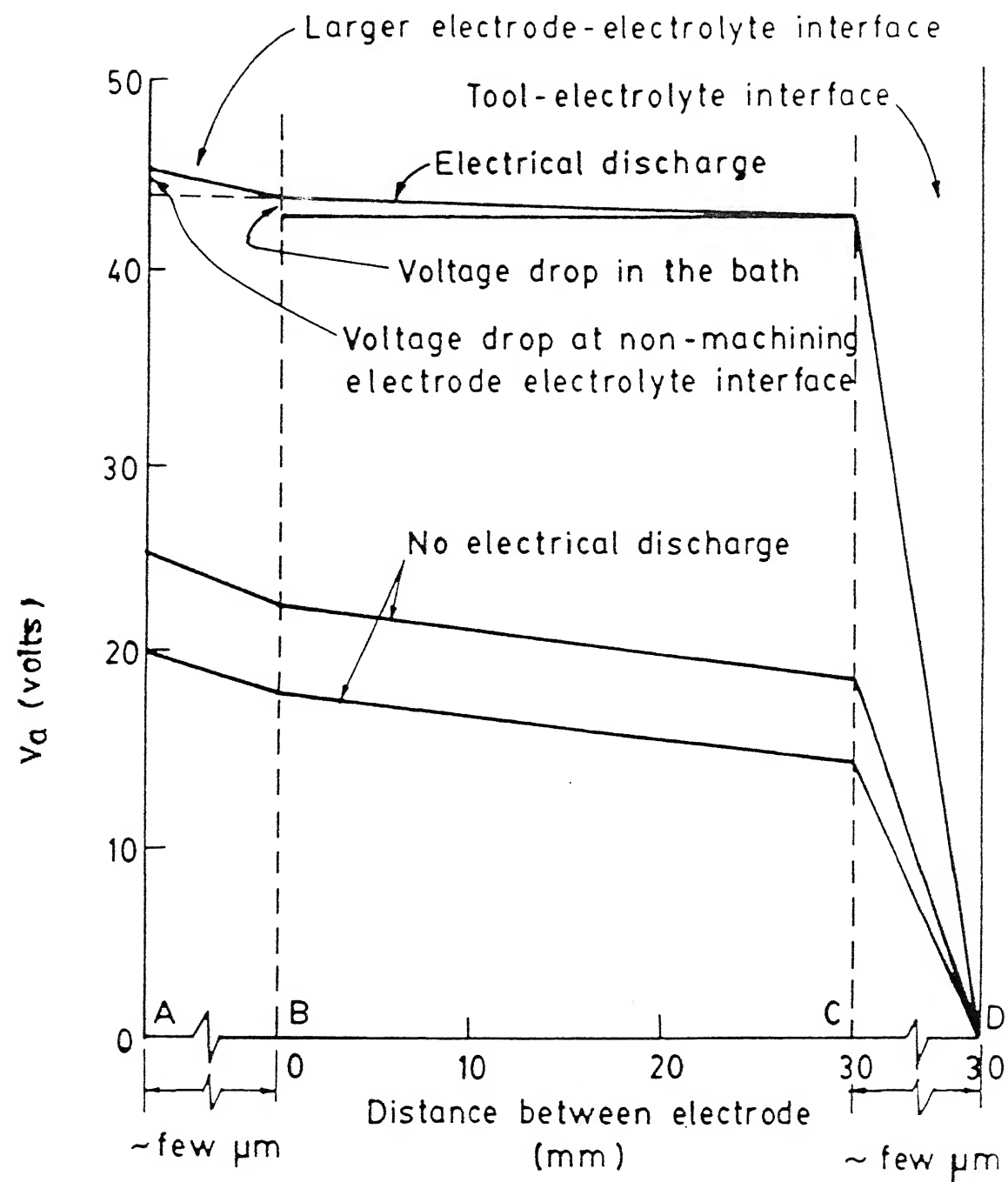
FIG 1.7   DISTRIBUTION OF VOLTAGE DROP IN AN ECDM BAT
[ELECTROLYTE – SODIUM HYDROXIDE (35 %); POWER SUPPLY
D.C.] [1]

20

Power supply unit

AC
main

Tool

R_1

R_2 Non-machining
electrode

R_e
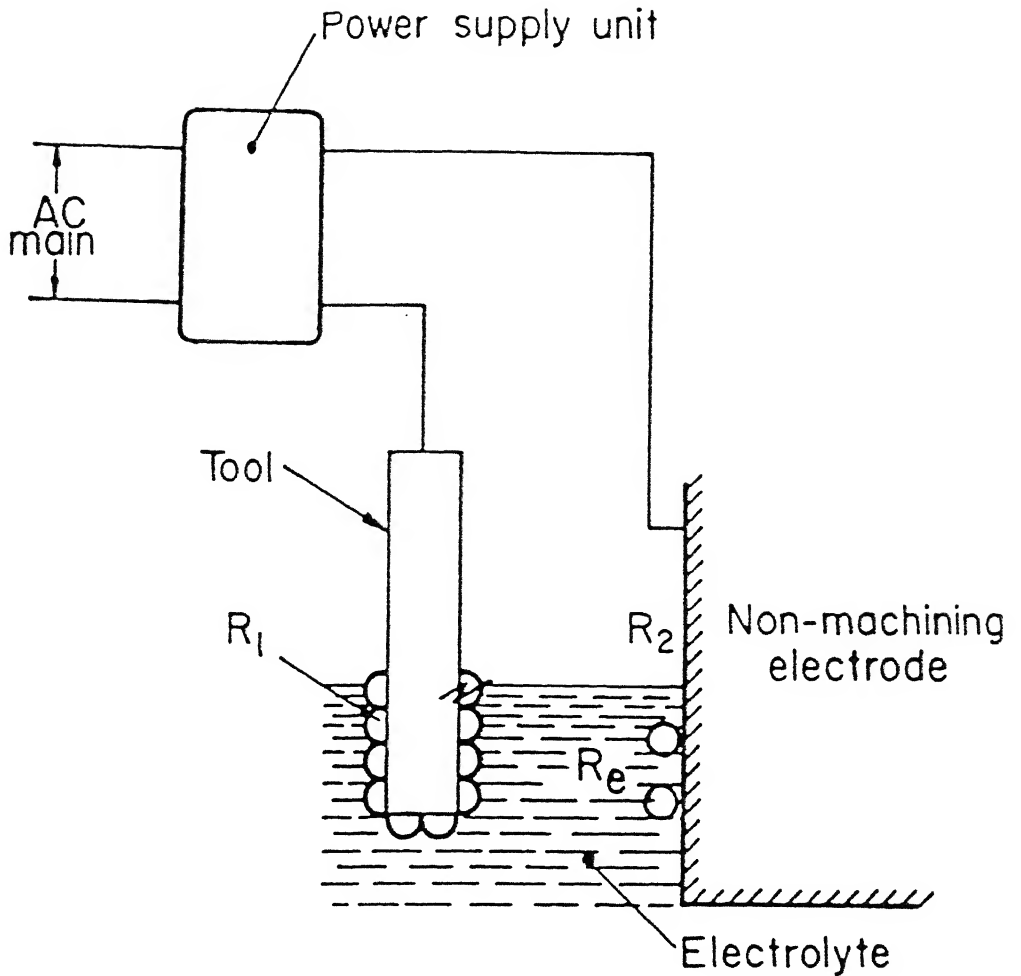
Electrolyte

R_e = Electrolyte path resistance

R_1 = Tool – Electrolyte interface resistance

R_2 = Non-machining electrode – electrolyte
interface resistance

R_1 Fluctuates depending on voltage

FIG 1.8   RESISTANCE   IN   ECD   (NON-CONDUCTOR   MACHINING)
CONFIGURATION [1]

1.8 Objective and Scope of present work

The objective of present work is to fabricate a travelling-wire electro-chemical spark machine (TW-ECSM). The machine should be capable of slicing the specimen. The performance of the machine is to be estimated.

In the second part, the feasibility of ECSM process for the machining of partially electrically conductive materials like piezoelectric ceramics, carbon fiber epoxy composite etc. is to be established. In piezoelectric ceramics, emphasis is made on Lead Zirconate Titanate (PZT).

The parameters (supply voltage and electrolyte concentration) and responses (material removal rate and average diametral overcut) are to be evaluated.

DESIGN OF THE TRAVELLING WIRE ELECTRO-CHEMICAL SPARK MACHINE

2.1 Introduction to the machine

The Travelling Wire Electro Chemical Spark Machining (TW-ECSM) machine has been deigned keeping in view the fundamental mechanism of the process and the basic requirements. The complete schematic drawing of the machine is shown in Fig. 2.1.

The TW-ECSM machine can be primarily divided into four distinct parts :

1. The workpiece holder, workpiece depth control mechanism and feed mechanism to the workpiece.

2. The wire drive mechanism and the electrode fixture.

3. Electrolytic tank.

4. Power supply.

2.2 Specification and Constraints on the TW-ECSM Machine

The following points have been considered in designing the TW-ECSM machine.

(i) Force exerted by the workpiece on the wire is negligible. It is assumed that there is no physical contact between the two

(ii) Maximum weight of the workpiece, W_o < 800 g

(iii) Vertical adjustment range of the workpiece of 25 mm

(iv) Fine adjustment of the workpiece to control its depth inside the electrolyte

1. STEPPER MOTOR
2. BALL SCREW AND SLIDE
3. TAKE-UP SPOOL
4. FEED SPOOL
5. SLIDE BLOCK
6. SLIDING MECHANISM FOR
   WIRE FEED DEVICE
7. PULLEYS
8. JOINT ROD
9. WORKPIECE HOLDER
10. GRAPHITE ANODE
11. ELECTROLYTIC TANK
12. POWER SUPPLY
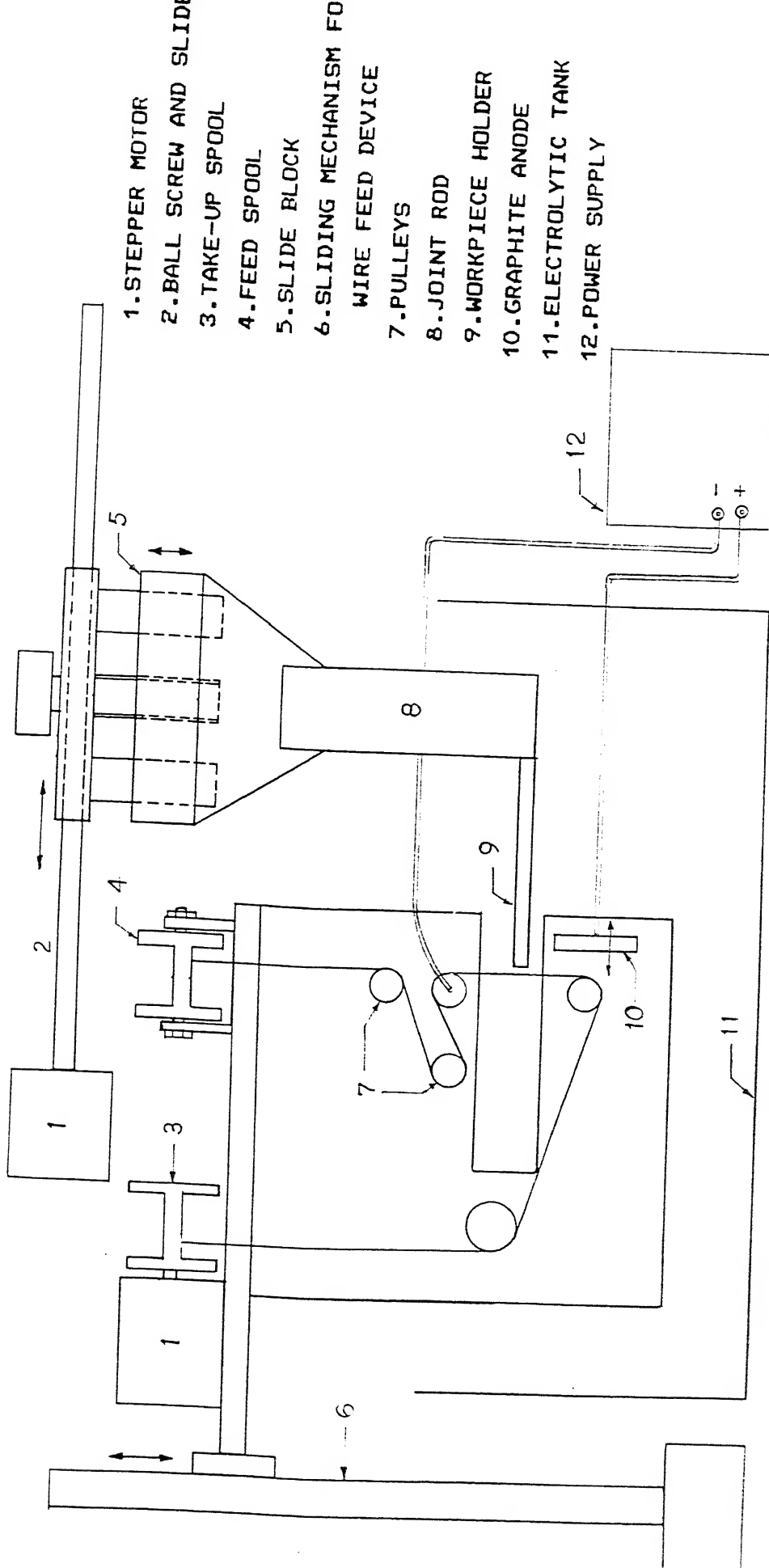
FIG 2.1   SCHEMATIC DIAGRAM OF TRAVELLING WIRE ELECTRO CHEMICAL
SPARK MACHINE (TW-ECSM)

(v) The workpiece surface must remain horizontal.

(vi) The cutting wire should not break frequently.

2.3 Design of the Machine

The machine has been designed by breaking the whole machine into four distinct sub-assemblies. Each sub-assembly has been further subdivided into smaller units for ease of fabrication and proper functioning of the unit.

2.3.1 Workpiece Holder, Depth Control Mechanism and Feed Mechanism

The workpiece holding device is to hold the workpiece rigidly during the cutting process.

The workpiece holder is assembled with depth control mechanism. A vertical adjustment range of 25 mm can be made to control the depth of the workpiece in the electrolyte. The workpiece holder is made of plexiglass to have its low weight and to avoid conducting material inside the electrolyte. Fig.2.2 shows the sub-assembly of the workpiece holder, depth control mechanism and feed mechanism.

The machine is designed to provide only linear sliding motion of the workpiece. The feed is given to the workpiece for which very low friction, rolled ball screw is used. A stepper motor is coupled to the ball screw to provide a very small and accurate movement to the workpiece. The T-block (ref. appendix A) to which nut of the ball screw is mounted is supported on a low friction linear motion (LM) slide. The details of the components can be viewed in Appendix A.

1. BALL SCREW AND SLIDE
2. SLIDE BLOCK
3. JOINT PLATE
4. GUIDE ROD
5. LIFT SCREW
6. HANG ROD
7. WORKPIECE HOLDER

FIG 2.2   WORKPIECE HOLDER, DEPTH CONTROL AND FEED CONTROL MECHANISM

2.3.2 The Wire Drive Mechanism and Anode Fixture

A metallic wire, working as the cathode, traverses from a feed spool through a set of pulleys to a take-up spool (Fig.2.3). A stepper motor drives the take-up spool to pull the wire gently at a constant speed. An anode of graphite is attached to the pulley mount and can be adjusted to maintain its distance from the cathode (wire). Also, this whole mechanism can be moved up by a sliding mechanism so as to clear the space for mounting a new workpiece or threading a new cutting wire through the pulleys. The details of the components are shown in Appendix B.

2.3.3 Electrolytic Tank

A tank made of plexiglass walls holds the electrolyte, of size 300×100×80mm. The tank being of plexiglass, cross-conduction does not affect the ECSM process. The tank is shown in Fig. 2.1.

2.3.4 Power Supply

A smooth rectified DC is supplied to the electrode. The connection of the supply at the anode and the pulley on which the wire slides, is shown in Fig 2.1.

The basic parameters selected for the power supply were

Voltage = 100 Volts (Max.)

Current = 25 Amps

Fig. 2.4 shows the schematic connection for smooth rectified output. A diode bridge (diode specification 2SM70) is used for rectification of A.C. and a bank of capacitors of capacitance 1980 μF and 400 Volts is used for filtering the ripples.

1. STEPPER MOTOR
2. TAKE-UP SPOOL
3. FEED SPOOL
4. SLIDING MECHANISM
5. PULLEY MOUNT
6. PULLEYS
7. GRAPHITE ANODE
8. WORKPIECE HOLDER
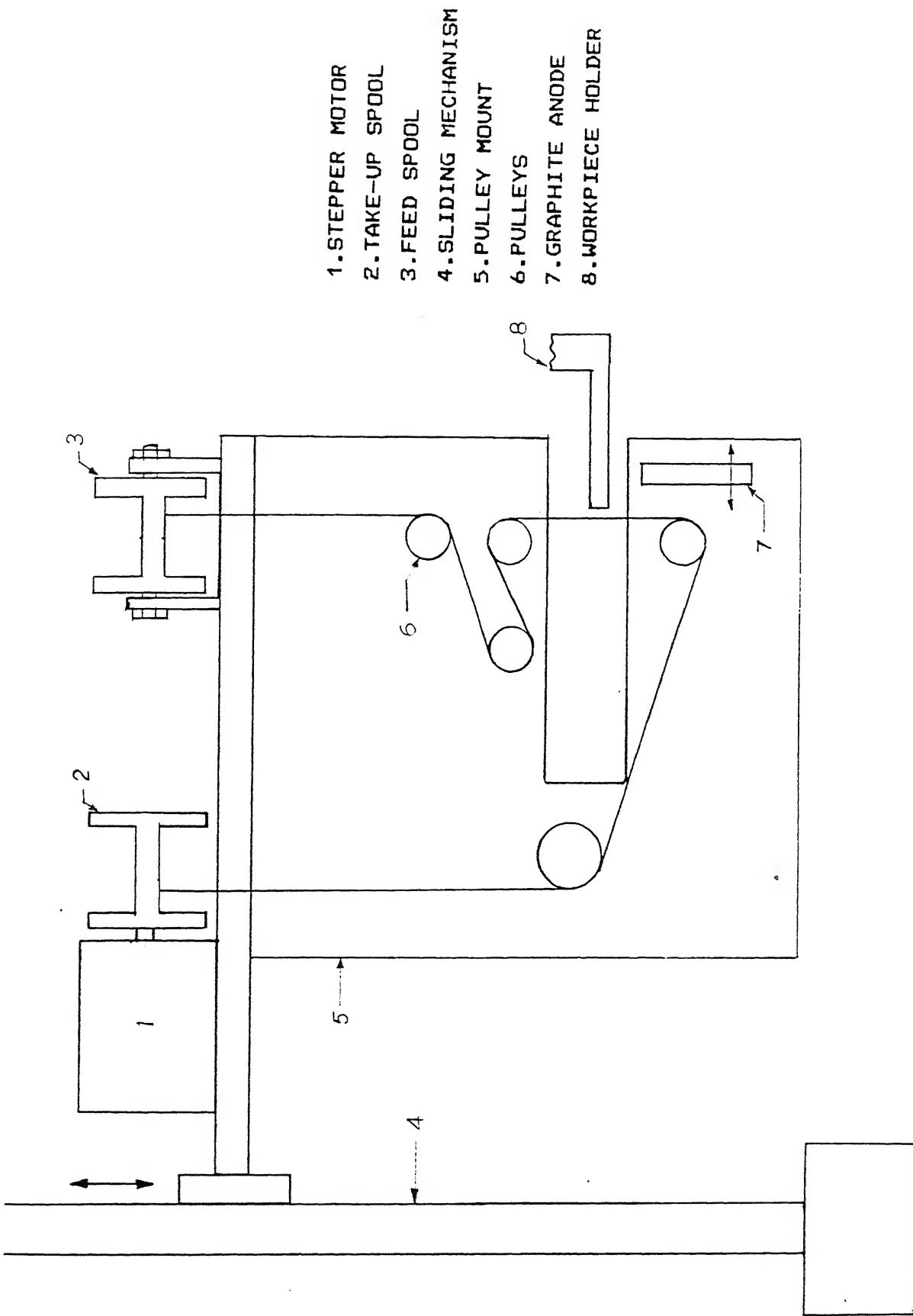
FIG 2.3   SCHEMATIC DIAGRAM SHOWING THE WIRE FEED MECHANISM

220 V AC

VARIAC

TRANSFORMER

DIODE BRIDGE

CAPACITOR BANK
2000 μF

DC OUTPUT

TO GRAPHITE ANODE

TO WIRE CATHODE
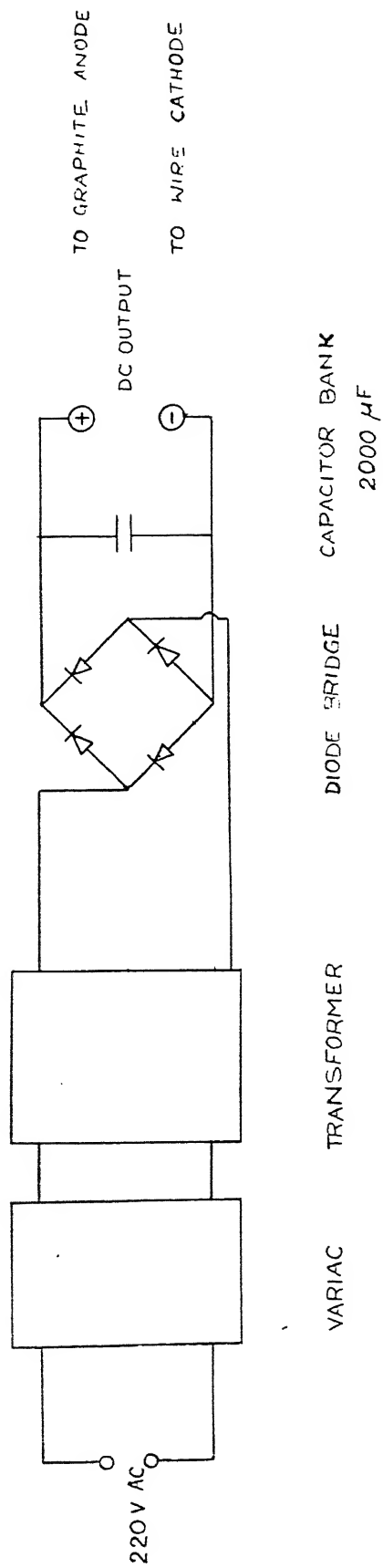
FIG 2.4   POWER SUPPLY FOR ECSM SET-UP

2.4 Working of the Machine

The whole ECD machine can be viewed in the plan and elevation drawing, shown in Fig.2.5(a) & 2.5(b)respectively. The support T-block is screw tightened to both the rolled ball screw and the LM-slide. The ball screw is coupled to the stepper motor with the help of a coupler. The rotation of the motor shaft now causes the support T-block to slide along the LM-guide in a horizontal plane. The support T-block is assembled with the depth control mechanism and workpiece holder on which the sample is mounted. By adjusting the speed of rotation of the motor we can adjust the feed of the workpiece.

The wire as the cathode, is driven with the help of a stepper motor. The speed of the wire can be adjusted by controlling the rotation of the motor.

The smooth rectified DC is supplied to the electrodes through a connection on the anode(graphite) and the copper pulley to the wire cathode.

PLAN

FIG 2.5(a)   TRAVELLING WIRE ELECTRO CHEMICAL SPARK MACHINE SET-UP
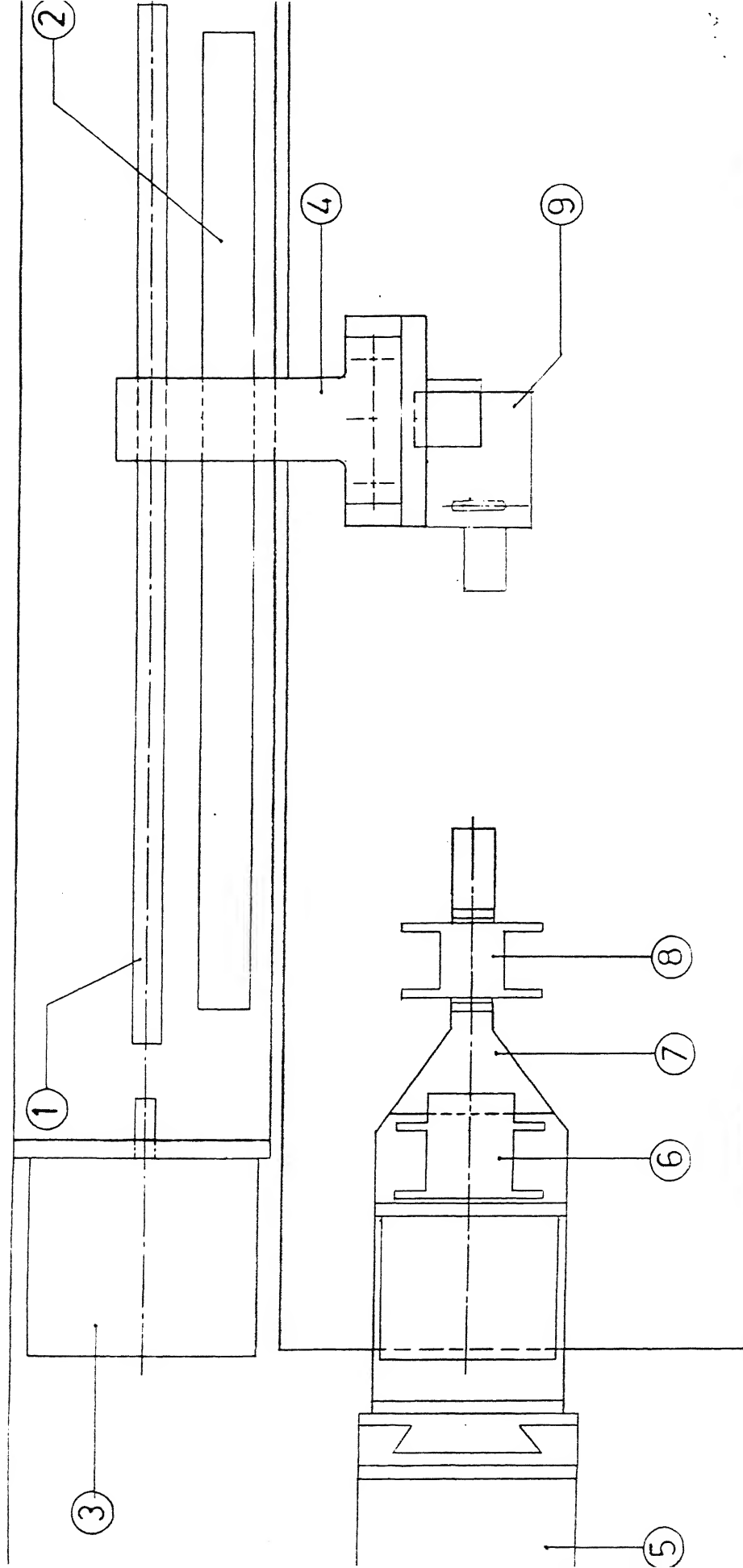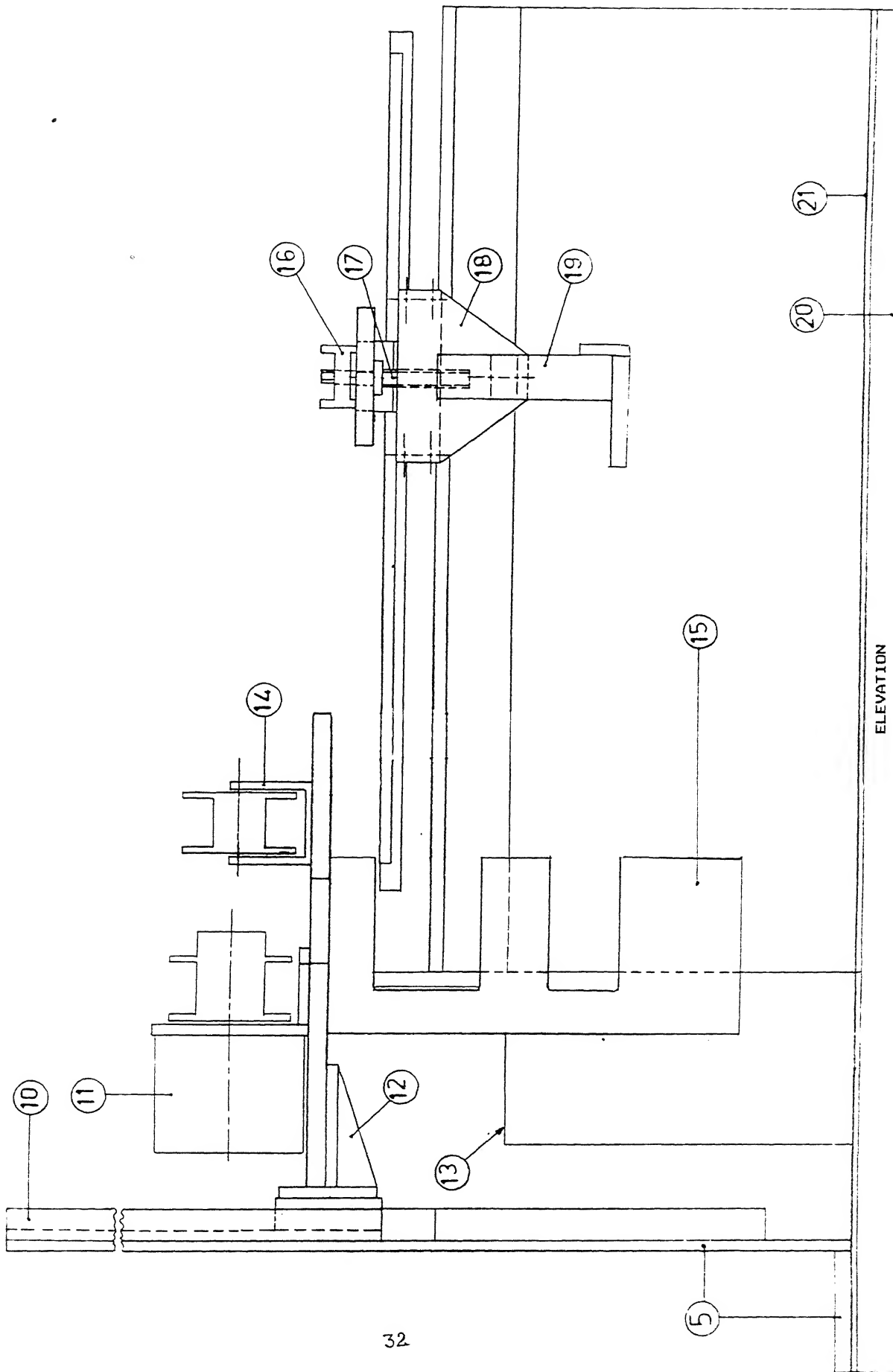
FIG 2.5(b)   TRAVELLING WIRE ELECTRO CHEMICAL SPARK MACHINE SET-UP

ELEVATION

32

Part no.	Description
1	ROLLED BALL SCREW
2	LINEAR MOTION SLIDE
3	BALL SCREW DRIVE MOTOR
4	SUPPORT T-BLOCK
5	SLIDING MECHANISM SUPPORT
6	TAKE UP-SPOOL
7	WIRE BASE
8	FEED SPOOL
9	WORKPIECE HOLDING DEVICE
10	DOVETAIL SLIDE
11	WIRE DRIVE MOTOR
12	WIRE BASE SUPPORT
13	ELECTROLYTE TANK
14	SPOOL BRACKET
15	PULLEY MOUNT
16	LIFT SCREW NUT
17	LIFT SCREW
18	JOINT PLATE
19	HANG ROD
20	MAIN STRUCTURE
21	BASE PLATE

FIG 2.5   ELECTRO CHEMICAL DISCHARGE MACHINE

CHAPTER 3

EXPERIMENTATION

3.1 Experimental Set-Up

Already available limited results of the previous investigators [18, 19, 21] formed the starting point and provided the guidelines for the experimentation in the present work.

The power was taken from A.C. mains through a variac, step-down transformer, bridge rectifier and capacitor bank. The output was smooth rectified D.C.

In all the experiments, the nonmachining electrode (i.e. anode) was the graphite plate (50×25×5mm) and positioned approximately 6 mm away from wire (cathode).

The potential was applied across the fixed copper pulley (cathode) on which the wire slides, and the graphite plate (anode).

An oscilloscope was connected in parallel to the D.C. power output for observing the voltage waveform. A digital voltmeter was also connected in parallel to record the supply voltage.

A conductivity meter is used to record the specific conductance of the electrolyte and a thermometer to measure the temperature. The initial conductivity of the electrolyte at the start of each experiment of a given concentration was kept in the range of ± 10 % of the fresh solution.

The feed was given to the workpiece, mounted on the ball screw and the LM-slide, with the help of stepper motor coupled with the ball screw. The stepper motor was controlled using the uni-step motor controller. The minimum feed which could be achieved by the

present controller was 0.009 mm/s. This was larger than the cutting rate observed during the experimentation. So the feed was controlled manually to avoid the arcing for a longer period.

The brass wire of 0.5mm diameter was selected as tool (cathode). We could not go for lower diameters as it was not readily available. The wire is driven with the help of the stepper motor and its controller. The speed of wire within an experiment was kept constant. However it was changed from one experiment to another depending upon the frequency of wire breakage (which was a function of voltage and concentration).

The change in voltage waveform (sharp and random peaks) indicated the onset of a spark. This minimum voltage required for initiating the spark is known as the discharge voltage.

The workpiece machined is a piezoelectric ceramic, Lead Zirconate Titanate (PZT), in the form of circular disc pellets of diameter 11 mm and thickness of 2-3 mm. The workpiece was immersed in the electrolyte at the depth of approximately 5mm.

An overall view of the TW-ECSM setup and the associated instruments can be seen in photograph no.3.1. The wire feed device is shown in photograph no.3.2 and workpiece sliding mechanism in photograph no.3.3.

Electrolyte:

The experiments were conducted with sodium hydroxide (NaOH) electrolyte, as it had higher specific conductance compared to sodium chloride (NaCl). The solution of different concentration was prepared by weighing the NaOH pellets on a single pan microbalance (accuracy of 0.00001g). The Table no.3.1 gives the weight of NaOH required for a concentration and the associated normality.
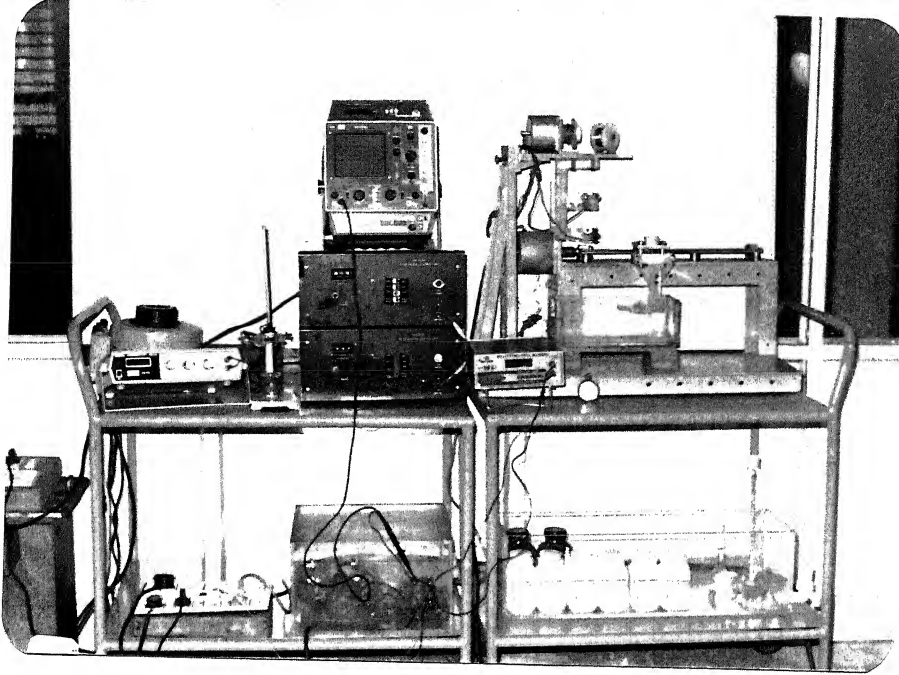
PHOTOGRAPH   NO. 3.1   OVERALL   VIEW   OF   TRAVELLING   WIRE   ELECTRO
CHEMICAL SPARK MACHINE ALONG WITH ASSOCIATED
INSTRUMENTS
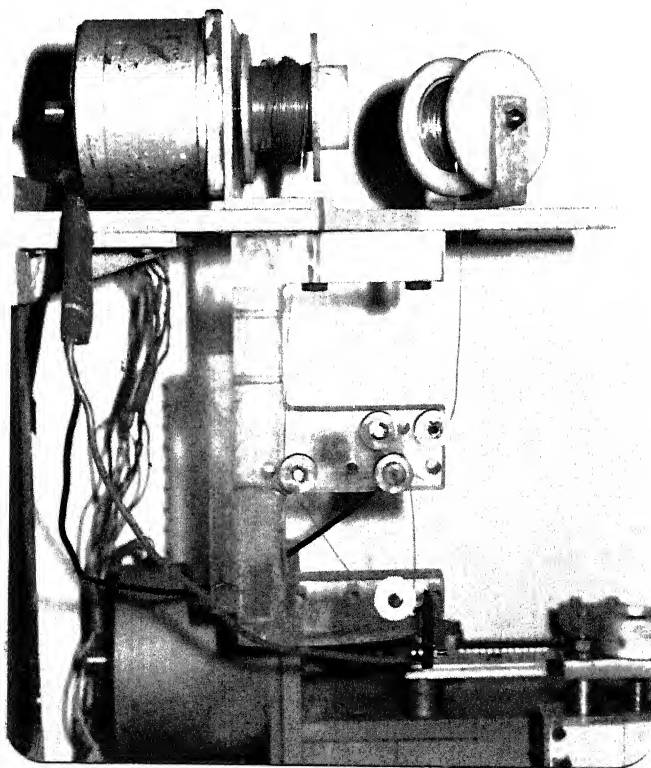
PHOTOGRAPH   NO. 3.2   WIRE FEED DEVICE

35

PHOTOGRAPH NO. 3.3   WORKPIECE SLIDING MECHANISM

SPARK PHOTOGRAPH

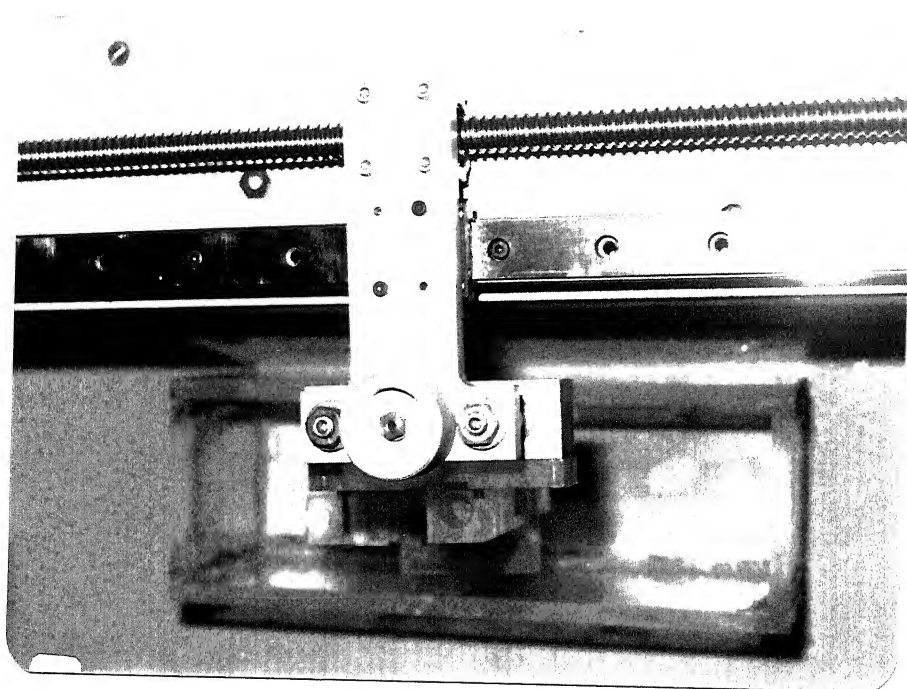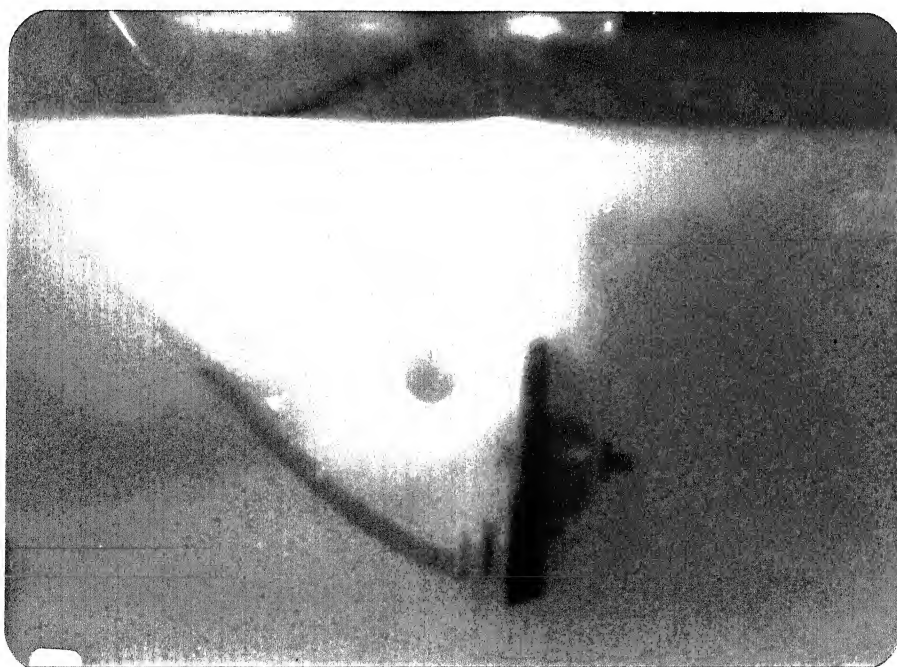The weighing was done upto four places of decimal on electronic alance (accuracy of 0.0001 g).

xing:

Intimate mixing of the powder constituents is necessary to liminate inhomogeneity of the compound and to obtain good operties. This is achieved by taking weighed amounts of PbO, ZrO_2 TiO_2 in a polyethylene jar and milling, using alumina balls in iple distilled water medium. The container is sealed and kept for lling for 5 hours. The slurry is then dried in an oven at 70°C for hours.

lcination:

After mixing, the dried powder is calcined. The purpose of lcination are:

1. To remove water of hydration, carbon-di-oxide from carbonates, and any volatile impurities.

2. To effect thermochemical reaction among the constituent oxides to form the desired solid solution.

3. As a consequence of reaction, to have reduced volume shrinkage in the final firing.

Ideally the temperature of calcination is chosen high enough to use complete reaction, but low enough to permit easy grinding [7].

In our study the dried powder was taken in a pure alumina icible, properly covered as shown in Fig.3.1 and were then cined at 960°C for 2 hours.

TABLE 3.1

Concentration (weight %)	Normality	Weight of NaOH (g/lit)
8	2N	80
15	3.75N	150
20	5N	200
25	6.25N	250
30	7.5N	300

The specific conductance of NaOH solution at various temperature and concentration [5] is shown in appendix F.

3.2 Sample Preparation

Lead Zirconate Titanate, a piezoelectric ceramic, having a composition given by $Pb(Zr_{0.535}Ti_{0.465})O_3$ was selected. This composition corresponds to the morphotropic phase boundary and yields the highest piezoelectric properties.

Material Composition:

The details of the chemicals used are given in Table no.3.2.

Table 3.2

Chemical	PbO	ZrO_2	TiO_2
Purity	98%	99.5%	98%
Molal ratio	1	0.535	0.465
Weight (g)	55.7975	16.4718	9.2860
Manufacturer	Loba Chemie, Bombay	Indian Rare Earth, Kerala	Sarabhai M Chemicals, Baroda

Atmosphere powder

Platinum crucible

Recrystallised
alumina crucible
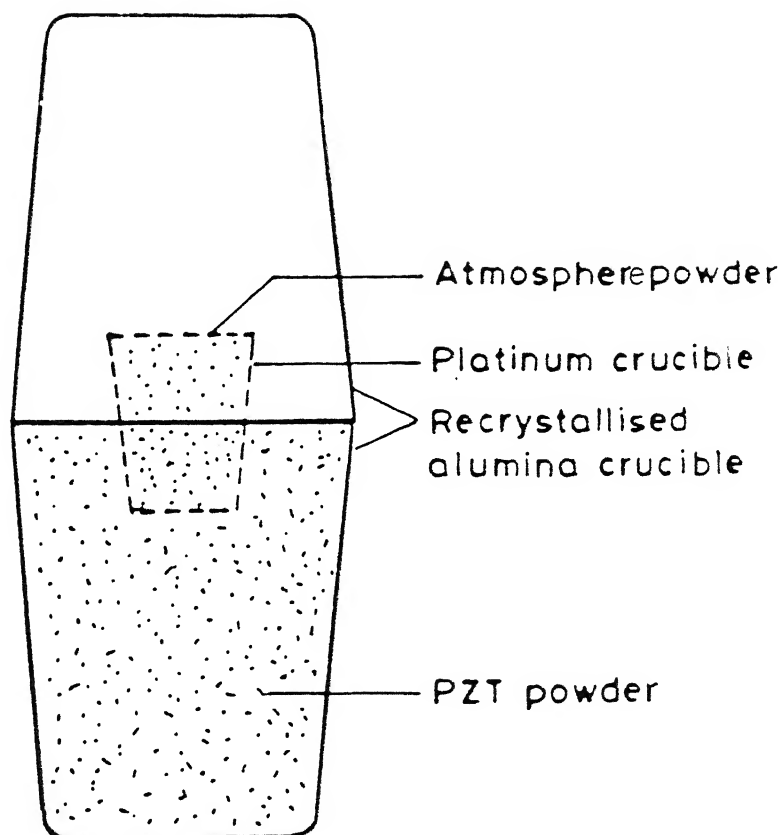
PZT powder

FIG 3.1   SCHEMATIC DIAGRAM OF CRUCIBLE ARRANGEMENT DURING
CALCINATION

Grinding and Sieving:

Grinding prepares the reacted material for ceramic forming and also helps to homogenize the compositional variations that may still exist. The powder was crushed in a mortar pestle and passed through 100 mesh screen.

Pelletization:

The powder is mixed thoroughly with 2% poly vinyl alcohol (PVA) solution in water, which acts as binder, and kept in oven at 70°C for 15 hours.

The dry powder (mixed with PVA) is compressed in a hydraulic press to form pellets of required size and shape using a die. The pellets are pressed in a 12mm diameter die at 550 MPa for 2 min.

Sintering:

Lead zirconate titanate bodies typically mature in the 1200°-1300°C range. These ceramics are subject to loss of PbO which can be prevented by including atmosphere powder in the refractory enclosure in which the pellets are sintered. The atmosphere powder is a mixture of Lead Zirconate, $PbZrO_3$ (also known as PZ) and 10wt % PbO.

The sintering was done in two steps, first at 600°C for 2 hours to remove the PVA binder and the second at 1200°C for 2 hours.

The configuration of the crucible arrangement during sintering is shown in Fig.3.2.

Alumina crucible

Al_2O_3 powder packing

Recrystallised alumina
crucible

Sample

Alumina sheet

Platinum disc

Atmosphere powder
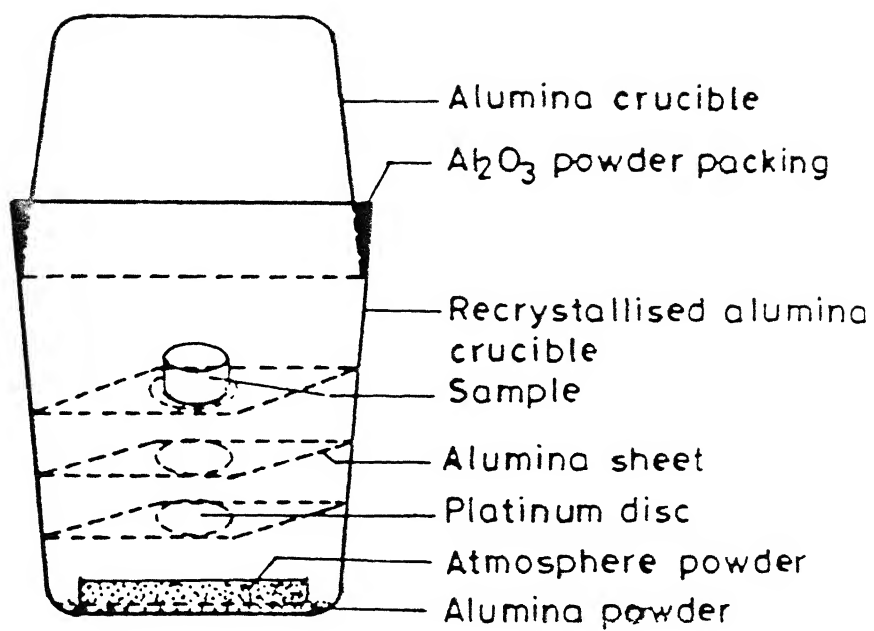
Alumina powder

FIG 3.2   SCHEMATIC DIAGRAM OF CRUCIBLE ARRANGEMENT DURING
SINTERING

3.3 Machining Experiments

Supply voltage and concentration of the electrolyte were considered as controllable parameters and their effects on material removal rate (MRR) and average diametrical overcut were studied as responses of the process.

The aqueous solution of NaOH was prepared and kept for sufficient time to dissipate the heat of reaction (as exothermic reaction takes place) and cool down the solution to room temperature. The specific conductance and the temperature of the electrolyte was recorded before the start of each experiment. After each experiment the solution was cooled down to the room temperature and filtered to remove the sludge formed during the experiment. The conductivity variation of the electrolyte was kept within the range of ± 10 % compared to the value of fresh electrolyte at room temperature. In case the value was more than ± 10 %, fresh electrolyte was prepared and used. Appendix E gives the procedure for measuring electrolyte conductivity.

The machining time was kept quite low (2-15 min) to avoid the dynamic changes occurring during the process in the electrolyte. A fan was used continuously to dissipate the heat generated during the machining process. In a set of experiments of same concentration and varying supply voltage the machining time was kept constant unless some problem arises during the cutting process, like, heavy arcing for long period or wire breakage due to arcing, rust or twist in the wire.

After machining, the workpiece was cleaned, dried to evaporate the water remaining on the surface and reweighed, with the help of a microbalance (accuracy of 0.00001g).

The amount by which the width of the machined slot exceeds the wire diameter, known as the *Diametral Overcut* (shown in Fig.3.3), was measured at a magnification of ×10, with the help of a shadowgraph. The wire diameter was also measured on the shadowgraph.

Wire speed was estimated from the product of the circumferential diameter of the spool and the rate of revolution. As the wire keeps on accumulating at the same point, the effective circumference of the of the wire increases with time, consequently the speed of the wire is not constant ($V=\omega R$). So after each experiment the wire is unwound from the take-up spool to reduce the speed error.

The responses thus obtained are plotted using grapher package to analyze the effect of supply voltage & concentration of the electrolyte on the MRR and overcut. Here, the author would like to emphasize about MRR in wire cutting machines like wire-EDM and wire-ECSM. In these machines, the performance of the machine and efficiency of the process is usually evaluated by Material Removal Rate (length, area) instead of MRR (gram or volume).

The current could not be recorded because of unavailability of high amperage ammeter (20-25A D.C.).

Few simple preliminary experiments were conducted to check the results obtained by the previous investigators. The following variations were studied through the set of experiments:

1. The variation of current with the length of the wire (cathode) immersed in the electrolyte.

2. Effect of gap between cathode and anode on current and voltage.
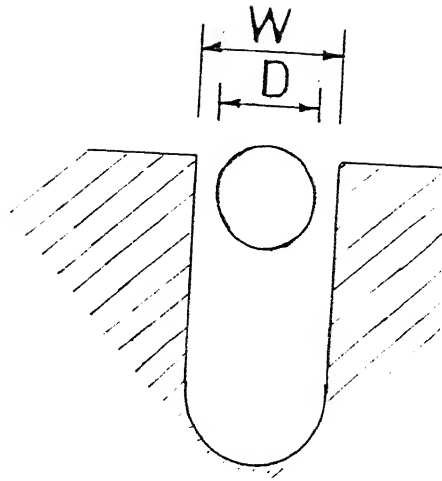
W = WIDTH OF CUT

D = DIAMETER OF WIRE

DIAMETRAL OVERCUT = W-D

RADIAL OVERCUT = (W - D) / 2

FIG 3.3   DIAMETRAL OVERCUT

Surface Analysis :

The machined surface characteristics were analyzed on the Scanning Electron Microscope(SEM). The properties studied from machining point of view were surface cracks & resolidified layer.

CHAPTER 4

RESULTS AND DISCUSSIONS

4.1 Mechanism of ECSM process

The mechanism of ECSM process is still not very clear. As already discussed in section 1.4, the sparking takes place across the tool electrolyte interface probably because of high potential gradient developed across the hydrogen gas bubble evolved at the cathode as a result of electrolytic action. It is observed that the reaction accelerates with the concentration of the electrolyte and consequently the minimum voltage for discharge onset (known as *Discharge Voltage* V_d) decreases with the increase in concentration up to 20 wt% and then remains constant up to 30% of concentration (as beyond 30% conc. experiments were not conducted). This is probably because a minimum potential gradient is required for the break-down of hydrogen gas bubble in the form of a spark. With an increase in the concentration of the electrolyte, the conductivity of the electrolyte increases, reducing the path resistance; hence the supply voltage required for discharge reduces.

The discharge results in the generation of heat in a very small localized area. Machining takes place, because the workpiece is in contact with the tool where the spark is occurring. The various possible mechanisms by which the material may be removed are:

1. Melting and vaporization of the work-material,

2. Electrochemical action and

3. Mechanical erosion.

Due to sparking, large amount of localized heat is evolved at the tool-workpiece interface, which melts and evaporates the work material.

PZT being partially conducting electrochemical action might have played a role in material removal. During the cutting process, the temperature, in the vicinity of the PZT cut surface, is very high. So there might be electrochemical reactions causing material to be removal. Though detailed examination of this has not been done.

The mechanical erosion may occur due to cavitation effect of the gas bubbles. The discharge is a result of violent rupture of the hydrogen gas bubble.

Besides this, the workpiece being electrically conductive, arcing occurs at the location where the debris gets entrapped in the cut slot or due to twist and bend in the wire, causing contact of the workpiece (PZT) and the wire. This results in a localized larger removal of the material and larger overcut at certain regions as can be observed in the shadow graphs shown in Fig.4.1(a) and 4.1(b).

4.2 Cutting of PZT Ceramics

The result of travelling wire electrochemical spark machining of PZT ceramic is presented in this section.

The experimental results are plotted, for understanding of effect of supply voltage and electrolyte concentration on MRRg and diametrical overcut. The plot indexes viz. *, +, ×..., are experimental values obtained under different conditions. The machined PZT specimens using ECSM can be seen in the photograph 4.1.
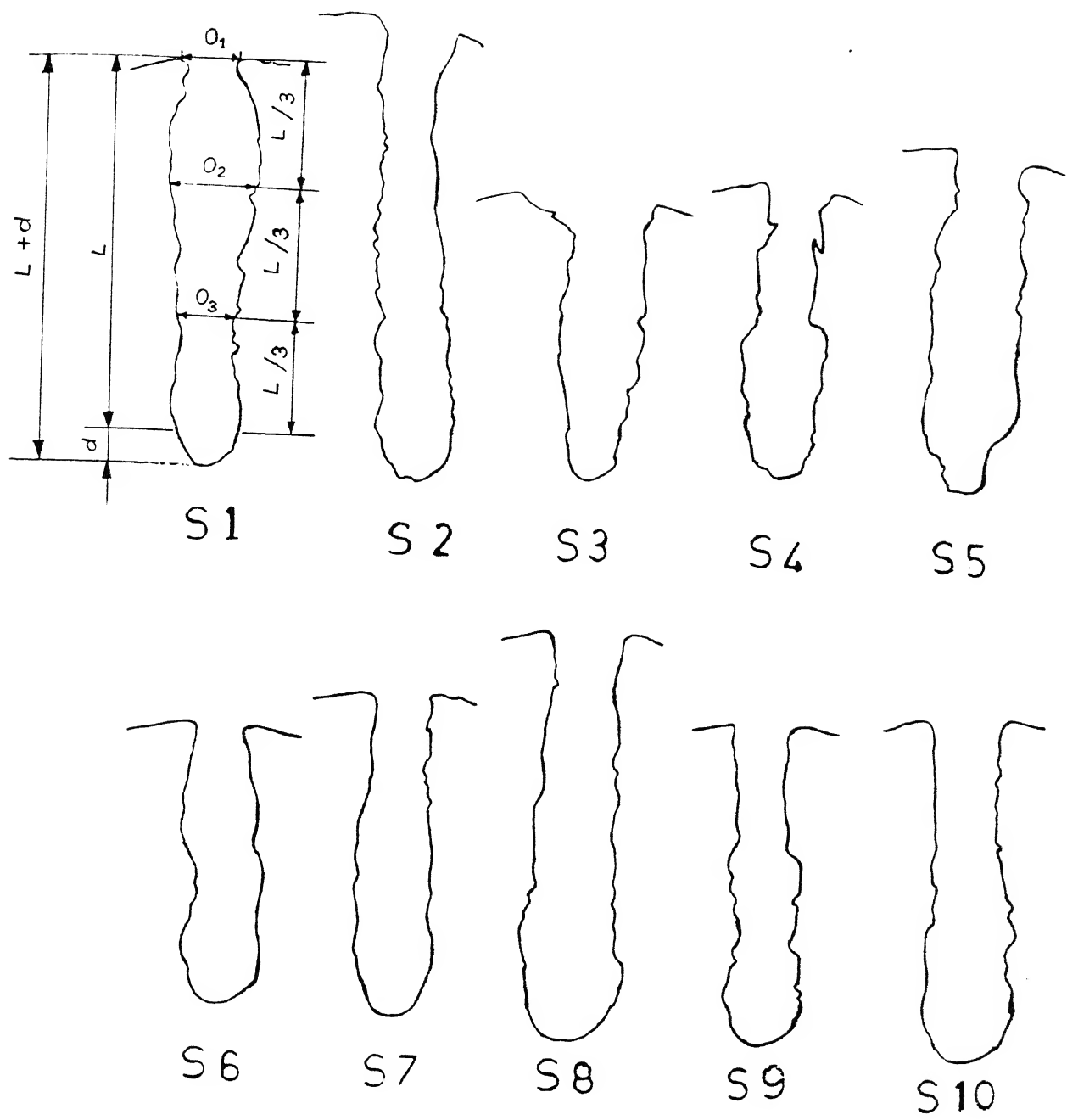
S1   S2   S3   S4   S5

S6   S7   S8   S9   S10

SCALE $\vdash\!\!-\!\!\dashv$ 1mm

4.1(a)   SHADOW GRAPHS SHOWING THE SHAPE OF GROOVE CUT IN PZT CERAMICS USING TW-ECSM PROCESS

S11   S12   S13   S14   S15

S16   S17   S18   S19   S20

S21   S22   S23   S24

SCALE $\vdash\!\!\!\!-\!\!\!\!-\!\!\!\!\dashv$
1 mm
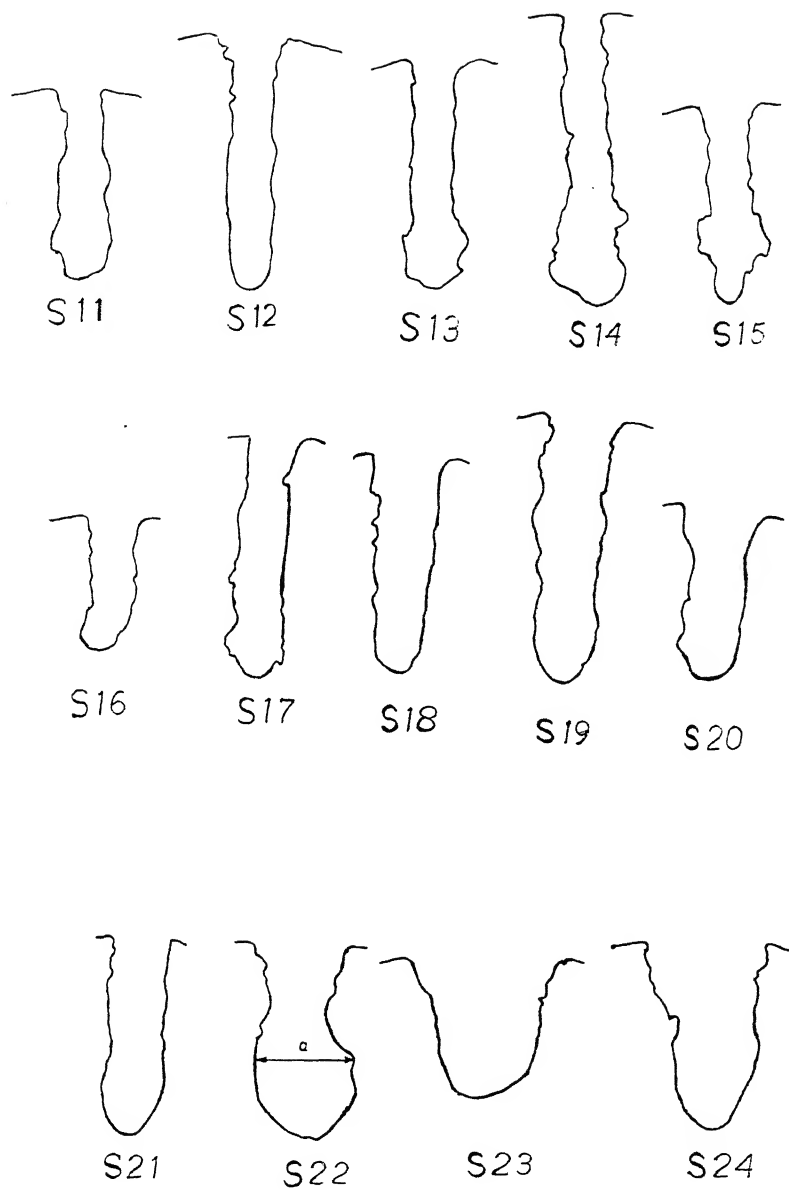
FIG 4.1(b)   SHADOW GRAPHS SHOWING THE SHAPE OF GROOVE CUT IN
                  PZT CERAMICS USING TW—ECSM PROCESS

49

8% CONCENTRATION   15% CONCENTRATION

20% CONCENTRATION   25% CONCENTRATION

30% CONCENTRATION
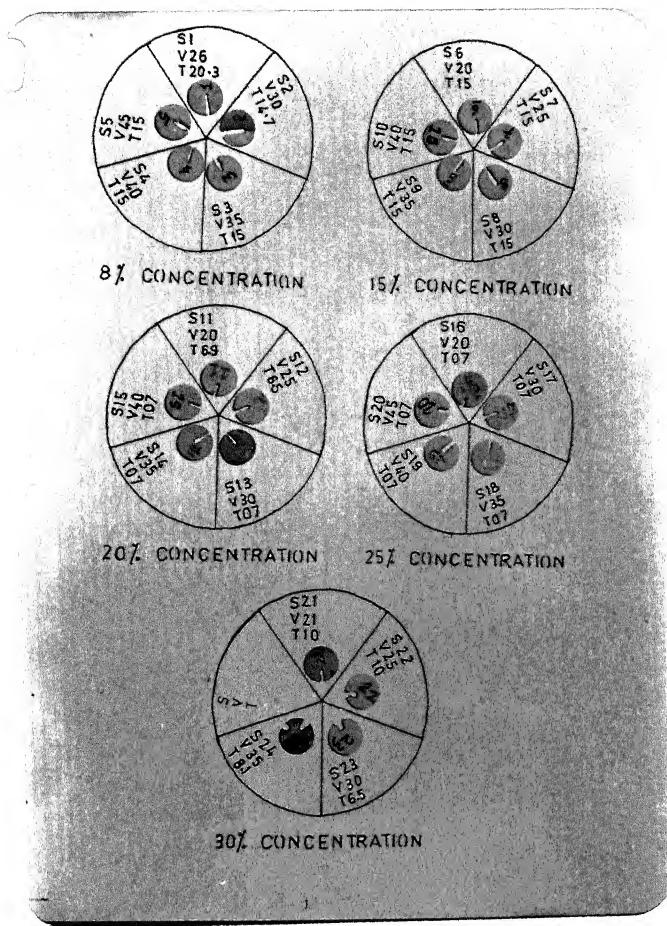
PHOTOGRAPH NO. 4.1   SHOWS THE PZT CERAMICS MACHINED AT DIFFERENT
                          EXPERIMENTAL   CONDITIONS   USING   TW-ECSM
                          PROCESS

The symbols,

        'S' stands for specimen no.,

        'V' for supply voltage and

        'T' for the machining time, in the photograph.

4.2.1 Material Removal Rate

Material Removal Rate (MRR) is defined as the amount of material removed in unit time. When the material removed is measured in grams the corresponding MRR is known as Gram Material Removal Rate (MRRg). The effect of supply voltage on MRRg for machining of PZT specimen is shown by a solid line in the Fig.4.2 for 30 % electrolyte concentration. MRRg is seen to increase with the increase in supply voltage at constant feed rate of 0.009mm/s. Increase in supply voltage implies higher discharge energy and hence more MRRg.

Other experimental values are not joined in the form of a curve as in those cases the experiments were not conducted with constant feed. In such cases feed was controlled by stepper motor but, at the instant of arcing it was manually interrupted. As soon as arcing was over it was again controlled by the stepper motor. This was done in order to avoid excessive overcut due to heavy arcing. This can be confirmed from the Fig.4.6 which shows that the overcut for 20% electrolyte concentration is much low than with a constant feed (with arcing). The experimental values are symbolized on the plot.

The material removal rate (length), MRR_l, defined as the length of cut achieved in unit time is plotted in Fig.4.3, for the PZT ceramic at 30% electrolyte concentration and a feed rate of
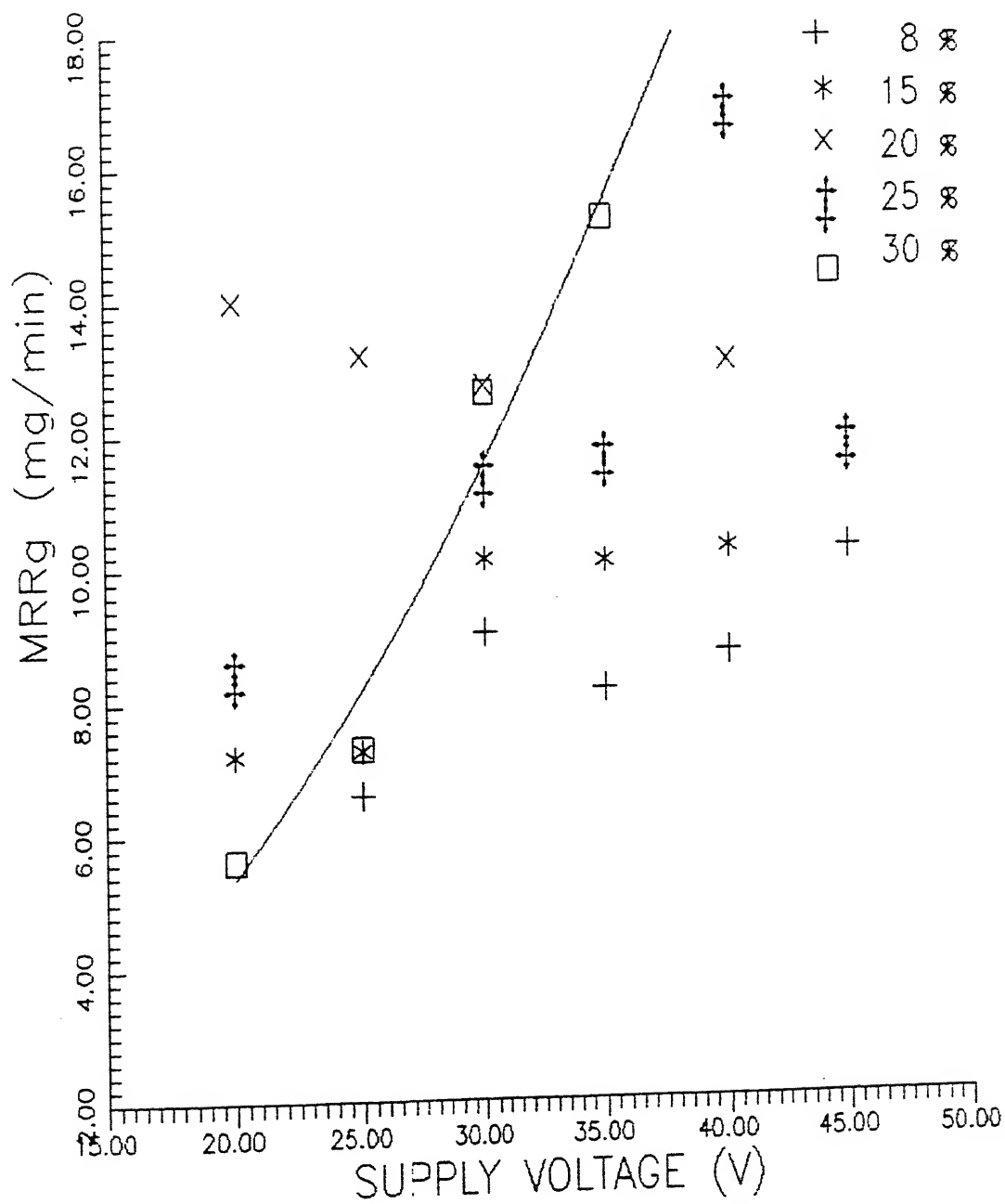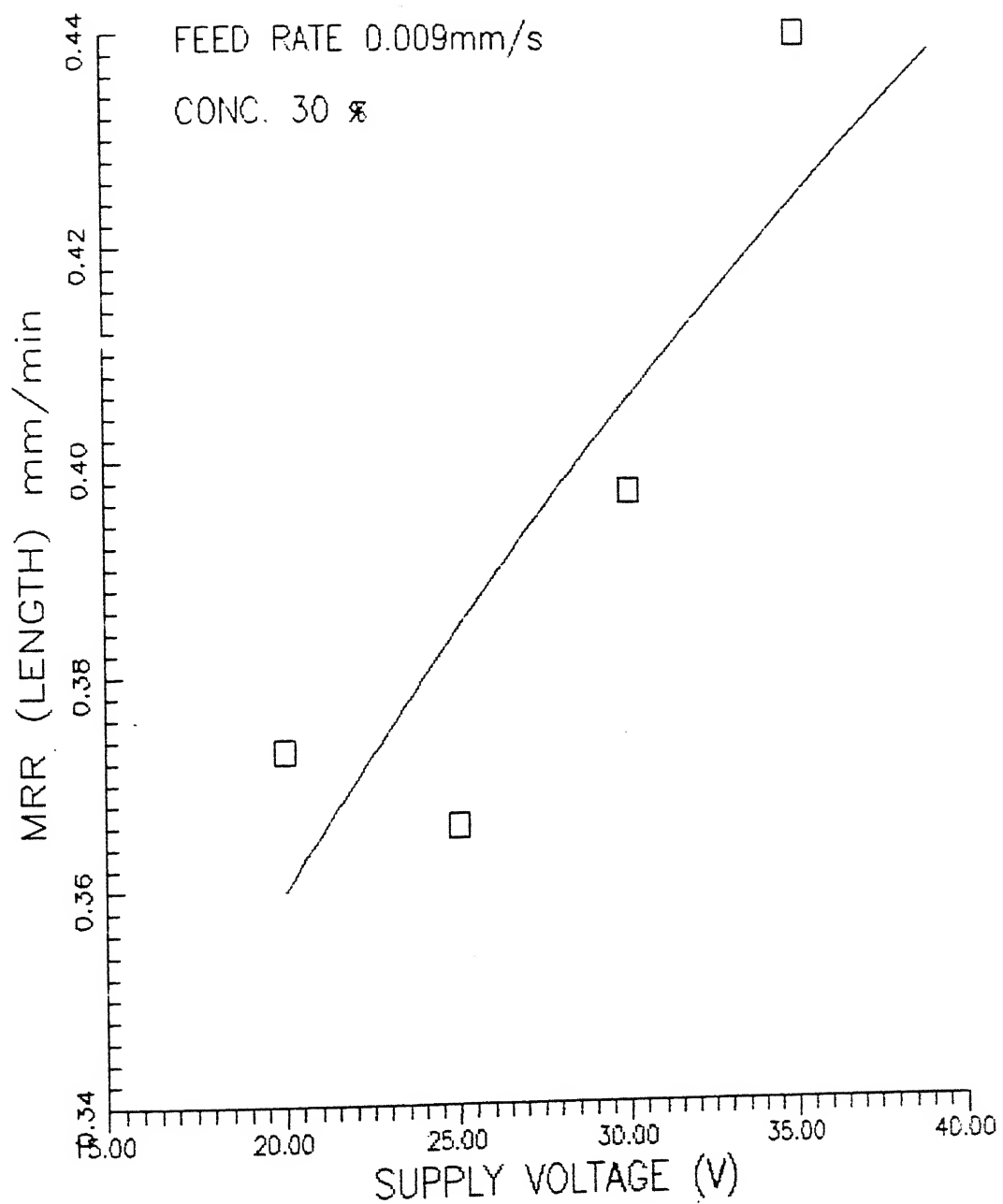
FIG 4.2   EFFECT OF SUPPLY VOLTAGE ON MRRg

FIG 4.3   EFFECT OF SUPPLY VOLTAGE ON MRR(LENGTH)

0.009mm/s. The MRR_l is seen to increase with the supply voltage for the reason that the discharge energy increases with the increase in supply voltage.

The material removal rate (area), MRR_a, is the area (product of length of cut and thickness of the specimen) removed in unit time. The MRR_a also increases for the reason that as the length of cut increases the MRR_a should also increase. The plot in Fig.4.4 shows the MRR_a for 30 wt% electrolyte concentration and feed rate of 0.009mm/s.

The effect of electrolyte concentration on MRRg at 20 volts of supply voltage is shown by a solid line in the Fig.4.5. MRRg increases with an increase in the electrolyte concentration up to a certain value i.e.20 wt% concentration, and then decreases. This is due to the fact that the specific conductance of NaOH solution increases approximately up to 20 wt% concentration. Theoretically, maximum specific conductance of NaOH solution is around 22.5 wt% for most of the higher temperature range (50-80°C), and after which it decreases (Refer Appendix F). An increase in specific conductance means an increased electrolyte conductivity (low path resistance) and consequently more electrolytic current. The process of electrolysis is accelerated by an increase in the electrolytic current. This results in a greater rate of evolution of hydrogen gas bubbles at the cathode surface. Since the sparking occurs across the bubbles, an increased rate of hydrogen gas bubbles formation implies an enhanced rate of sparking and hence higher MRRg. Therefore, MRRg is found to increase with the increasing concentration up to 20 wt% and then decreases on further increase in the concentration.
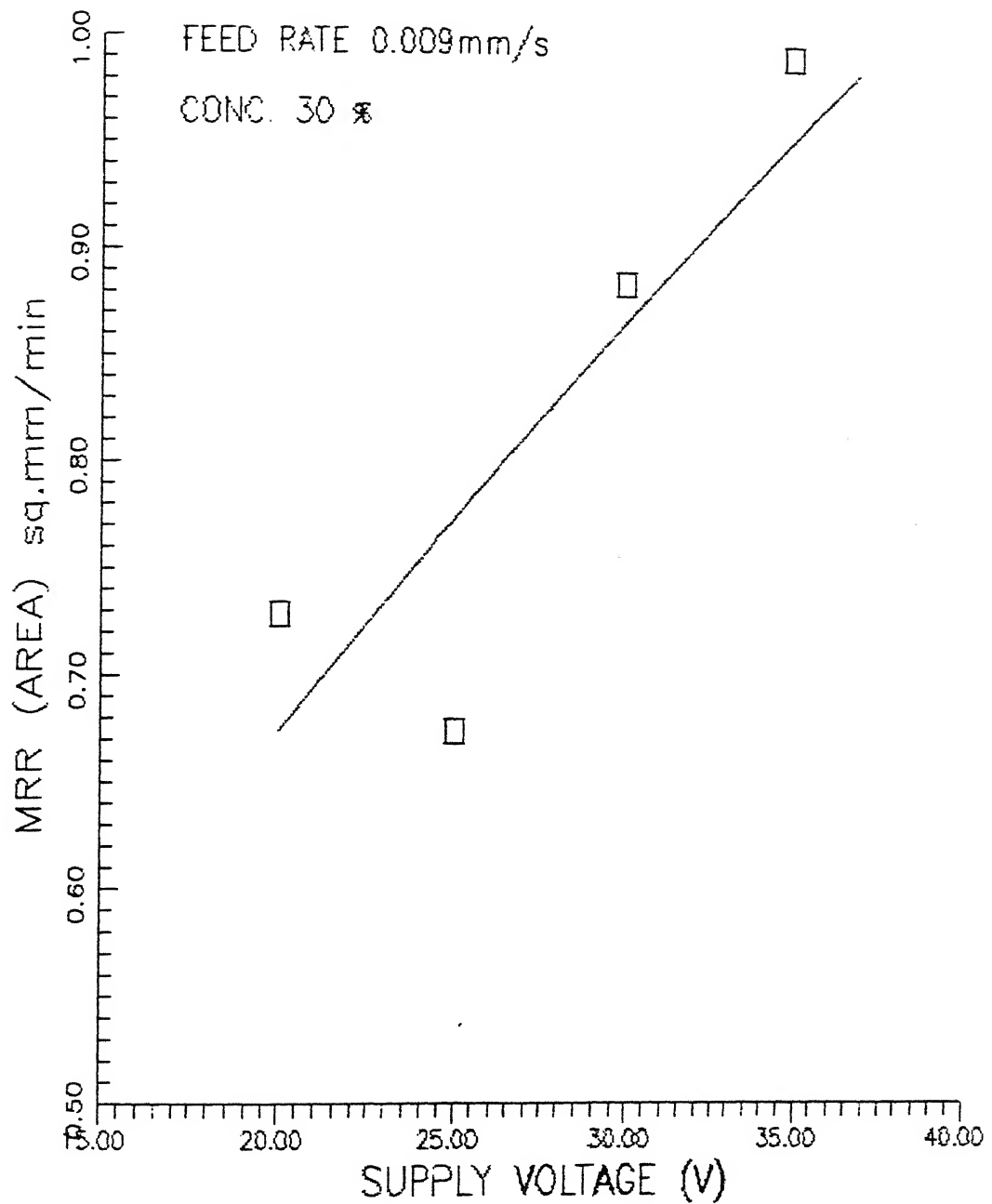
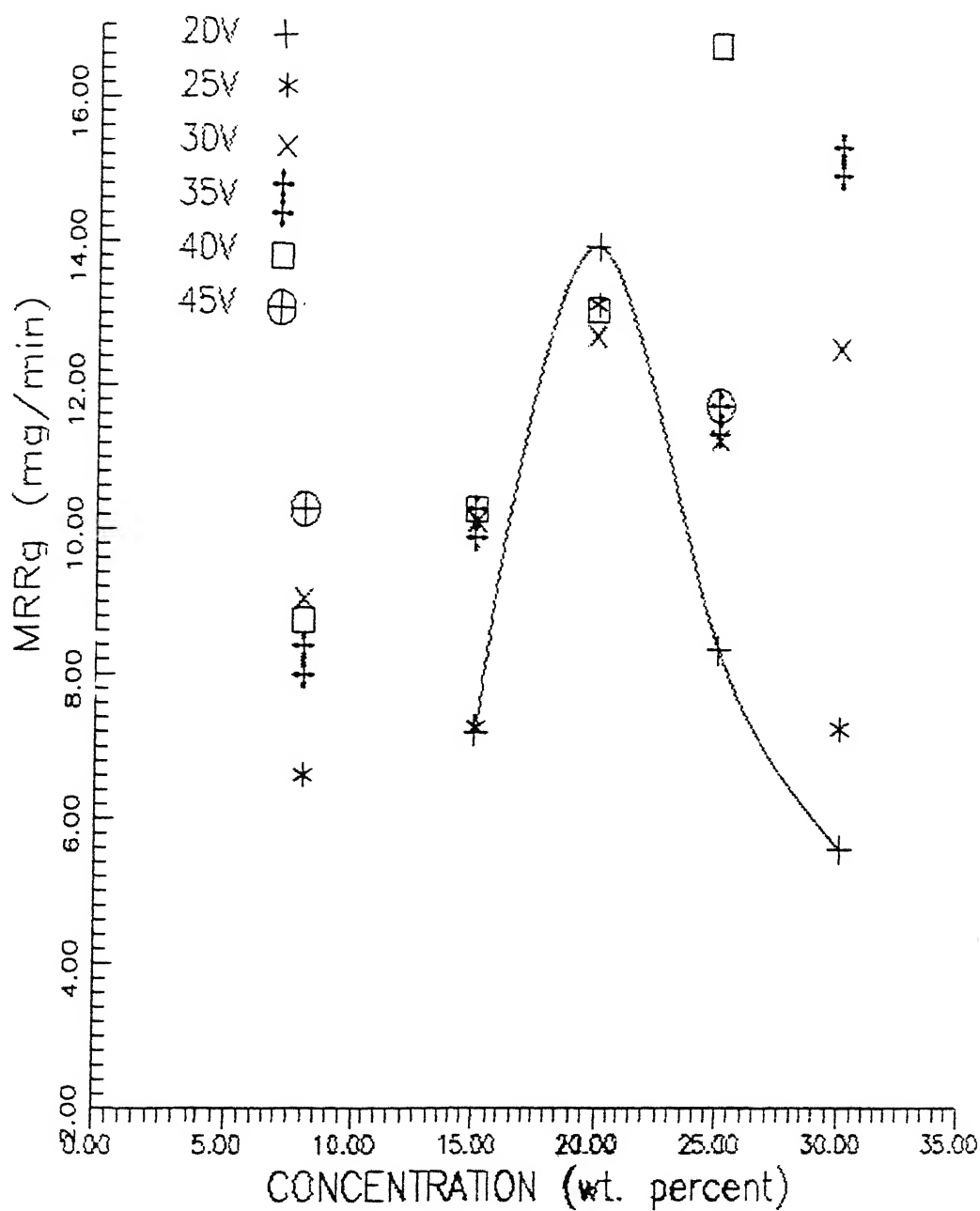FIG 4.4   EFFECT OF SUPPLY VOLTAGE ON MRR(AREA)

FIG 4.5 EFFECT OF CONCENTRATION ON MRRg

Here too, the other points are not plotted because of the reasons mentioned above. But it can be seen that for the different supply voltages the peak MRRg is at around 20 wt% of the electrolyte concentration. Table no.4.1 gives the observed values of the MRRg in mg/min.

4.2.2 Average Diametral Overcut

In most of the cases, overcut was measured at four different locations, taking values at 0, L/3, 2L/3 and L as shown in Fig.4.1(a), L is the length of cut and d is wire diameter, except at those locations where the overcut is exceptionally high [for example Fig.4.1(b), S22]. The average of these readings was used for plotting. The dependence of the average diametral overcut on supply voltage can be viewed in the Fig.4.6. With the increase in the supply voltage, the current density increases resulting in high electrochemical reactions evolving large amount of hydrogen gas bubbles. This probably increases the frequency of sparking (no. of sparks per sec.) and the energy per spark, removing large amount of material from the specimen in the same time as at lower supply voltages, hence wider cuts.

Only for 30 wt% electrolyte concentration experimental points are joined as a curve for the reason that the feed for other experiments was not constant to avoid arcing during the machining process. This can be seen from the plot in Fig.4.6. Compared to 15% electrolyte concentration curve, the overcut for 30% electrolyte concentration is quite high. Generally, the average overcut for other experiments is found to be in the range of 0.3 to 0.8mm for

0.5mm wire diameter.

TABLE 4.1

Supply Voltage	Material Removal Rate (MRRg) mg/min				
	Conc.8%	Conc.15%	Conc.20%	Conc.25%	Conc.30%
20V	----	7.213	14.010	8.394	5.620
25V	6.609	7.280	13.206	---	7.316
30V	9.044	10.140	12.760	11.328	12.646
35V	8.198	10.113	19.803*	11.617	15.288
40V	8.747	10.307	13.131	16.863	----.
45V	10.285	----	----	11.814	----

* Very high value, not considered in the plot.

TABLE 4.2

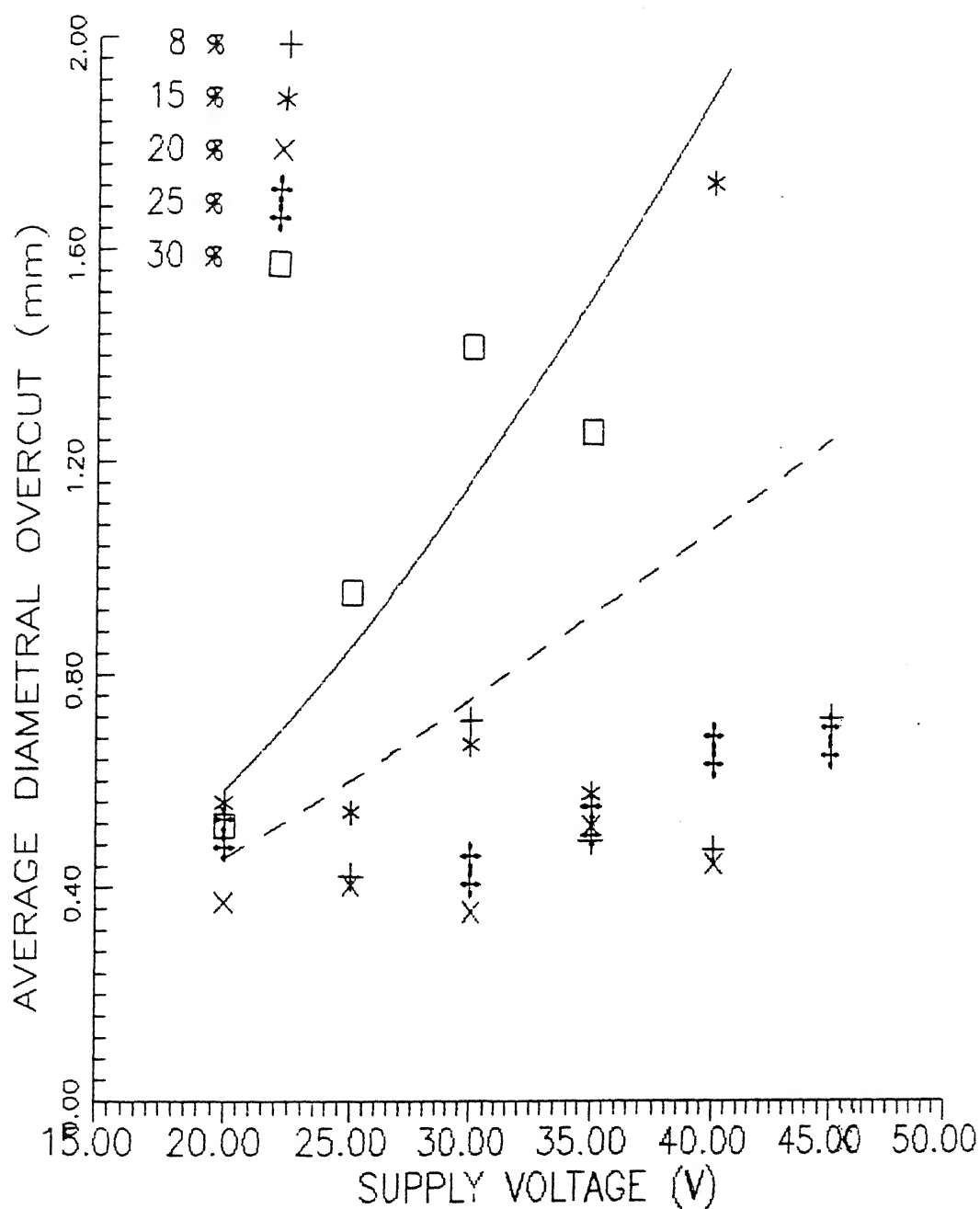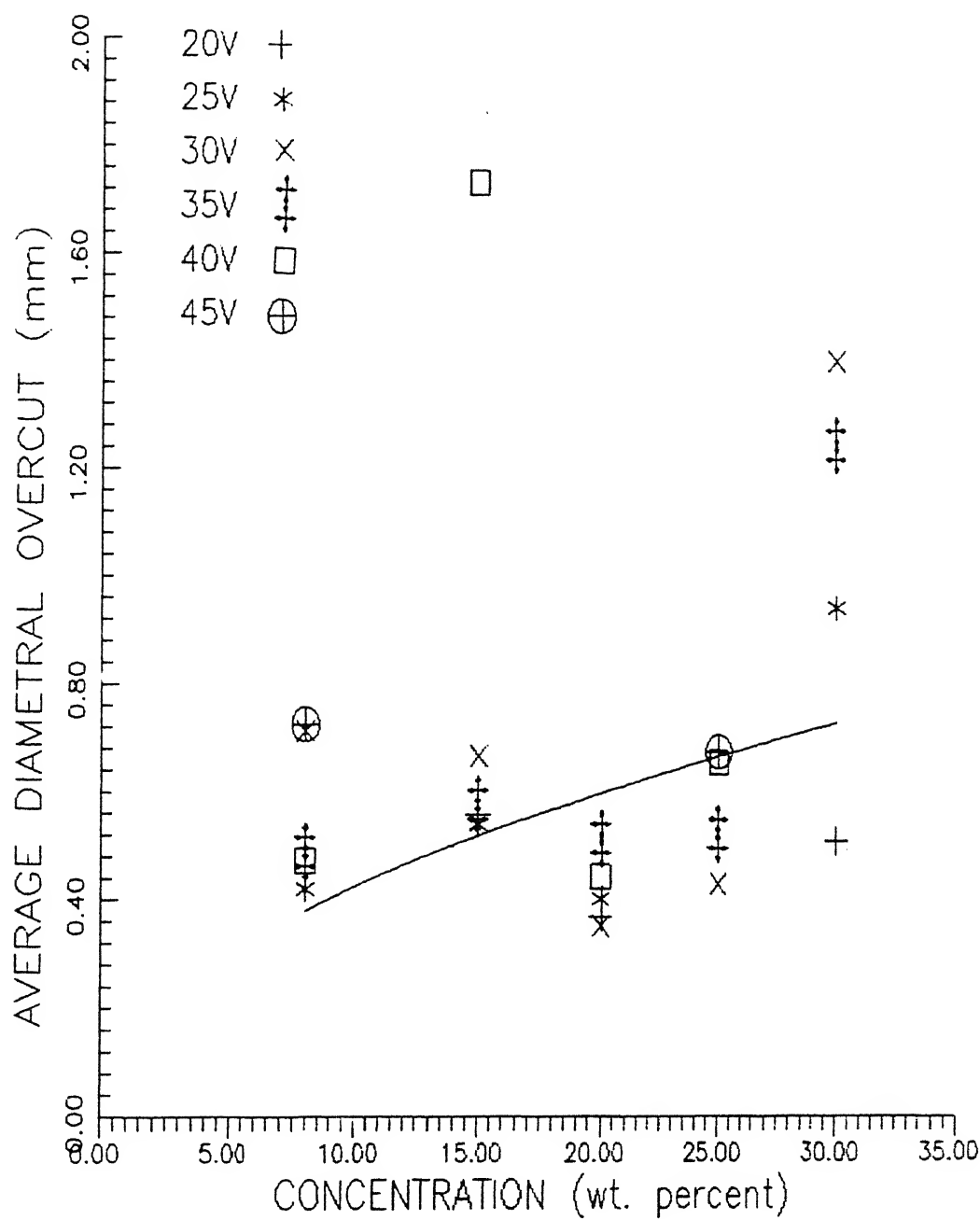| Supply Voltage	Average Diametral Overcut (mm)				
	Conc.8%	Conc.15%	Conc.20%	Conc.25%	Conc.30%
20V	----	0.560	0.372	0.502	0.516
25V	0.421	0.542	0.405	----	0.953
30V	0.714	0.670	0.355	0.434	1.419
35V	0.490	0.579	0.518	0.528	1.260
40V	0.474	1.738	0.447	0.663	----
45V	0.726	----	----	0.682	----

FIG 4.6 EFFECT OF SUPPLY VOLTAGE ON OVERCUT

FIG 4.7 EFFECT OF CONCENTRATION ON OVERCUT

The effect of electrolyte concentration on average diametrical overcut is shown for 25volts of supply voltage in the Fig.4.7. Here, even after 20 wt% of electrolyte concentration the overcut keeps on increasing. This is due to the fact that as the length of cut increases, the probability of arcing increases, for the reason that there are more chances of the debris being present in the slot which may lead to arcing. Thus, increasing average diametral overcut. Table 4.2 gives the observed values of average diametral overcut. Fig.4.8 shows the shape of the cut obtained in machining of the PZT ceramics.

Table 4.3 gives the details of the machining parameters of the PZT specimens.

4.2.3 Surface Integrity

The surface structure was studied on SEM. It was observed that the PZT grains after machining had acquired small round granule form as compared to the cluster of grains in random shape of the initial PZT sample. This can be seen in the Photograph no.4.2. This is due to the fact that large heat generated during the cutting process melts the PZT, which recrystallizes in round shape because of the surface tension. This also confirms that the material removal is by melting and vaporization.
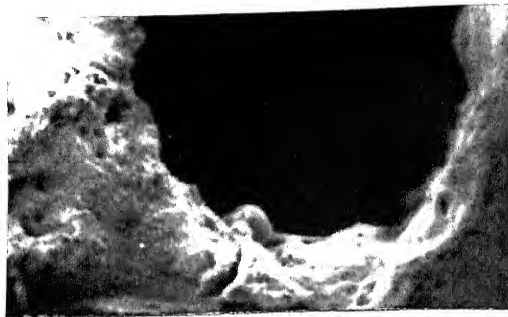
Photograph no.4.3 shows the crack developed at the machined surface. The probable reason for the crack is rupture of large hydrogen bubble in the vicinity of the specimen. At high supply voltages, the potential gradient becomes sufficiently high to cause the larger bubbles rupture and release heat of spark. This violent

(a) S13, 30V, CONC.20%
X23

(b) S21, 20V, CONC.30%
X30

(c) S24, 35V, CONC.30%
X35

FIG 4.8   SHOWS THE SHAPE OF GROOVE CUT IN PZT CERAMICS USING
TW-ECSM PROCESS, TAKEN ON SEM

The following chart shows the specimen no. and its machini

parameters.

Sample No.	Supply Voltage (volt)	Conc. (wt %)	Specific conductance(mho/cm)		Thickness (mm)
S1	25	8	0.183^*	at 32°C	2.16
S2	30	8	0.189	34°C	2.08
S3	35	8	0.192	36°C	2.40
S4	40	8	0.195	36°C	3.02
S5	45	8	0.183	32°C	2.97
S6	20	15	0.244^*	35°C	3.09
S7	25	15	0.246	36°C	2.76
S8	30	15	0.248	37°C	2.83
S9	35	15	0.241	32°C	2.99
S10	40	15	0.241	30°C	3.08
S11	20	20	0.253^*	33°C	3.58
S12	25	20	0.271	36°C	2.96
S13	30	20	0.274	37°C	3.11
S14	35	20	0.256	34°C	2.95
S15	40	20	0.261	36°C	3.03
S16	20	25	0.256^*	34°C	3.92
S17	30	25	0.246	30°C	2.42
S18	35	25	0.253	34°C	2.38
S19	40	25	0.264	36°C	2.27
S20	45	25	0.267	37°C	3.40
S21	20	30	0.255^*	37°C	1.95
S22	25	30	0.247	35°C	1.84
S23	30	30	0.251	35°C	2.23
S24	35	30	0.242	34°C	2.28

* It signifies the specific conductance of fres
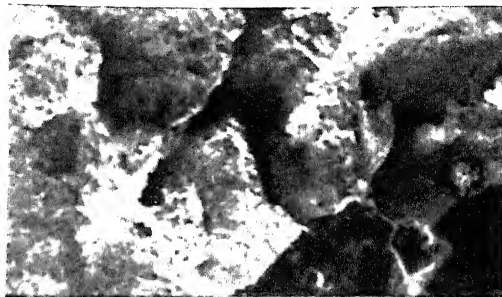
electrolyte.

63
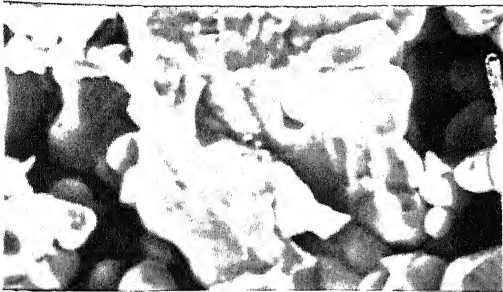
(a) UNCUT SURFACE OF PZT CERAMICS
X5000

(b) CUT SURFACE OF PZT CERAMICS
S2, 30V, CONC.8% , X5000

HOTOGRAPH NO. 4. 2   THE STRUCTURE OF PZT CERAMICS TAKEN ON SEM

S2, 30V, CONC.8%
X 50

PHOTOGRAPH NO. 4. 3   SHOWS THE CRACK OBSERVED   IN   MACHINED
CERAMICS ON SEM

rupture causes mechanical shock which may be one of the factors
responsible for the damage of the specimen by introducing cracks.
Sometimes chipping of the surface layer is also caused as can be
seen in photograph no.4.8(a).

4.3 Efficiency of the ECSM process

The spark is observed over the full length of wire immersed in
the electrolyte (approx. 60mm). The specimen thickness is in the
order of 3 mm.

Therefore, approximately, $(3/60) \times 100 = 5\%$ of the whole
energy is utilized. Large amount of energy is being wasted.

4.4 Miscellaneous Observation:

4.4.1 Effect of immersed wire (cathode) length in the electrolyte It
was observed that with the increase in the immersed length of the
wire, value of the current increased as the voltage was increased.
Just before the onset of discharge, current drop was observed. At
the onset of the discharge, further drop in the current was
recorded.

This might be due to the reason that at the onset of the
discharge the bubble bursts, giving rise to a spark. This spark,
heats up the electrolyte locally and accelerates the electrolysis
mechanism, evolving hydrogen bubbles at faster rate at the cathode
surface. Thus a multi layer of non-conducting hydrogen bubbles is
formed at the cathode, increasing the effective resistance and hence
lowering the current. Table no.4.4 gives the observed supply voltage

and current values.

TABLE **4.4**

Effect of wire length immersed in the electrolyte on current.

Supply voltage (volts)	Electrode gap = 5mm		
	L_*= 1mm	L_*= 25mm	L_*= 60mm
	Current(A)	Current(A)	Current(A)
10		0.6	1.5
20	0.5	1.6	4.1
30	0.8	2.8	6.6
35	1.0	3.4	9.0
40	–	3.9	10.0[#]
50	1.1	4.2	
60	1.0	4.9	
70	0.6	3.8	

L_*= Length of wire immersed in the electrolyte.

\#   The maximum limit of the ammeter was   10amps,   so   beyond
    this value of current, it could not be measured.

For L_* = 1mm, Discharge Voltage was 70 V,

For L_* = 25 and 60mm, it could not be recorded because of the
constraint on maximum voltage output from the transformer was
70 volts.

4.4.2 Effect of electrode gap

It is observed that the variation in current value with increased electrode gap (from 6.5mm to 25mm) before the onset of discharge is small but after which the values are same for both the electrode gap of 6.5 and 25mm. The Table no.4.5 shows the experimental results obtained. It can be deduced that the effect of electrode gap is negligible. It can also be said that the electrolyte resistance is very small and major potential drop is across the bubbles at the electrodes.

TABLE 4.5

Effect of electrode gap on current.

Supply Voltage (volts)	$L_* = 10$mm	
	Electrode gap = 6.5mm	Electrode gap = 25mm
	Current (amp)	Current (amp)
10	0.4	0.3
20	1.0	0.9
30	1.6	1.5
40	2.1	2.0
50	2.5	2.5
60	2.2	2.2
65*	1.9	1.9
70	1.7	1.7

* Discharge Voltage

L_* - Length of wire immersed in the electrolyte.

4.4.3 Effect of Electrolyte Concentration on Discharge Voltage

This is an obvious deduction from the main experiments conducted that the discharge voltage decreases with the increase in the electrolyte concentration.

As the electrolyte concentration increases the conductivity of the solution increases because of more ions in the solution. This reduces the electrolyte resistance and the supply voltage required for discharge lowers. But at higher concentration again higher voltage should be required because of collision of too many ions will now obstruct the free movement of the ions.

The discharge voltage recorded for electrolyte concentration of 15 wt% and above was around 20 volts and for 8 wt% it was 25 volts.

4.4.4 Experiments on carbon fiber epoxy composites :

Few experiments of cutting and drilling were conducted on carbon fiber epoxy composites. The detail of the specimen is given in Appendix D. It was observed that the arc intensity in the machining of the carbon composite were quite high as compared to that of PZT ceramics. The shadow graph of the cut groove is shown in Fig.4.9.

Drilling was done using a 2mm diameter copper rod. It was noticed that after a depth of around 2mm, the tool(i.e. the copper rod) tip got melt because of heavy arcing. As depth increases, the debris probably gets entrapped in the drilled hole causing severe arcing.

Photograph no.4.4 shows the machined and drilled hole in the specimen.

C1

C2

SCALE ⊢———⊣
0.5 mm
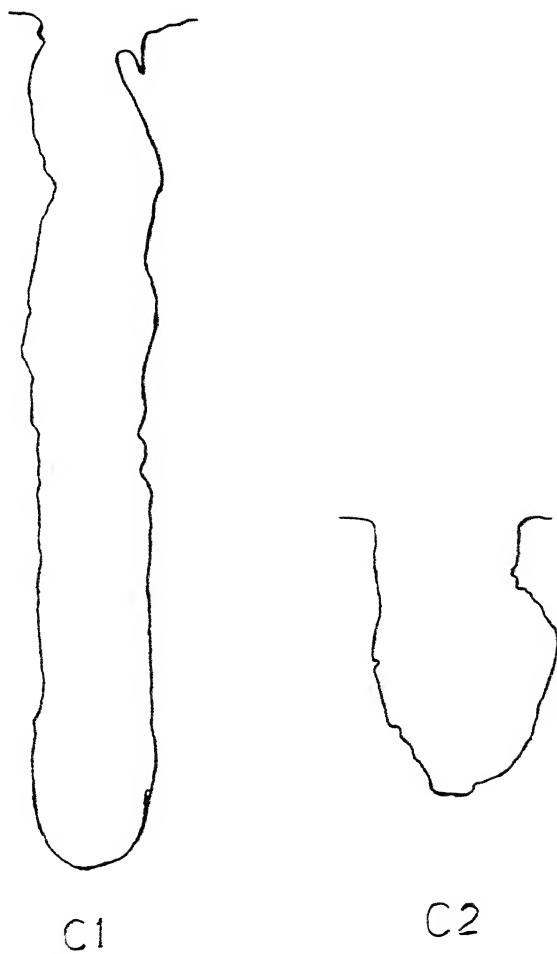
C_1 O_D = 0.260mm   L = 5.768mm   V = 20 volts   C = 20 wt%
C_2 O_D = 0.52mm   L = 1.90mm   V = 40volts   C = 20 wt%

where, O_D is average diametral overcut,
          L is length of cut,
          V is supply voltage and
          C is electrolyte concentration

FIG 4.9   SHADOW GRAPHS SHOWING THE SHAPE OF GROOVE   CUT   IN
CARBON FIBER EPOXY COMPOSITE USING TW-ECSM PROCESS
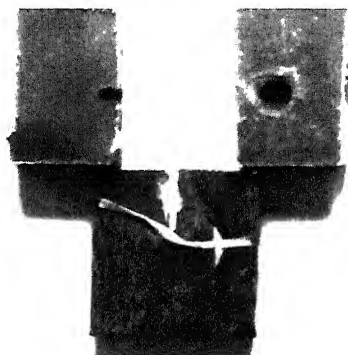
PHOTOGRAPH NO. 4. 4   MACHINED AND DRILLED   SPECIMENS   OF   CARBON
                          FIBER EPOXY COMPOSITES ON TW-ECSM SET-UP

5.2 Suggestions for Future Work

From the difficulties faced in the present work and with more in view of the literature surrvey the authors presents the following points which could be emphasized in the future.

1. The feed given to the workpiece should be provided through a servo motor instead of a stepper motor. This will avoid the physical contact of the workpiece and the wire through the sensors and retrieve the feed. Thus arcing could be prevented and better surface finish could be achieved for partially conductive materials.

2. Since the process generates excessive heat, it is suggested to have a continuous flowing electrolyte system. A pump can be used for the purpose. The flow rate should be such that hydrogen bubble is stable for sufficient time to generate spark and fast enough to carry away the generated heat. A cooling and sludge filtering device should be incorporated prior to the pump to maintain a constant value of the conductivity of the electrolyte.

3. From the literature survey it has been studied that in process like wire EDM and EDM the MRR and the surface finish of the machined component improves when a pulsed supply is used instead of smoothed rectified D.C. supply. Hence, a pulsed D.C.supply could be used to enhance the MRR and better surface finish.

4. A second axis could be added to the workpiece sliding mechanism. This can generate cut of any shape (2-D) in the specimen.

REFERENCES

1. Allesu K.- Ph.D. Dissertation, I.I.T., Kanpur, India, 1988.

2. Allesu K., Muju M.K., Ghosh A.- *"Experimental Observation in the ECD machining of Non-conducting materials"*, Proc.of International Symposium for Electro-Machining(ISEM-9), 1989.

3. Basak I.- Ph.D. Dissertation, I.I.T., Kanpur, India, 1992.

4. Cook N.H., Foote G.B., Jordan P., Kalyani B.N.- *"Experimental studies in electro-machining"* Trans ASME, Jl. of Engg.for Ind., pp 945, Nov.1973.

5. Dobos D.- *"Electrochemical Data"*, Elsevier Scientific Publishing Company, Amsterdan, New York 1975.

6. Ito S., Nakamura M., Kanemabu W.- *"Machining of High Performance Ceramics"* Bull. Japan Society of Prec. Engg., Vol.21 No.3, pp167, Sept.1987.

7. Jaffe B., Cook W.R. and Jaffe H.- *"Piezoelectric ceramics"*, Academic Press Inc.(London) Ltd., 1971.

8. Jain V.K., Rao P.S., Choudhary S.K. and Rajurkar K.P.- *"Experimental Investigation into Travelling-Wire ElectroChemical Spark Machining (TW-ECSM) of Composites"*, Trans ASME, Jl. of Engg. for Ind., Vol.113, pp75, Feb.1991.

9. Kiso H., Taguchi T., Fukuhara M., Kimora T.- *"Machining of advanced ceramics by turning with sintered polycrystalline Diamond tool"*, Bull. Jap. Soc. of Prec. Engg., Vol.21 No.2, pp142, June 1987.

10. Koing W. and Dauw D.F.- *"EDM-Future steps towards the machining of ceramics"* Annals of CIRP, Vol.37, pp623, 1988.

11. Larsson C.N. and Bauxter E.M.- *"Tool damage by sparking in ECM"*,

Proc. of the IMTDR, pp499, 1977.

12. Loutrel S.P. and Cook N.H.- *"High rate electrochemical Machining"*, Trans. ASME, Jl of Engg. for Ind., Nov.1973.

13. McGeough J.A. and Crichton I.M.- *"Studies of the discharge Mechanism in Electrochemical arc machining"*, Jl. of Applied Electrochemistry, Vol.15 pp 113, 1985.

14. Nag S.K.- *"Ceria doped Lead Zirconate Titanate Ceramics"*, M.Tech Thesis, I.I.T. Kanpur 1990.

15. Nancy F.Petrofes and Ahmed M.Gadalla — *"Electrical Discharge Machining of Advanced Ceramics"*, Ceramic Bulletin, Vol.67 No.6, pp 1048, 1988.

16. Paschen F. — mentioned in *" Electric contact — Theory and Application (4th Edition 1981)"* pp 276, 1967.

17. Ricci W.S., Blumenthal W.R. and Skeele H.A.- *"Electrical discharge machinability of ceramics"*, US Army Materials Technology Laboratory, Massachusetts, pp281.

18. Sanjiv Tandon — *"Machining of composites — A New Approach"* M.Tech.Thesis, I.I.T., Kanpur, 1987.

19. Sreenivasa Rao — *"Application of travelling wire — ECSM process for machining of composites. An experimental study of electrical machining of non-conducting materials"*, M.Tech. Thesis, I.I.T., Kanpur, 1988.

20. Tonshoff H.K., and Emmelmann C.- *"Laser cutting of Advanced Ceramics"*, Annals CIRP Vol.38, pp219, Jan.1989.

21. Umesh Kumar — *"An experimental study of Electrical Machining of Non-conducting materials"*, M.Tech. Thesis, I.I.T., Kanpur, 1985.

WORKPIECE HOLDER, DEPTH CONTROL MECHANISM AND FEED MECHANISM

The workpiece holding and sliding subassembly can be viewed in Fig.A.1(a) [Plan], A.1(b) [Elevation] and A.1(c) [Right side view].

The workpiece is to be mounted on the workpiece holding fixture shown in Fig.A.2(a), which can slide on the workpiece slider, shown in Fig.A.2(b), to align the position of cut on the workpiece. The workpiece slider is fixed to the joint plate (Fig.A.3) and the hang rod (Fig.A.4).

The lift screw subassembly is shown in Fig.A.5. The lift screw nut Fig.A.6(a) and lift screw Fig.A.6(b) are made with high precision for fine vertical adjustment. The lift screw nut is push fitted and screw tightened to a slide block (Fig.A.7). The slide block is made of aluminum for low weight. The slide block has two holes bored and force fitted with brass bush [Fig.A.8(a)]. A stainless steel guide rod [Fig.A.8(b)] can slide in the brass bush. Two guide rods are provided to prevent rotation in vertical axis. A block-washer [Fig.A.9(a)] is fitted between the lift screw and the block slide to prevent the lift screw from vertical play.

The lift screw and guide rod have standard thread cut which helps it in mounting on the support T-block (Fig.A.10). The lift screw is fitted with the lift nut [Fig.A.9(b)] on the upper surface of the support block. The lift nut is made of relatively

large diameter with knurling at its outer surface for easy hold and rotation, to facilitate the vertical adjustment of the workpiece. As the feed is provided to the specimen, a mechanism of very low friction and precision is needed. For this, Linear motion (LM) guide Fig.A.11, and rolled ball screw Fig.A.12, is used The specification of these components are as follows :

Linear motion slide   1 RSR 12 W M UU + 470 L M

Rolled ball screw   BNT 1404 A C + 500 LT

PLAN

WORKPIECE HOLDING AND SLIDING SUBASSEMBLY

FIG A.1(a)

ELEVATION

FIG A.1(b)   WORKPIECE HOLDING AND SLIDING SUBASSEMBLY

PART NO.	DESCRIPTION
1	SUPPORT T-BLOCK
2	ROLLED BALL SCREW
3	LINEAR MOTION SLIDE
4	WORKPIECE HOLDER
5	WORKPIECE SLIDER
6	LIFT NUT
7	LIFT NUT SCREW
8	GUIDE ROD
9	JOINT PLATE
10	HANG ROD

RIGHT SIDE VIEW
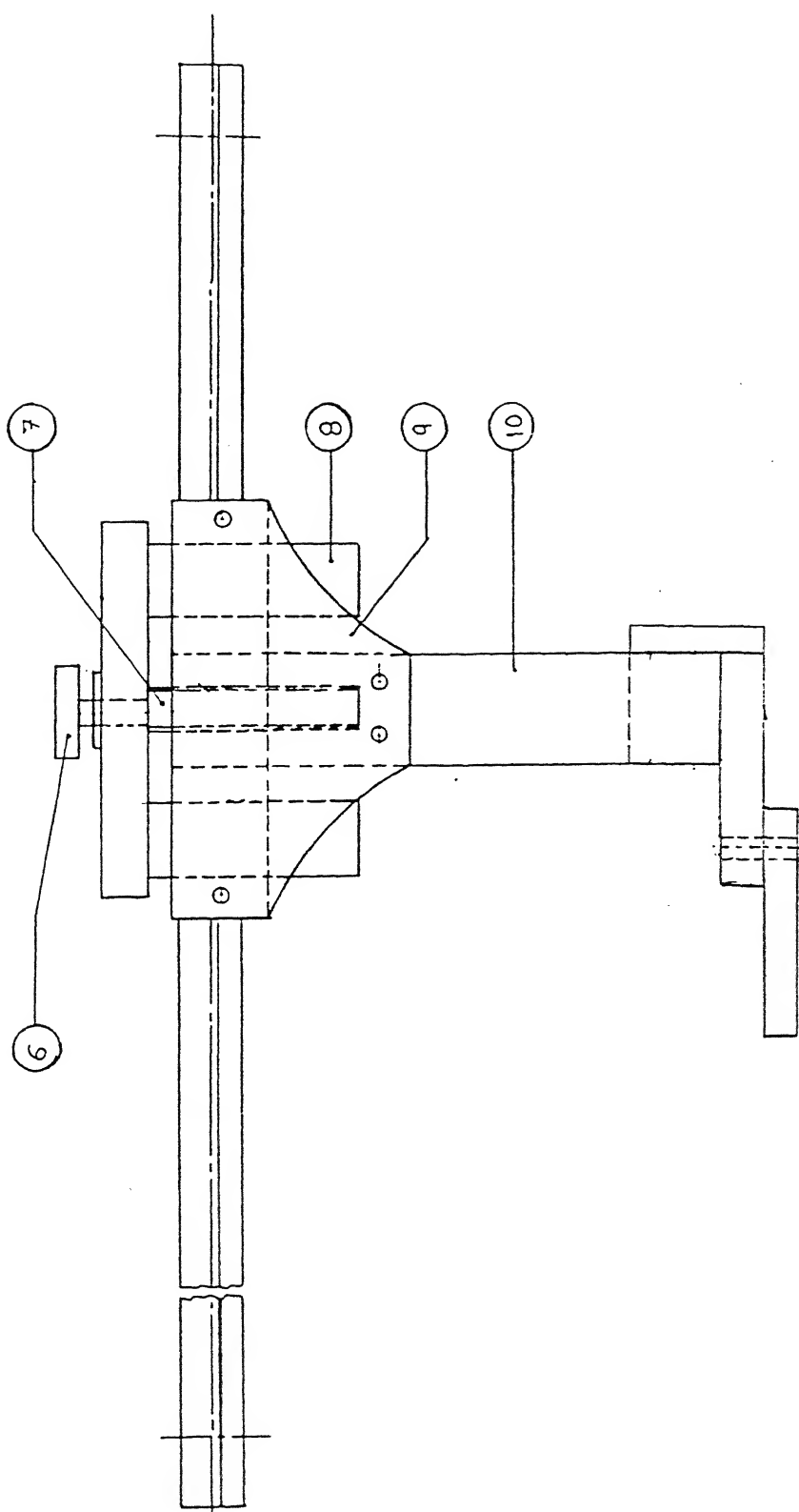
FIG A.1(c)   WORKPIECE HOLDING AND SLIDING SUBASSEMBLY

80
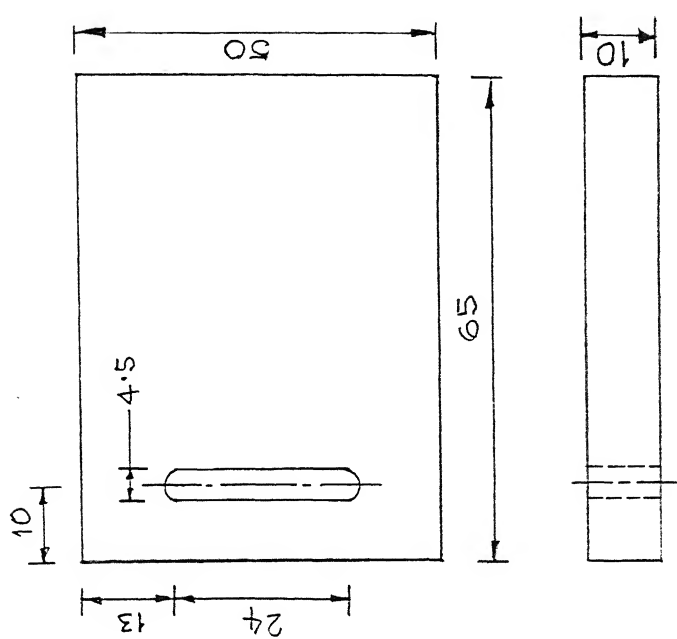
FIG A.2(b)   W.P.SLIDER
              PLEXIGLASS/1NO.
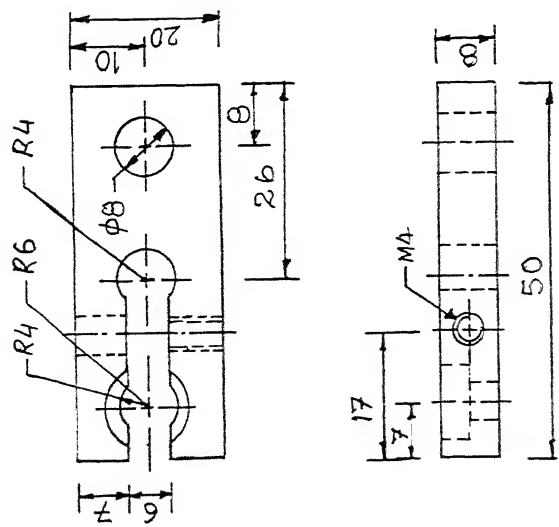
FIG A.2(a)   W.P. HOLDER
             PLEXIGLASS/1NO.

81
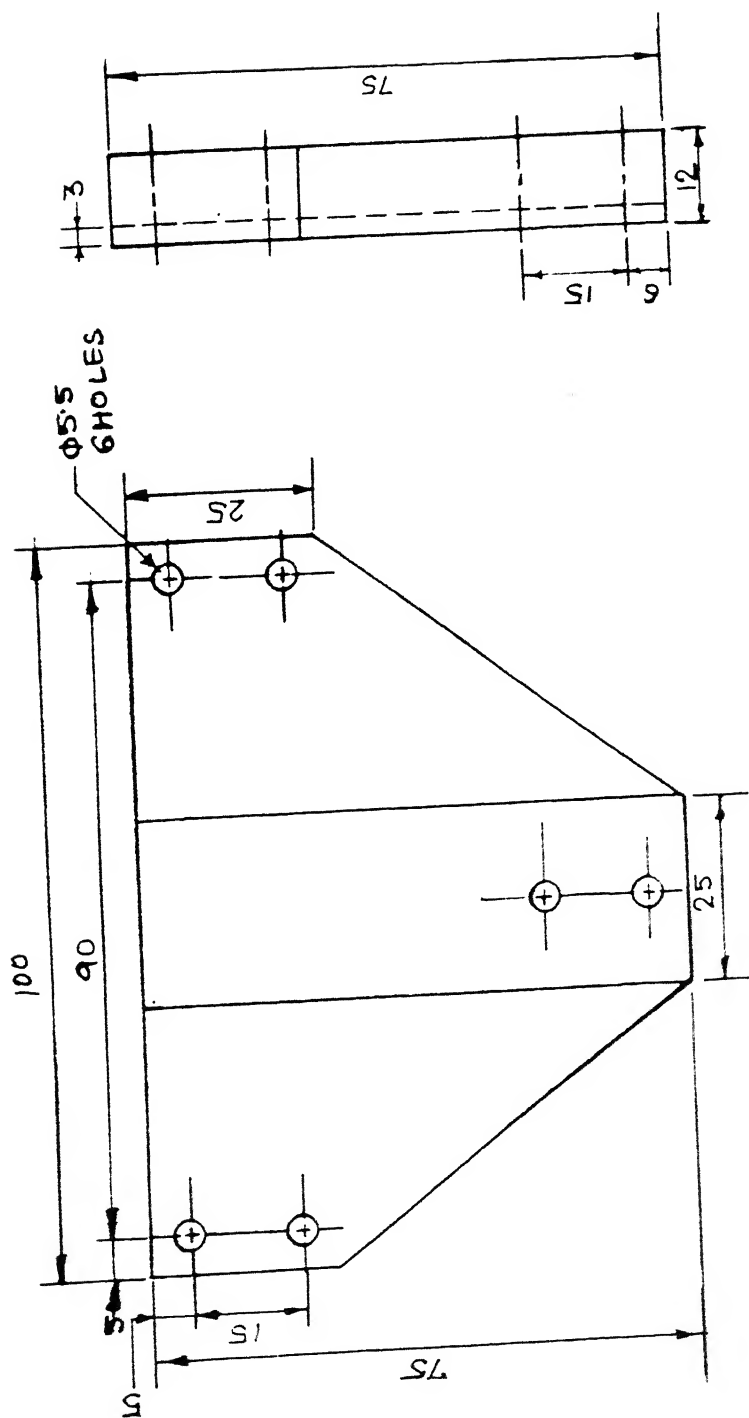
JOINT PLATE
PLEXIGLASS/1NO

FIG A.3
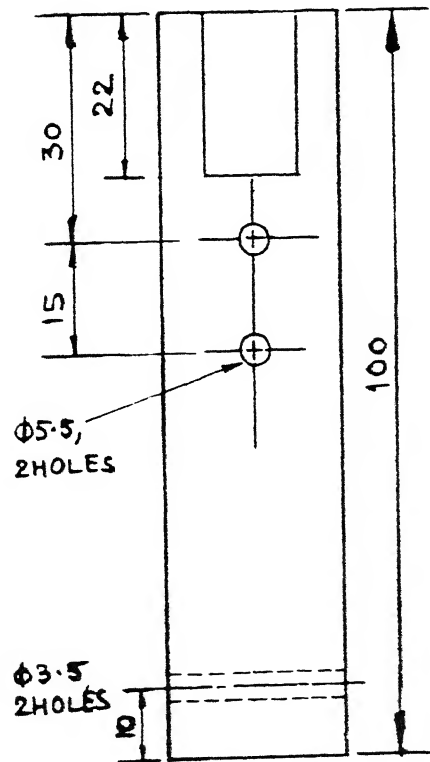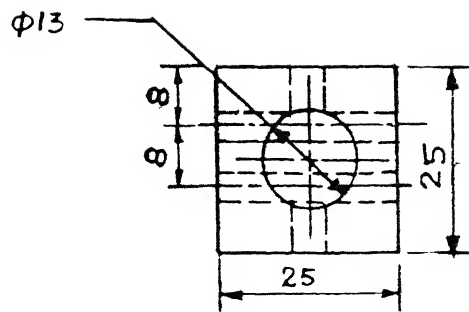
FIG A. 4   HANG ROD
                           PLEXIGLASS/1NO.
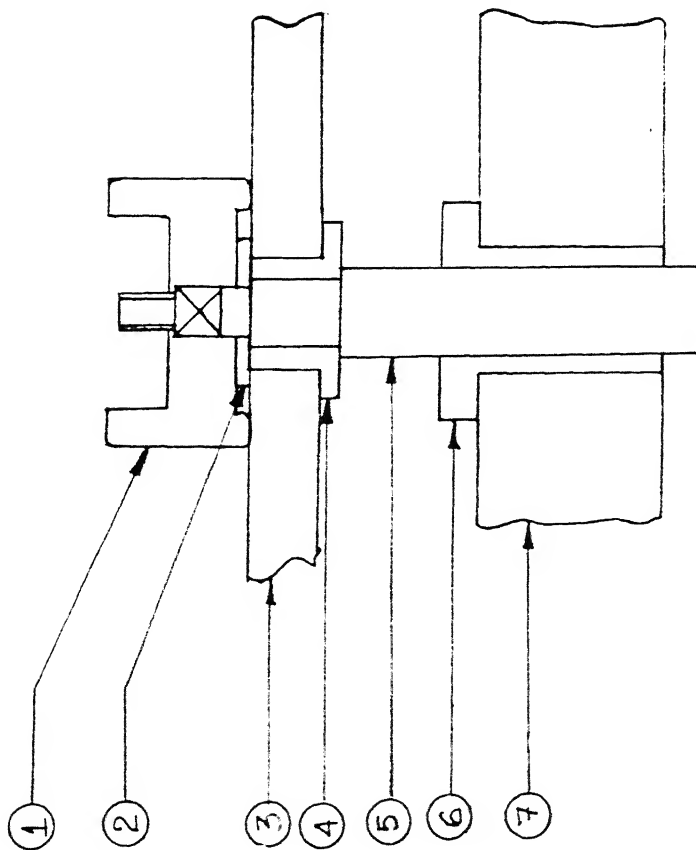
1. Lift Nut
2. Washer
3. Support Block
4. Block Washer
5. Lift Screw
6. Lift Screw Nut
7. Slide Block

LIFT SCREW SUBASSEMBLY

FIG A.5

84

LIFT SCREW
S.S. / 1NO.

80

50

13

7

6

9

Φ 9

Φ 4
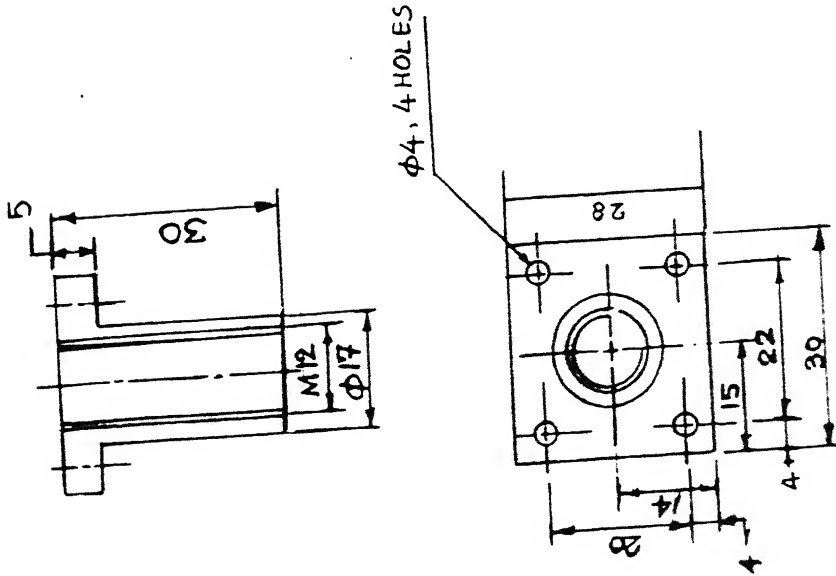
FIG A.6(b)

LIFT SCREW NUT
BRASS / 1NO.

Φ4, 4 HOLES

28

22

30

15

4

14

28

5

30

M12
Φ17
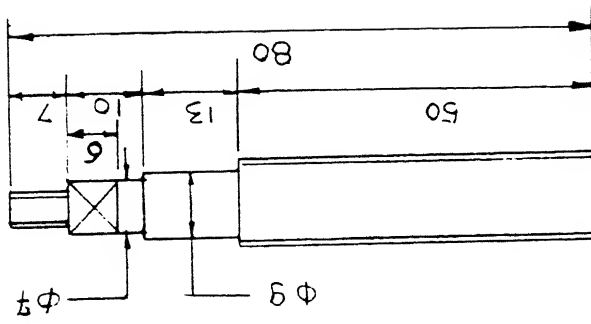
FIG A.6(a)
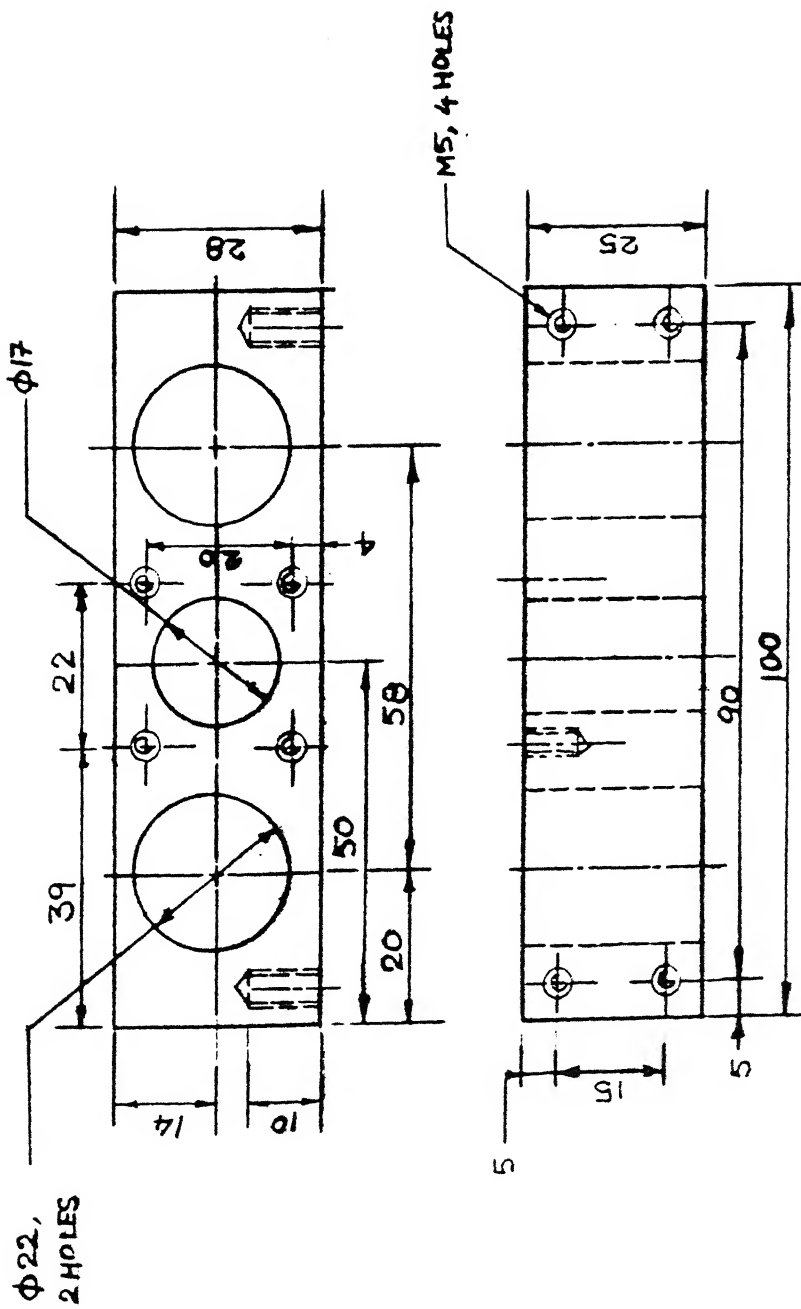
FIG A.7

SLIDE BLOCK
ALUMINIUM/ 1NO.

86

M8

20

65

45

∅16

SMOOTH SURFACE

FIG A.8   GUIDE ROD
S.S./2 NO.

FREE RUN ON
GUIDE ROD

FORCE FITTED IN
SLIDE BLOCK

∅16

∅22

25
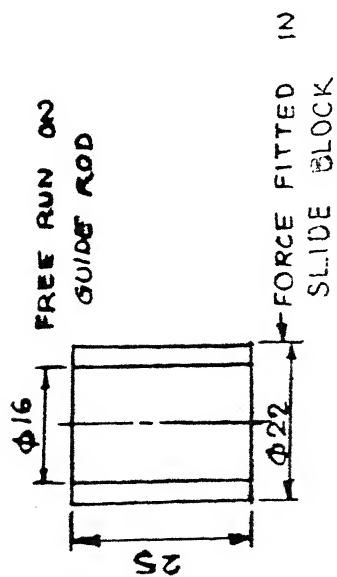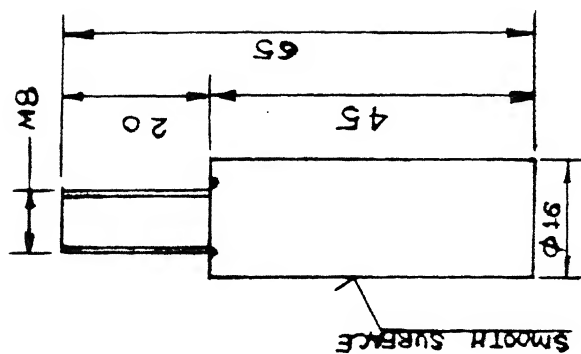
FIG A.8(a)   BUSH
BRASS/2 NO.
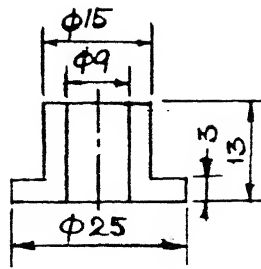
FIG A.9(a)   BLOCK WASHER
              BRASS/1NO.
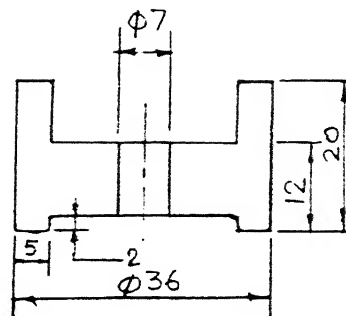
FIG A.9(b)   LIFT NUT
              ALUMINIUM/1NO.
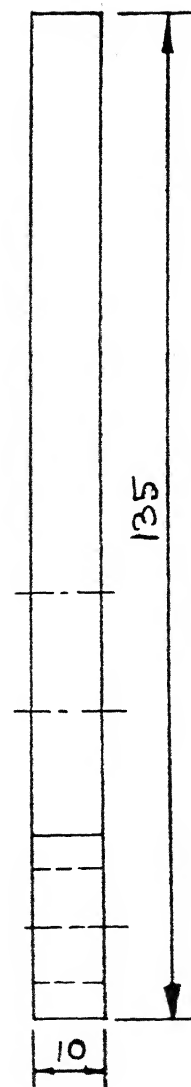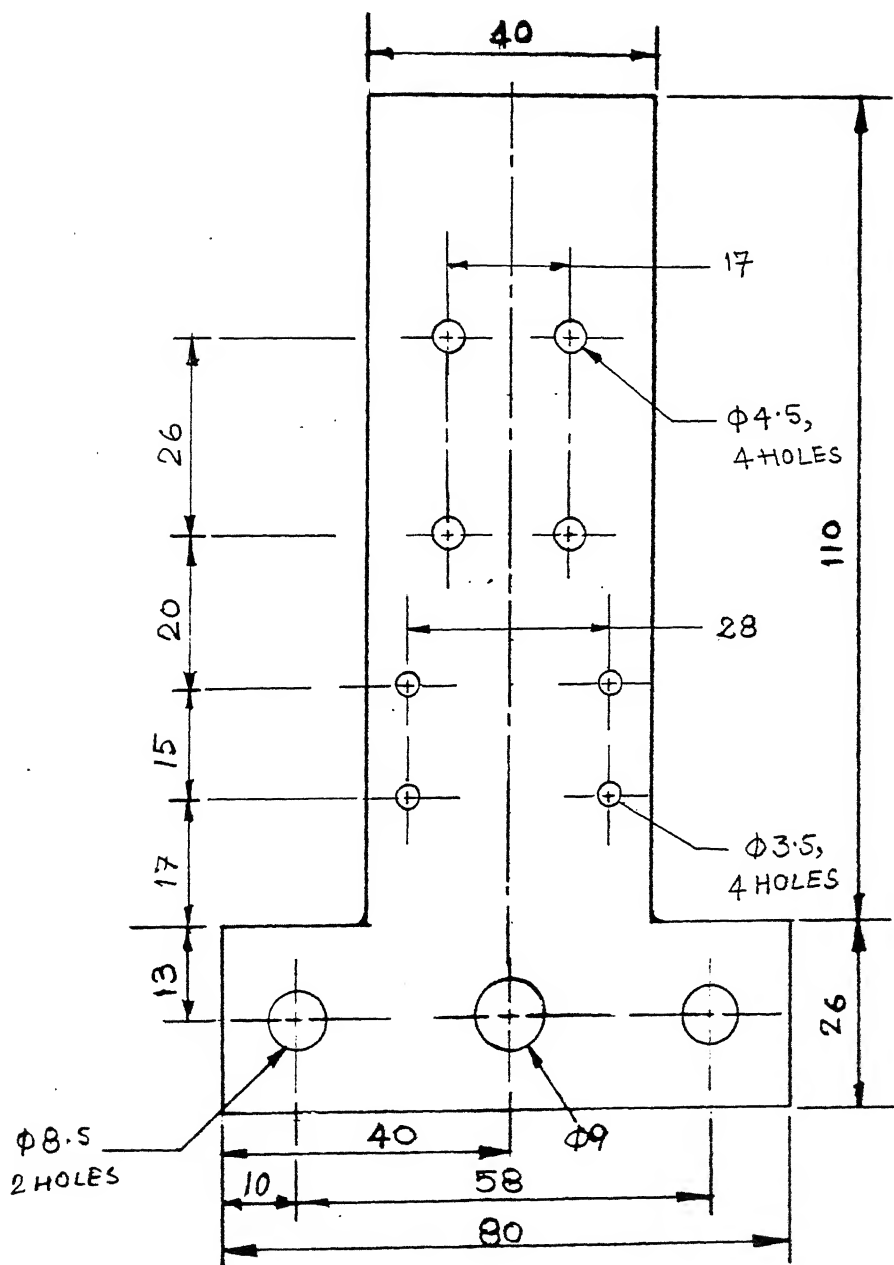
FIG A.10   SUPPORT T-BLOCK
ALUMINIUM/1NO.

59

Type RSR9W, 12W

LM block stopper
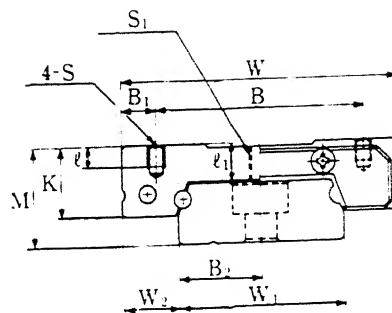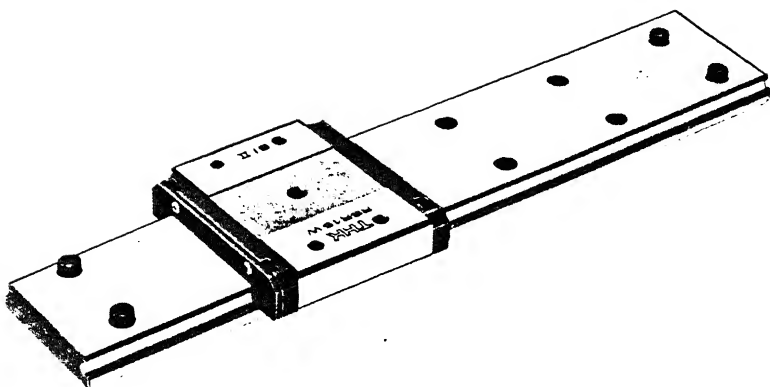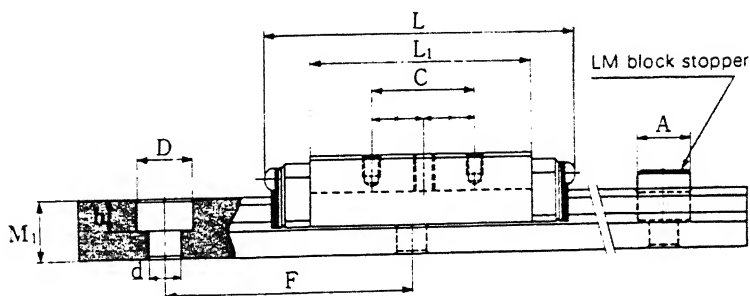
| Model No. | LM block dimensions | | | | | | | | | | | mm | |
| | Width | | | Length | | | Height | | | | | W_1 | W_2 |
	W	B	B_1	L	L_1	C	M	$S \times l$	K	S_1	l_1		
											5.2	24	8
RSR12W	40	28	6	44.5	32.5	15	14	$M3 \times 3$	10	M4	5.2	24	8
RSR12WM	40	28	6	44.5	32.5	15	14	$M3 \times 3$	10	M4	5.2	24	8

| LM rail base dimensions | | | | mm | | Basic load rating | | Static permissible moment (incl.) | | | Weight | |
| | | Height | | | | C | Co | M_A | M_B | M_C | LM block | LM rail |
W_3	B_2	M_1	$d \times D \times h$	F	A	kgf	kgf	kgf·m	kgf·m	kgf·m	kgf	kgf·m
—	12	8.5	$4.5 \times 8 \times 4.5$	40	8	410	620	1.75	1.90	4.86	0.075	1.5
—	12	8.5	$4.5 \times 8 \times 4.5$	40	8	410	620	1.75	1.90	4.86	0.075	1.5

FIG A.11   **LINEAR MOTION SLIDE**
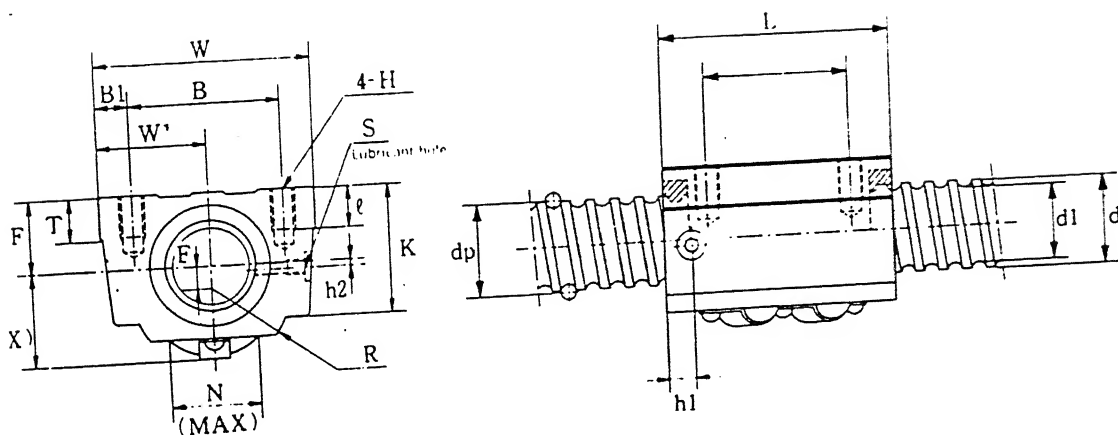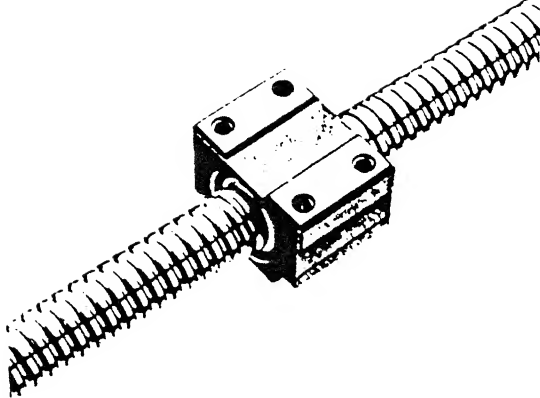
Designation	Threaded shaft O.D	Lead	Ball Diameter	Ball circle diameter	Root diameter	Turns × rows	Ca	Coa	Width	W₁ ±0.15	B	B₁	Overall length
	d	l	Da	dp	d₁		kgf	kgf	W				L
BNT 1404C	14	4	2.778(7/64″)	14.4	11.5	1×3.65	520	1200	34	17	26	4	35

	Nut dimensions									Standard shaft length
H×l	F ±0.15	K	T	R	E	h₁	h₂	S	M	N
4×7	13	20.2	6	14	2.5	6	2.5	M6×1	17	16	500, 1000

FIG A.12   ROLLED BALL SCREW

91

WIRE FEED MECHANISM AND ANODE FIXTURE

The subassembly drawing of the wire drive mechanism is shown in figures B.1(a) [Plan], B.1(b) [Elevation], and B.1(c) [Right side view].

1. Wire support unit

The wire (cathode), as it moves is guided through free pulley units and one fixed copper cathode pulley [Fig.B.2(a)]. The pulley unit consists of idler pulley Fig.B.2(b), idler pin Fig.B.2(c), circular locks and nuts. The idler pulley which is dipped in the electrolyte is made of non-conducting teflon, the rest is of brass. This is done to avoid electrical continuity to the pulley unit thus preventing it to act as cathode. The fixed cathode pulley and cathode nut [Fig.B.2(d)] is made of copper for electrical connection.

These pulleys are mounted on the pulley mount [Fig.B.3] in such a way to have minimum wire length immersed in the electrolyte. The holes in the pulley mount for the idler pin is done to accommodate the various size of the specimen. A slot of 60mm is made in the pulley mount for the workpiece holding device to move across the wire and facilitate the cutting process. The pulley mount is screw tightened to the wire base Fig.B.4.
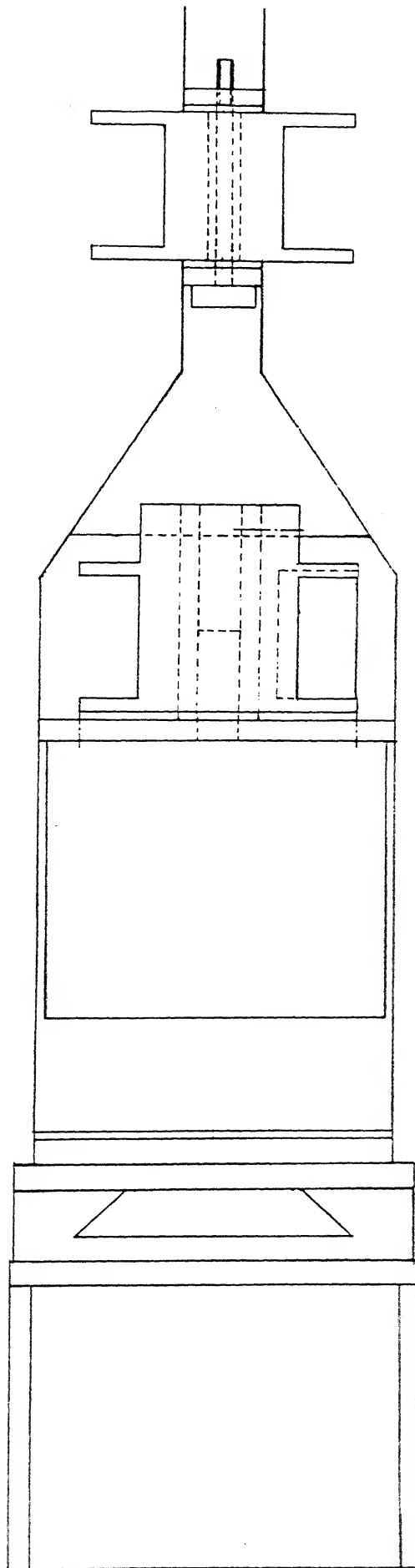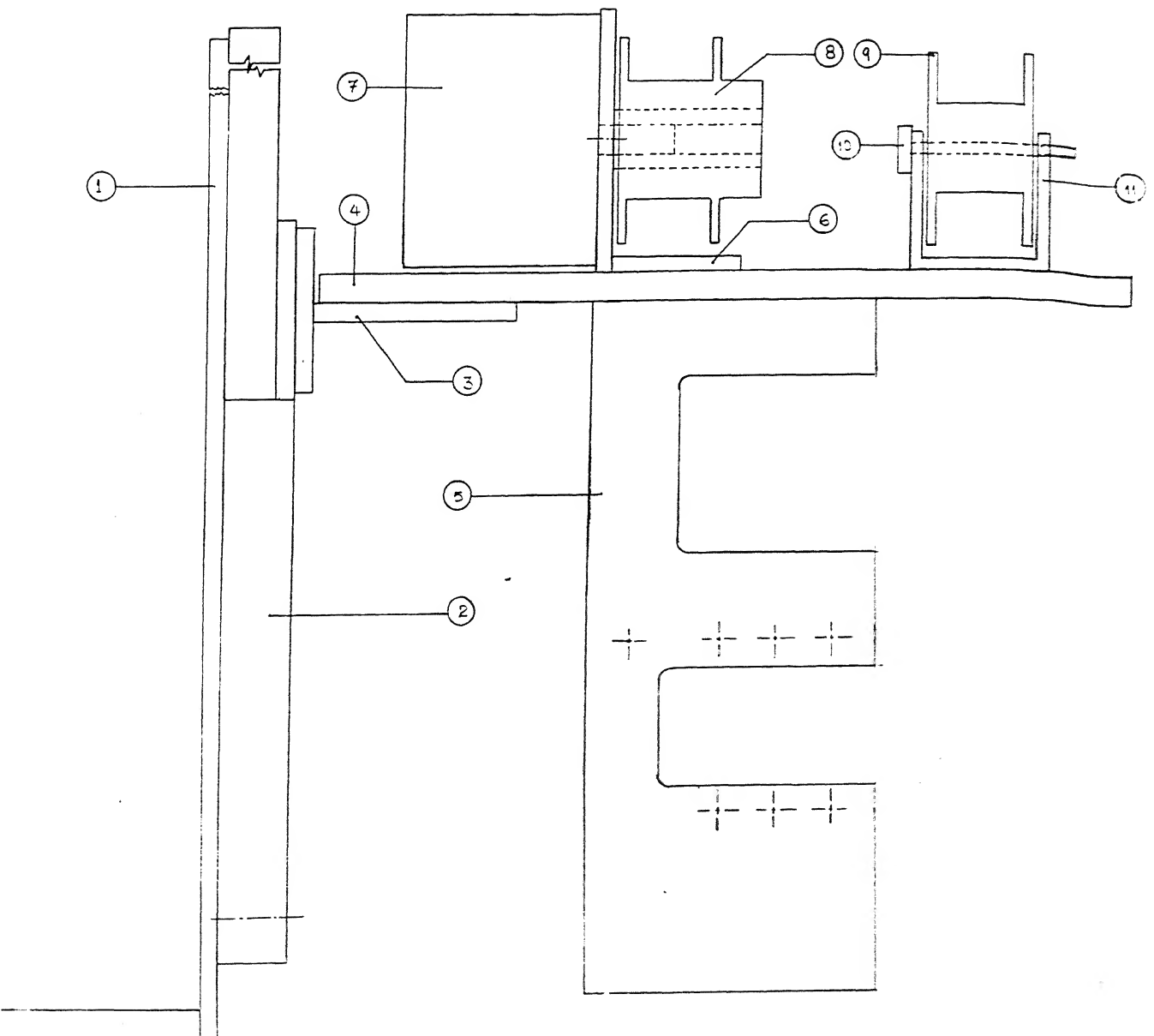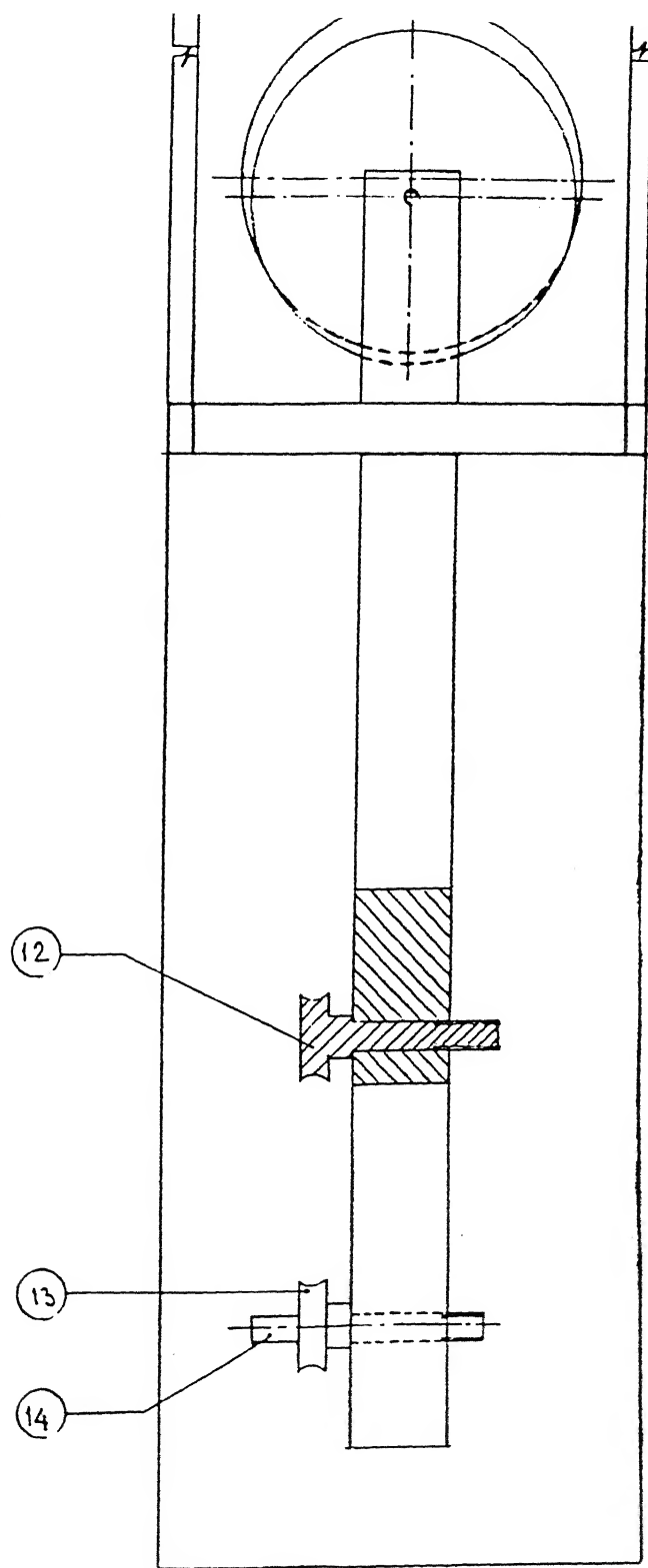
PLAN

WIRE DRIVE MECHANISM

FIG B.1(a)

Part No.	Part Description
1	SLIDING MECHANISM SUPPORT
2	SLIDING MECHANISM
3	WIRE BASE SUPPORT
4	WIRE BASE
5	PULLEY MOUNT
6	WIRE MOTOR MOUNT
7	WIRE MOTOR DRIVE
8	TAKE UP SPOOL
9	FEED SPOOL
10	SPOOL PIN
11	SPOOL BRACKET
12	COPPER CATHODE
13	IDLER PULLEY
14	IDLER PIN

ELEVATION

RIGHT SIDE VIEW

FIG B.1(c)   WIRE DRIVE MECHANISM

(a) CATHODE PULLEY
COPPER/1 NO.
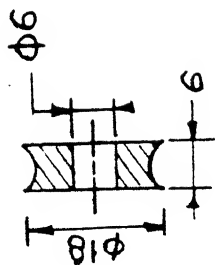
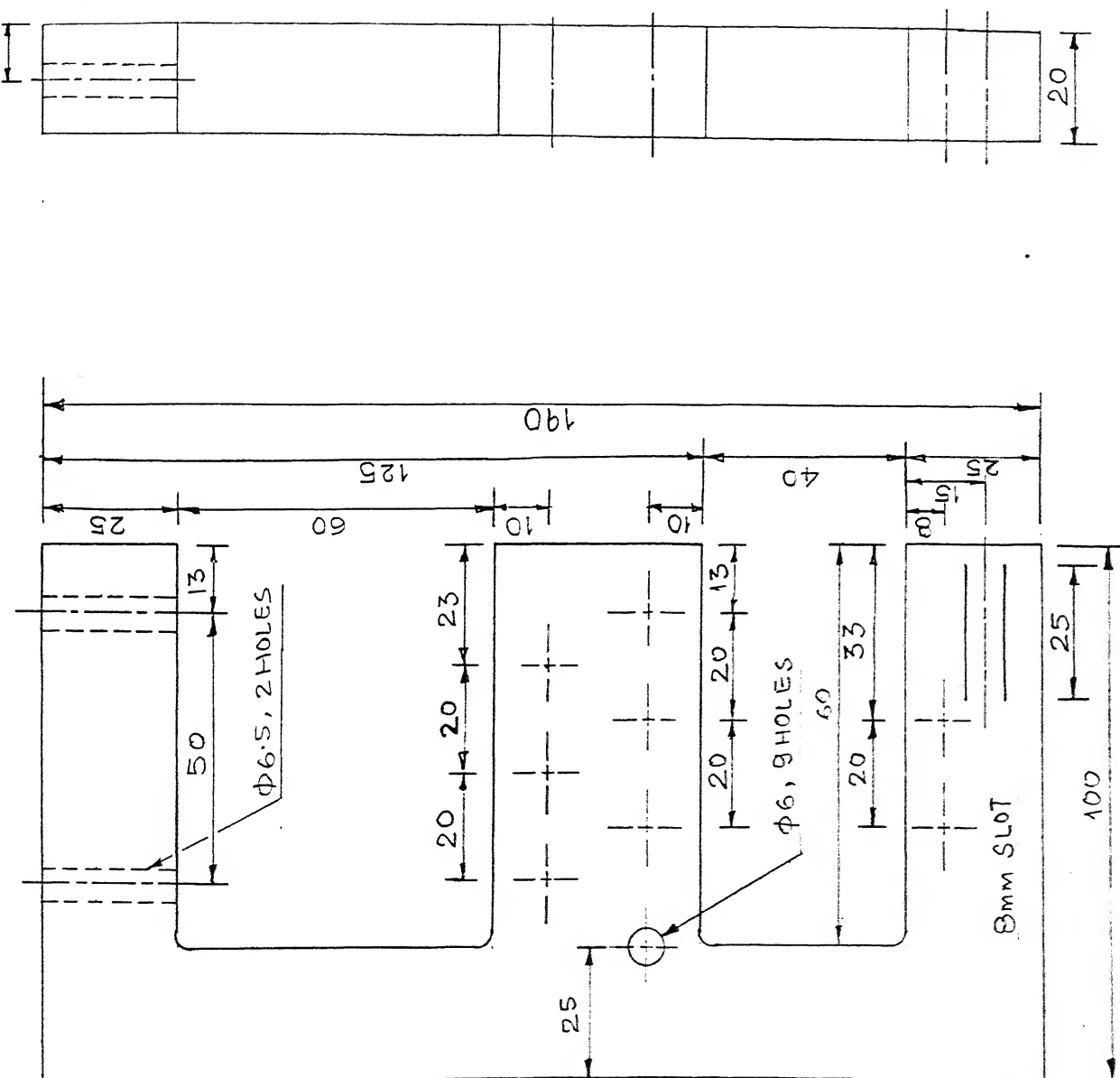(b) IDLER PULLEY
BRASS/4 NOS.

(c) IDLER PIN
S.S/5 NOS.
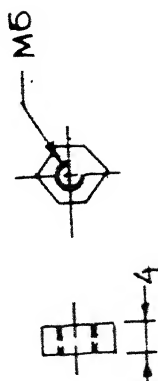
(d) CATHODE NUT
COPPER/2 NOS.

PULLEY UNIT

FIG B.2

96

PULLEY MOUNT
PLEXIGLASS/1 NO.

20

190

125

60

25

10

40

10

25

5

8

25

13

Φ6·5, 2 HOLES
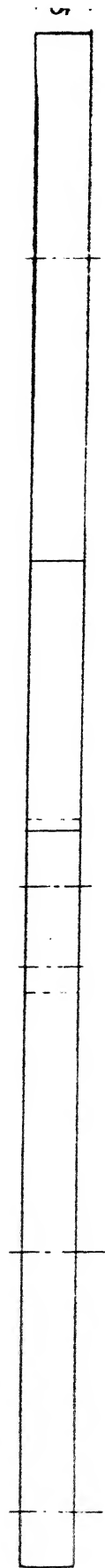
50

23

20

20

20

13

20

20

Φ6, 9 HOLES

60

33

20

8mm SLOT

100

25

25

FIG B.3

95
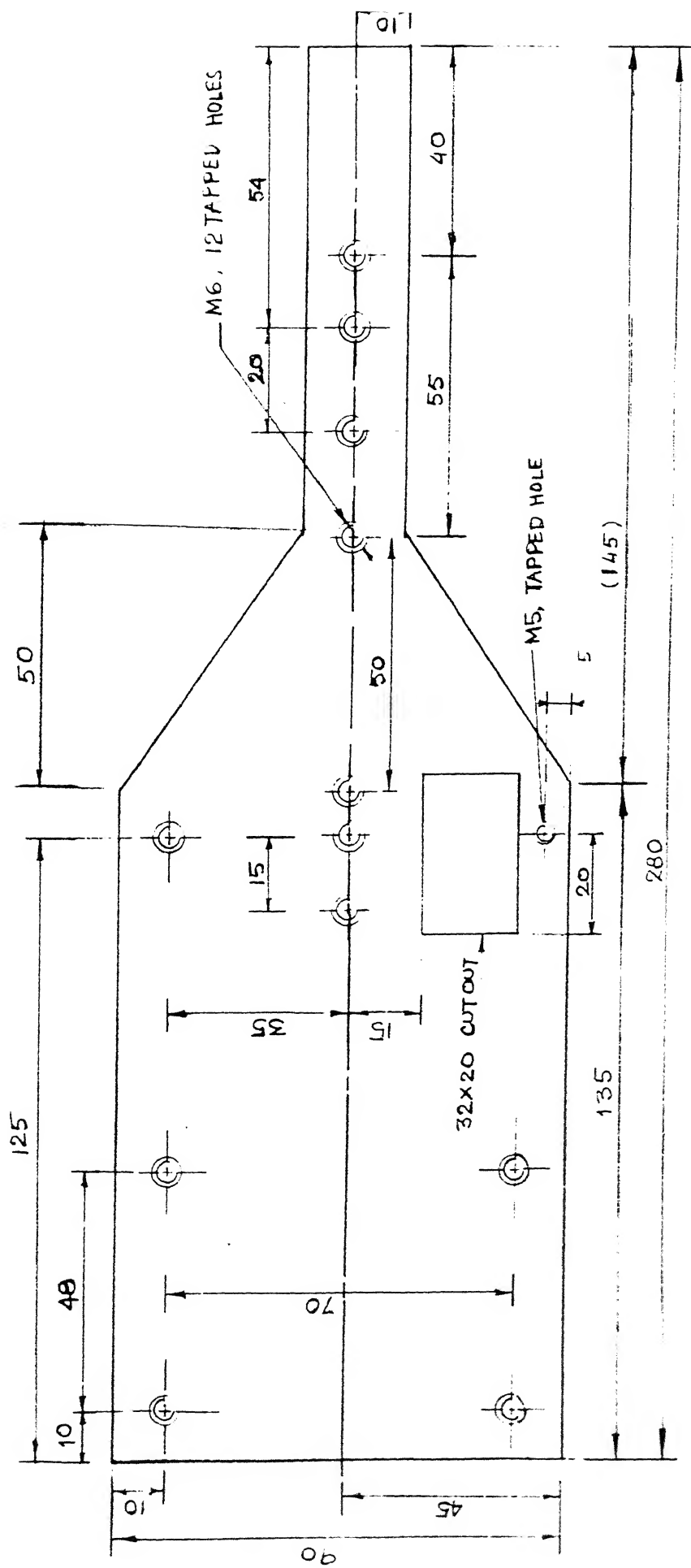
WIRE BASE
MILD STEEL/1 NO.

FIG B.4

M6, 12 TAPPED HOLES

M5, TAPPED HOLE

32×20 CUTOUT

110
54
40
20
55
50
50
(145)
5
15
35
15
20
280
135
125
48
70
10
10
45
90
5

SPOOL UNIT

FIG B.5

MACHINED PARALLEL
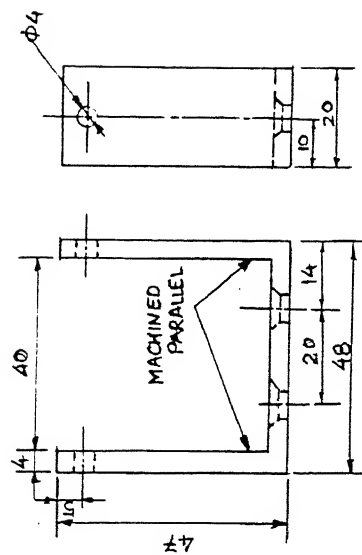
(c) SPOOL BRACKET
ALUMINIUM/ 1 NO.

M4

SMOOTH SURFACE
FINISH WITH
EMERY PAPER.
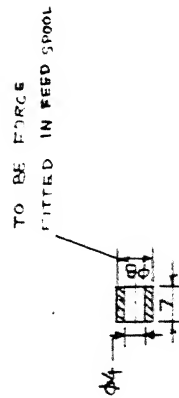
(d) SPOOL PIN
MILD STEEL/ 1 NO.

(a) FEED SPOOL
NYLON/2 NOS.

TO BE FORCE
FITTED IN FEED SPOOL

(b) SPOOL BUSH
BRASS/4 NOS.

2. Wire drive

The fresh wire is wound on the feed spool [Fig.B.5(a)], made of nylon. The feed spool is fitted with spool bush [Fig.B.5(b)] for low friction and free rotation. This feed spool is supported on feed spool bracket [Fig.B.5(c)] with the help of spool pin [Fig.B.5(d)].

The take up spool [Fig.B.6(a)] is driven by a stepper motor, SYM901, operated on 12 volts. A spool sleeve [Fig.B.6(b)], free fitted on the take-up spool, is set-screw tightened on the motor shaft. The take up spool is then mounted on the spool sleeve and screw tightened to the spool sleeve to provide positive rotation to the spool. The motor is mounted on the wire motor mount (Fig.B.7).

The feed spool and take up spool is mounted on the wire base (Fig.B.4).

3. Anode fixture

The anode is a rectangular piece of graphite (size 50×20×5mm) with a hole of 3.5mm diameter at the center of 50×20mm side. The anode is tightened on the anode holder (Fig.B.8). The anode is held and can be adjusted on the pulley mount.

4. Sliding mechanism for wire feed device

This mechanism is to hold the wire feed mechanism at two positions, at the working condition and off condition for replacing wire, etc. A dovetail assembly is used for this purpose
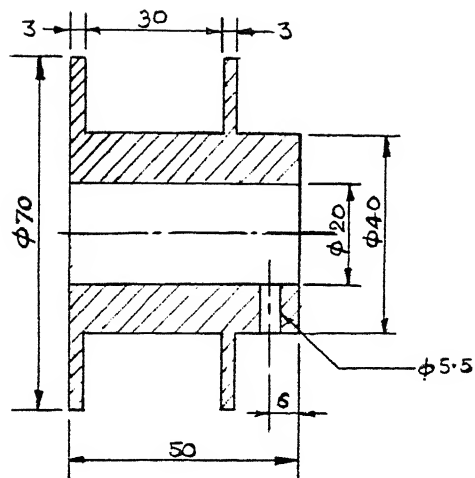
FIG B. 6(a)   TAKE-UP SPOOL
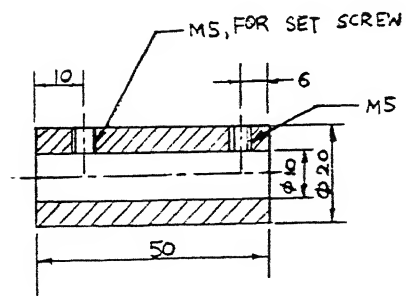   NYLON/2 NOS.
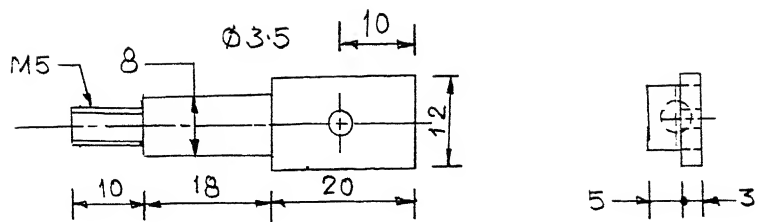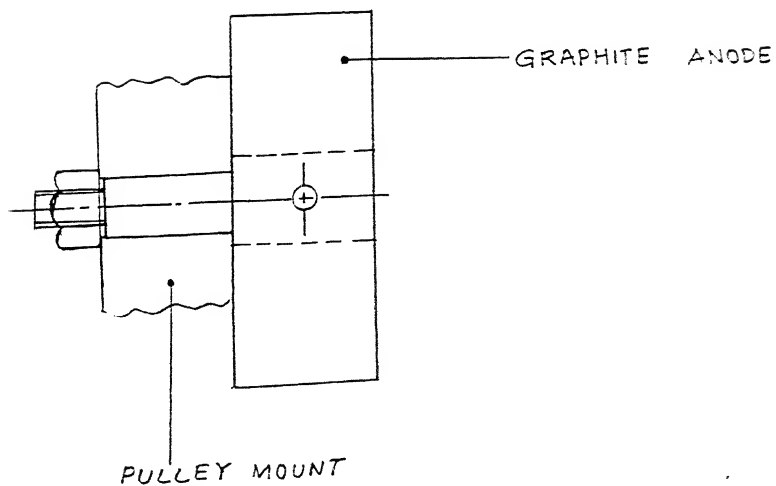

FIG B. 6(b)   SPOOL SLEEVE
               BRASS/1 NO.

FIG B.7

WIRE MOTOR MOUNT
MILD STEEL/1 NO.

The following labels appear in the drawing:

- 30
- 10
- 35
- φ6·5, 3 HOLES
- 15
- 15
- WELDING ...OSE TO THE ...NTRE HOLE.
- 10
- 32
- 20
- 40
- 5
- ...TOUT
- 5
- φ5·5
- 70
- M6, 4 PC'S.
- φ25
- 90
- 70
- 45
- 45
- 90
- 90°
- 5
- 50

102

FIG B.8

ANODE HOLDER
PLEXIGLASS/1 NO.

GRAPHITE ANODE

PULLEY MOUNT

SUBASSEMBLY SHOWING ANODE MOUNTING
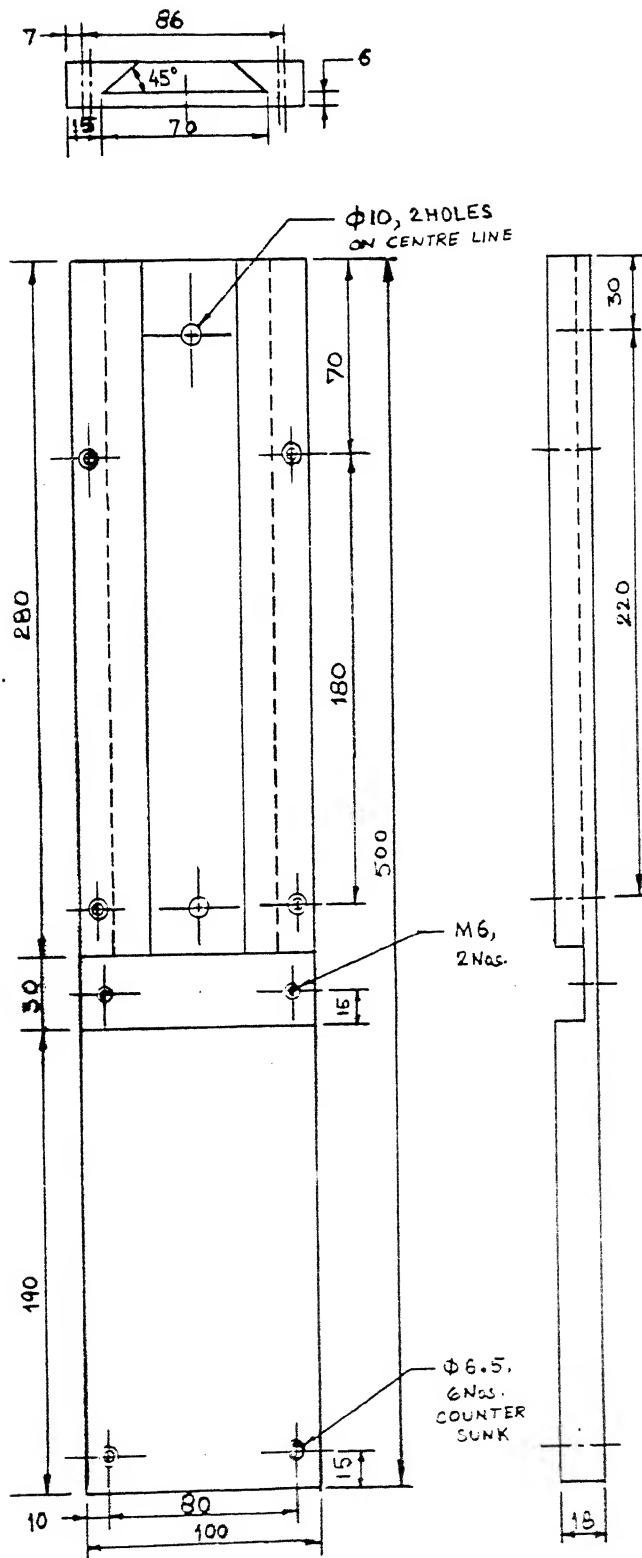
FIG B.9

DOVETAIL FEMALE SLIDE
MILD STEEL/1 NO.

80

10

15

φ6, 2Nos.
COUNTER
SUNK.

30

12

100
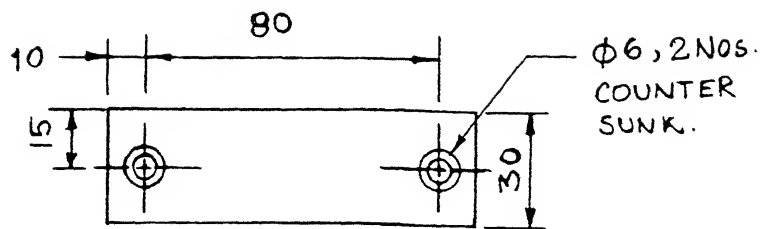
TO BE FITTED IN THE SLOT OF 100×30×12 OF FIG B.9

70

6

18

15

70

50

M10   M6. 4Nos.

30

10

40

60

100
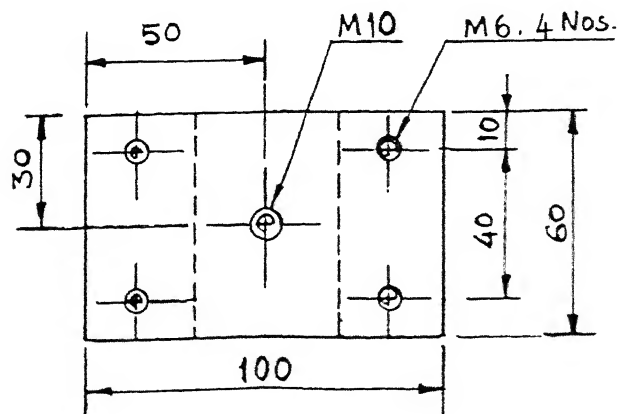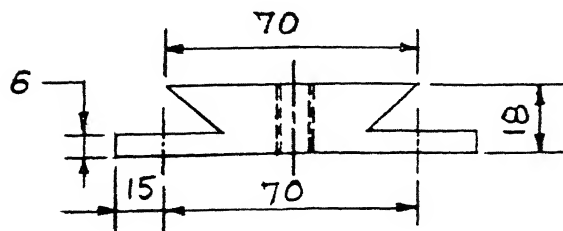
FIG B.10

DOVETAIL MAIL SLIDE
MILD STEEL/1 NO.

Φ6.5, 4 HOLES

M6, 4 Nos.

56

70

10

26

42

90

6

70

48
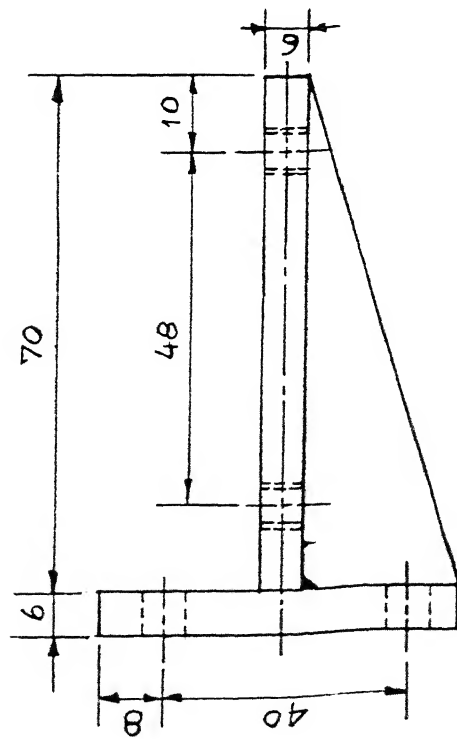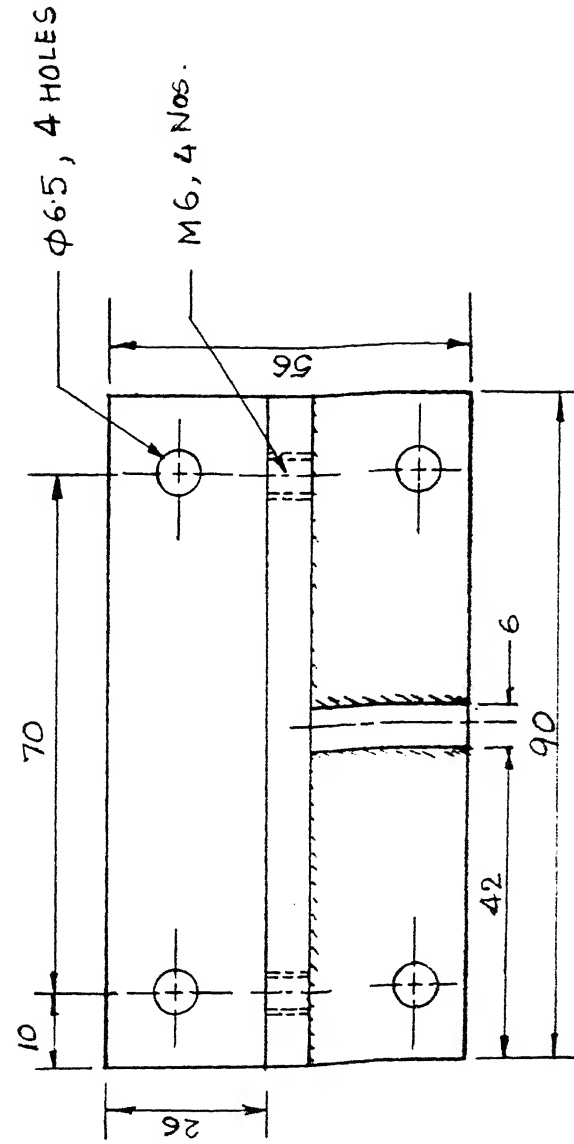
10

6

8

40

6

WIRE BASE SUPPORT
MILD STEEL/1 NO.

FIG B.11

comprising of dovetail female slide (Fig.B.9), dovetail male slide (Fig.B.10) and wire base support (Fig.B.11).

The wire base support is screw tightened on the dovetail male slide. Thus the whole wire feed mechanism slides along with the male slide. To hold rigidly at the two positions, a clear hole is made in the female slide and tapping is done in the male part. A bolt is tightened from the rear side of the female slide to the male slide. This assures stable and fixed position. This mechanism is screw tightened to the sliding mechanism support (Fig.B.12)which can slide on the base plate (Fig.B.13) for small alignment.
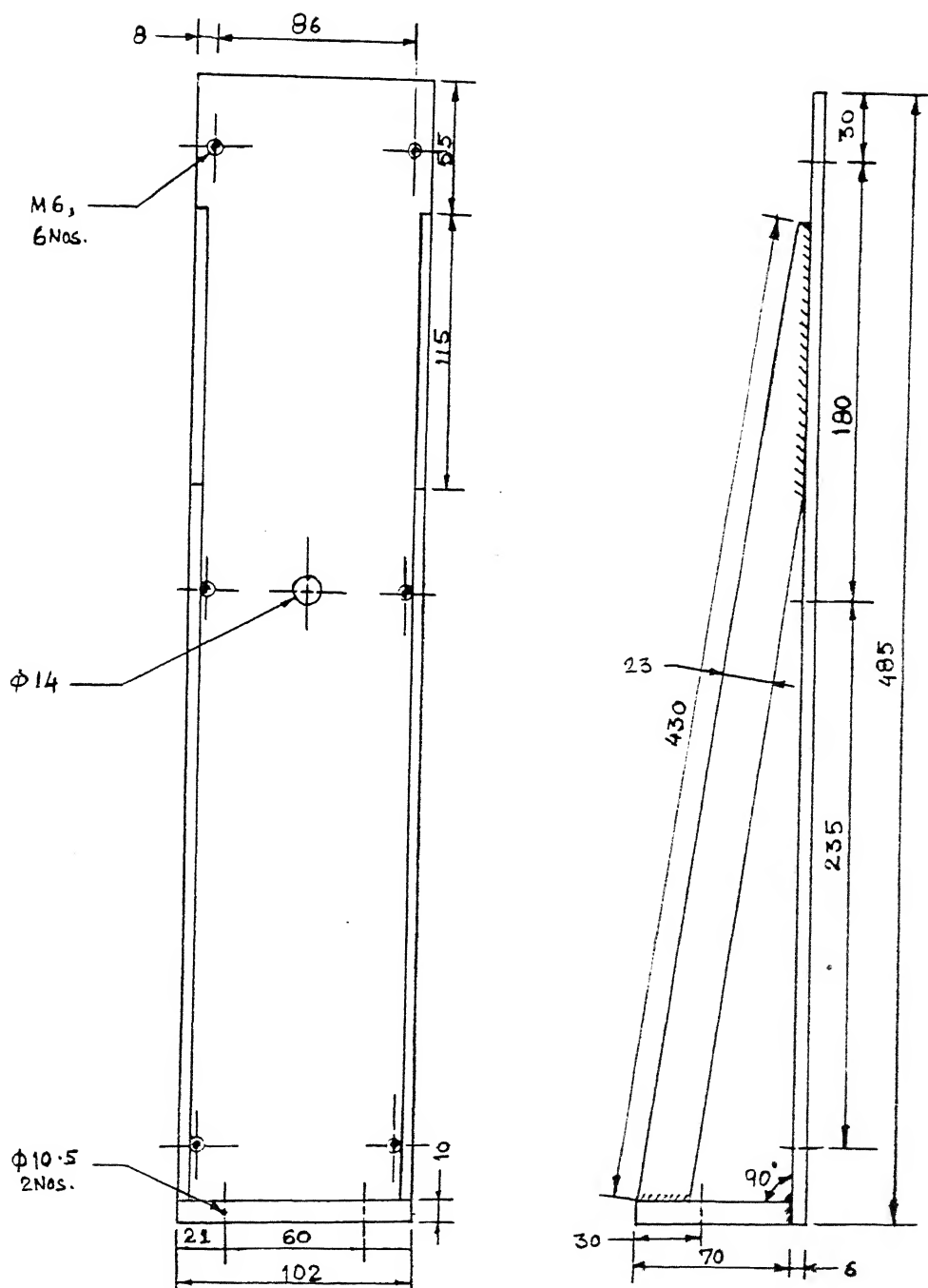
FIG B.12   DOVETAIL SLIDING MECHANISM SUPPORT
             MILD STEEL/1 NO.

M8

14

⌀14

5 4

⌀20

TO BE FITTED IN THE
SLOT OF FIG B.13

225

560

790

120

230

30
20

40

72
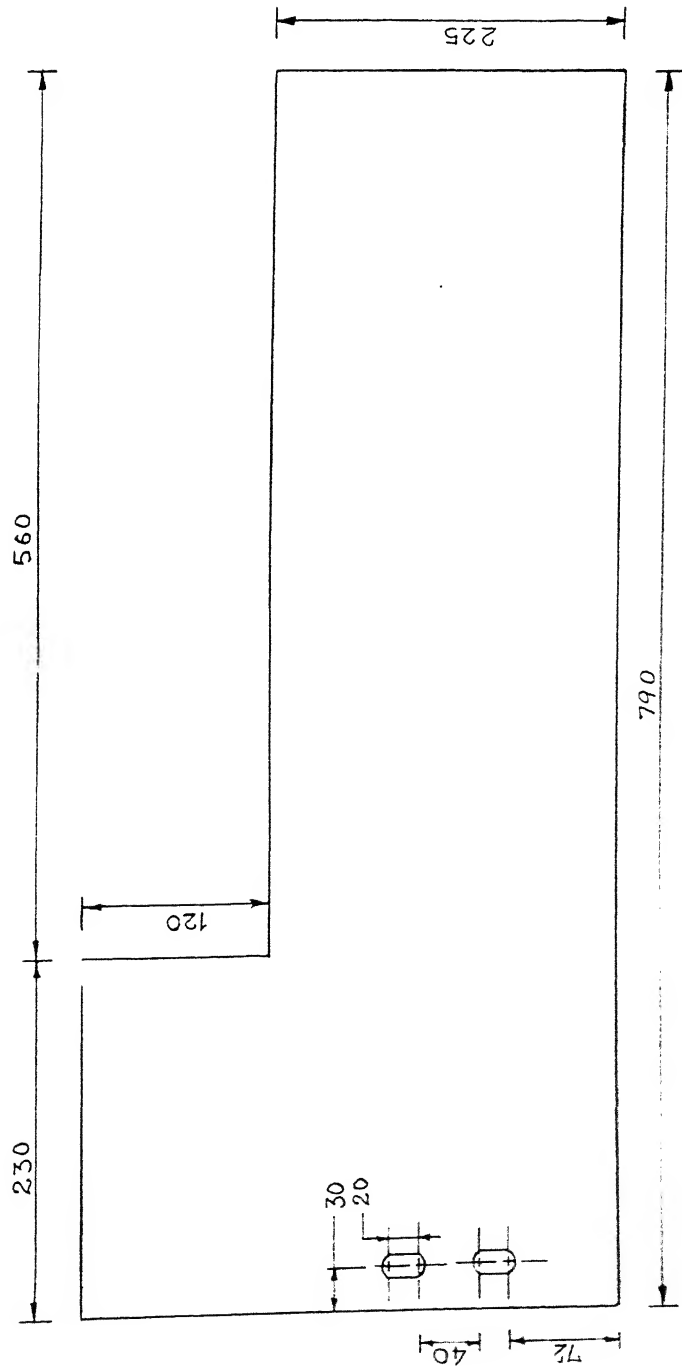
BASE PLATE
MILD STEEL/1 NO.

FIG B.13

PROPERTIES OF PZT CERAMICS

1. Mechanical Properties of PZT ceramics

Vickers Hardness $121.5 kg/mm^2$ at load of 2.5kg

Modulus of Rupture 48.8MPa

Young's Modulus 30.83GPa

Fracture Toughness 1.219MPa

2. Physical Properties

Melting Temperature $1560^{\circ}C$

Density $6.78 \ gm/cm^3$

3. Electrical property

Specific Electrical $10^{-11} mho/cm$

Conductivity

DETAILS OF CARBON FIBER EPOXY COMPOSITES

Purchased from   Fothergile Englineered Fabrics Ltd.,
                                  England

Type   Unidirectional carbon fabrics

Area Density, AD_{CF} $200g/m^2$

Density of carbon fibers, D_C $1.9g/cm^3$

Fiber Volume Fraction, V_F $(AD_{CF} \times N)/(D_C \times t)$

    where,   N is no of fiber and

        t is thickness of sample

    In our case, N = 16

        t = 3.7mm

    Therefore, V_F = 45.52 %

MEASUREMENT OF ELECTROLYTE CONDUCTIVITY

The specific conductance of the electrolyte is measured using a conductivity meter. The conductivity meter primarily consists of two parts, namely,

1. Digital direct reading (D.D.R.) conductivity meter, and

2. Conductivity Cell

The D.D.R. conductivity meter can measure conductivity of 0-1000 mMho in 4 ranges, with the accuracy of $\pm 1\%$. The conductivity can be read directly on the digital panel without manual balancing.

The conductivity cell has two platinum electrodes separated by a gap of "L" and each having cross sectional area of "A".

$$\text{Since} R = \rho(L/A)$$

$$\text{or,} (1/\rho) = (L/A) \times (1/R),$$

where, R = resistance in ohm

ρ = specific resistivity in ohm-m

$(1/R)$ = conductivity in mho

$(1/\rho)$ = specific conductance in mho-m

(L/A) is known as the cell constant and is fixed for a given cell electrode, since L & A are fixed.

Therefore, specific conductance is,

$$\sigma = \text{cell constant} \times \text{conductivity} (1/R)$$

The electrode cell constant of the apparatus was 0.841

APPENDIX F

The following chart shows the specific conductance of NaOH electrolyte in mho/cm [5]

Conc. wt.%	Temperature (degree celcius)						
	55	55	60	65	70	75	80
15	0.635	0.685	0.750	0.800	0.853	0.861	0.956
17.5	0.655	0.710	0.769	0.827	0.885	0.941	1.000
20[#]	0.663*	0.724*	0.786	0.855	0.919	0.982	1.046
22.5[#]	0.658	0.722	0.790*	0.859*	0.925*	0.993*	1.060
25	0.632	0.700	0.775	0.847	0.919	0.990	1.063*
27.5	0.591	0.638	0.743	0.820	0.895	0.971	1.047
30	0.562	0.634	0.718	0.796	0.857	0.952	1.032
32.5	0.520	0.606	0.690	0.769	0.850	0.930	1.61
35	0.513	0.590	0.664	0.745	0.833	0.907	0.989
37.5	0.475	0.556	0.640	0.722	0.805	0.887	0.969
40	0.448	0.525	0.610	0.693	0.777	0.859	0.945

* Maximum value of the specific conductance at constant temp.
# Concentration at which maximum value of the conductivity lies.